2015

Novel acceleration approaches of accurate and efficient modeling of high speed interconnects in layered media

Hongsheng Xu
Iowa State University

Recommended Citation

Xu, Hongsheng, "Novel acceleration approaches of accurate and efficient modeling of high speed interconnects in layered media" (2015). *Graduate Theses and Dissertations*. 14439.
https://lib.dr.iastate.edu/etd/14439

Novel acceleration approaches of accurate and efficient modeling of high speed interconnects in layered media

by

Hongsheng Xu

A dissertation submitted to the graduate faculty
in partial fulfillment of the requirements for the degree of
DOCTOR OF PHILOSOPHY

Major: Electrical Engineering

Program of Study Committee:
Jiming Song, Major Professor
John R. Bowler
Mani Mina
Nathan Neihart
Wensheng Zhang

Iowa State University
Ames, Iowa
2015

DEDICATION

This dissertation is dedicated to my beloved grandmother Tianying Dai and my parents, Zaolin Xu and Yimei Chen, whose affection, love, encouragement and prays of day and night make me able to get such success and honor.

This dissertation is also in memory of my grandfather. The absence during the last moments of his life is my biggest regret in my PhD career. He taught me to understand "The happiness comes from the ordinary."

TABLE OF CONTENTS

LIST OF TABLES

LIST OF FIGURES

ACKNOWLEDGEMENTS

I would like to take this opportunity to express my thanks to those who helped me with various aspects of conducting research and the writing of this thesis.

First and foremost, Dr. Jiming Song for his guidance, patience and support throughout this research and the writing of this thesis. His insights and words of encouragement have often inspired me and renewed my hopes for completing my graduate education. I would also like to thank my committee members for their efforts and contributions to this work: Dr. John R. Bowler, Dr. Mani Mina, Dr. Nathan Neihart and Dr. Wensheng Zhang. I could not have reached this far without Professor Tiejun Cui at Southeast University, who introduced me to the realm of electromagnetics.

I am also grateful to Dr. Telesphor Kamgaing, from Intel Corporation, Chandler, Arizona for his helpful suggestions about the publications of my research works. I am thankful to China Scholarship Council (CSC), Beijing, China and Intel Corporation, Arizona, USA for funding my PhD research.

I am thankful to Dr. Fugang Hu, Dr. Sidharath Jain, Dr. Hui Xie, Teng Zhao, Kun Chen, Siming Yang and other students in Dr. Song's group for their kind and friendly association and enlightening discussions. I appreciate all the departmental staff for their time and help, especially to Vicky Thorland-Oster.

I am also very grateful to my friends Jie Huang, from University of Glasgow, Scotland, UK, Renliang Gu, Ren Yan, Yifei Li, Ran Bi, Chunyu Zhang, Hongyan Sun, Yu Tian, Yuqing Chen, Dr. Depeng Mao and others who provided a very loving and friendly atmosphere without which all this would not have been possible.

ABSTRACT

Accurate modeling of interconnect structures is an important issue in modern high-frequency circuit and chip design; such as the accurate computation of the frequency-dependent internal impedance of interconnect structures, like wires and conducting strips, and the accurate and efficient electromagnetic (EM) modeling for shielded microstrip structures, especially in multilayered medium.

In the first part of this dissertation, a rigorous volume integral equation (VIE) is developed for the current distributions over two-dimensional conducting cylinders. For very low frequencies, it can be reduced to the widely-used quasi-static approximation. The different VIEs, surface integral equation (SIE), and partial differential equation (PDE) with Dirichlet boundary condition method are used to calculate the current distributions. The VIE with quasi-static approximation for good conductor is not accurate enough for the current distributions as there is a constant ratio between the results calculated from the quasi-static VIE and SIE. Two more leading terms from the Hankel function have been added into the integral kernel to solve this problem. We also calculate the internal impedance by using the different VIEs and the PDE with Dirichlet boundary condition method. The different results between VIE and PDE methods are due to the different boundary conditions.

In the second part of this dissertation, the novel acceleration approaches for spectral domain approach (SDA) over single layer substrate and for spectral domain immitance approach (SDIA) over multilayered substrates have been developed using one of the most promising extrapolation method–the Levin's transformation. It avoids the leading term extraction of the Green's functions and the Bessel's functions (basis functions) by re-

casting the summation kernel to a suitable form which can be applied in the Levin's transformation. The extrapolation delay has been introduced to successfully apply the Levin's transformation. Accurate results have been obtained for the propagation constant by only using twenty to thirty terms. The final accuracy could be further improved if only the first leading term added with the Levin's transformation. The new techniques match with or are even better than other acceleration techniques with high order leading term extraction. The two-dimensional PMCHWT formulation was developed from internal and external equivalent problems, along with the spatial and spectral domain dyadic Green's functions to deal with the arbitrary cross section and finite conductivity of multiple metal lines over multilayered substrates. The pulse and triangular basis were chosen to be applied in the Galerkin method. The matrix elements were calculated from spatial domain integration in internal equivalent problem, while in external equivalent problem we need to transfer the spatial domain integration into spectral domain summation.

CHAPTER 1. INTRODUCTION

The dissertation introduces and discusses of the electromagnetic modeling for high speed interconnects, and is comprised of two parts. Part I is on the accurate modeling of the current distribution and internal impedance of interconnects in homogeneous medium. Different integral equations and different definitions are developed to analyze the current distribution and the internal impedance. Part II is focused on the novel acceleration approaches of accurate and efficient electromagnetic modeling for the generalized shielded microstrip line structures with single or multiple metal lines in multilayered medium. Extrapolation methods are used to accelerate the spectral domain approach with the method of moments (MoM) to calculate the propagation constant and the effective permittivity of the microstrip lines.

1.1 Introduction to Current Distribution and Impedance of Interconnects

1.1.1 Research motivation

Accurate modeling of interconnect structures is an important issue in modern high-frequency circuit and chip design. Especially the accurate computation of the frequency-dependent internal impedance of interconnect structures, like wires and conducting strips, of the type encountered in planar integrated circuits (ICs) is an important consideration for the accurate assessment of loss and dispersion in high-speed signaling. The on-chip interconnect structure in modern very large scale integrated (VLSI) circuits is a highly complicated electromagnetic system as shown in Figure 1.1. The full structure may connect more than one million transistors that are hosted on a silicon substrate and may contain up to seven metalization layers. Now, the electronics industry has entered an era where interconnect delays are the most significant limitation in the overall performance of a high speed digital system. For the submicron-geometry chips, it is the interconnection delays rather than the device delays that determine the chips. Interconnect delay will soon become the main bottle neck for increasing the operation frequencies of the fully integrated circuits. New approaches are needed to lower the interconnection delays. One of the key part of an excellent interconnect is to minimize skin effect. Skin effect occurs when the high-frequency currents flow on the outer skin of the conductors whereas lower frequencies have more uniform current distribution across the conductor cross-section. The effect is that the impedance is different for low frequencies than high frequencies. This difference in impedance can cause serious problem such as attenuation, dispersion and phase shifts in signal integrity. The losses also have an important impact on the signal integrity due to attenuation and dispersion.

Signal integrity primarily involves the electrical performance of the wires and other packaging structures used to move signals about within an electronic product. This topic is an important activity at all levels of electronics packaging and assembly, from internal connections of an IC, through the package, the printed circuit board (PCB), the backplane, and inter-system connections [2]. On PCBs, signal integrity becomes a serious concern when the transition times of signals start to become comparable to the propagation time across the board. As speed increases, a larger and larger fraction of signals need integrity analysis. Roughly speaking, essentially all signals must be designed with signal integrity in mind when frequency larger than 100 MHz. In modern IC industry, scaling trends brought electrical effects back to the forefront in recent technology nodes. With scaling of technology below 0.25 μm, the wire delays have become comparable or even greater than the gate delays. So the wire delays are needed to be considered to

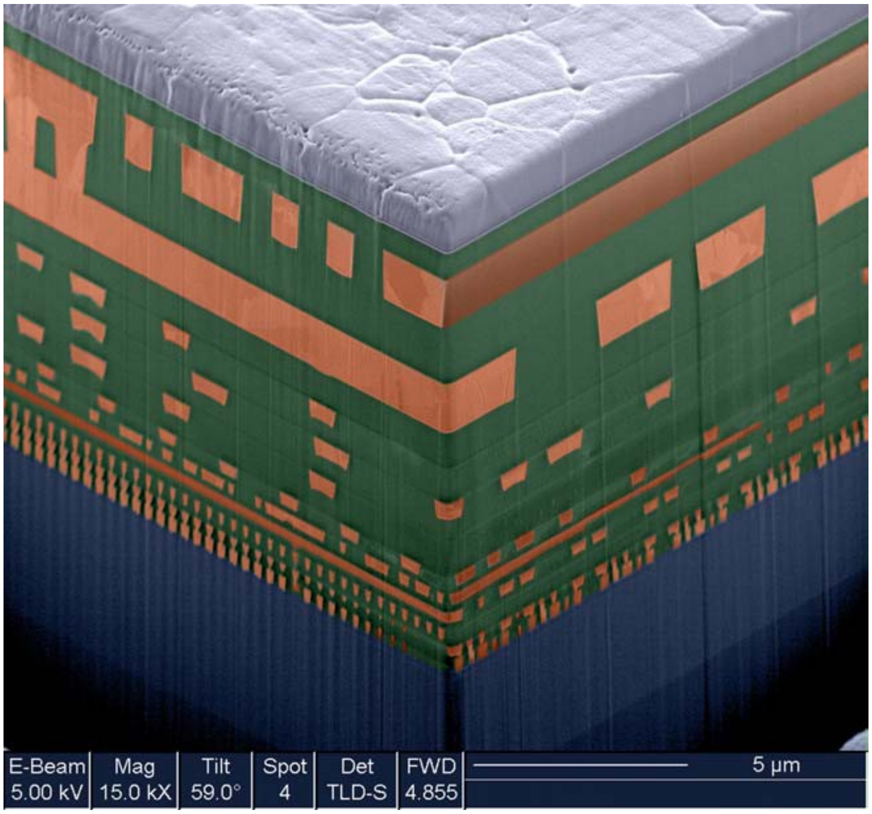

Figure 1.1 The cross section of an IBM multi-level interconnect structure [1]

achieve timing closure. In nanometer technologies at 0.13 μm and below, unintended interactions between signals (e.g. crosstalk) become an important consideration for digital design. At these technology nodes, the performance and correctness of a design cannot be assured without considering noise effects.

To do a good signal integrity analysis, parasitic extraction can be a huge help. Parasitic extraction is calculation of the parasitic effects in both the designed devices and the required wiring interconnects of an electronic circuit: detailed device parameters, parasitic capacitances, parasitic resistance and parasitic inductances. The major purpose of parasitic extraction is to create an accurate analog model of the circuit, so that detailed simulations can emulate actual digital and analog circuit responses [3]. Another fact is that parasitic capacitances and inductances associated with the interconnections in the high density environment of the IC have become the primary factors in the evolution of the very high speed IC technology. In early ICs the impact of the wiring was negligible, and wires were not considered as electrical elements of the circuit. However, below the 0.5 μm technology node resistance, capacitance and inductance of interconnects start making a significant impact on circuit performance. The continuous downscaling of the pitch implies that parasitic effects become a major design concern.

For accurate signal integrity simulations of on-chip interconnect structures, a broadband transmission line model is required. In the near future, systems with speed of 40 Gbit/s and higher will be developed, for which undesired effects as mentioned above (signal delay, attenuation, dispersion, loss, and cross-talk) on interconnects are becoming problematic. These effects can be predicted by a transmission line model that rigorously takes into account the material properties and geometry of the considered structures. An accurate modeling of interconnects is necessary for the development of high speed systems. Such a 2-D model is developed for the determination of the quasi-TM resistance and inductance. Predicting signal delay, attenuation, and dispersion on these interconnects demands the accurate determination of the circuit parameters, i.e., capacitance, inductance, conductance and resistance per unit length (p.u.l.), and hence demands the accurate calculation of the current distributions flowing inside the conducting wires. For the usual application to transmission line problems, the conductors are assumed infinitely long so that the computation of these parameters is a 2-D problem in the transverse or cross-sectional plane of the line.

1.1.2 Literature review

Many scientists have focused on this topic discussed here, and some good work was done for the skin effect and losses in rectangular conductors [4–18]. The earliest research on interconnect losses is well summarized in [10], for example, Wheelers incremental inductance rule, where the magnetic field generated by the axial current flow is used to calculate the losses, under an assumption that the real and imaginary parts of the high-frequency internal impedance per unit length is equal. The calculation of p.u.l. internal impedance for an isolated 2-D conducting cylinder with circular cross section (a wire) is well known as the analytical result of [19]. The p.u.l. internal impedance for an isolated 2-D conducting rectangular cylinder can be calculated by means of a volume integral equation (VIE) and volume discretization with Galerkins method in [20], which showed an important deviation from Wheelers rule. However, this topic has prompted some intriguing discussion in the literature [21–23]. The quasi-static approximation is widely used in practical engineering problems like analysis of current carrying conductors [24], and internal impedance of conductors [20, 25]. In addition to VIE, Surface integral equation (SIE) can also be used to calculate the surface equivalent currents along the boundary of a conductor [26], and then get the current distribution within the conductor by using these surface equivalent currents to calculate the electric field everywhere inside the conductor [27]. Given the same excitation sources, the numerical results calculated from VIE and SIE should be the same, but we found there is a constant ratio between them. Another way to calculate the current distributions of rectangular cross sections cylinder is given by an analytical series expression by solving partial different equation (PDE) with Dirichlet boundary conditions [25].

1.1.3 Research work

In Chapter 2, we develop an accurate volume integral equation (VIE) rigorously for the current distribution within a conductor with arbitrary cross section. This accurate VIE is compared with widely used quasi-static VIEs and surface integral equations (SIE) by using MoM to solve the current distribution within a rectangular cross section conductor. The different partial differential equations (PDEs) obtained in quasi-static approximation and rigorous approaches require different Green's functions to get the solutions: logarithm and Hankel functions, respectively. By expanding the Hankel function for small arguments, two more leading terms should be added into the quasi-static VIE's integral kernel to cancel the constant ratio mentioned above.

We analyze the influence of different definitions and different boundary conditions on the calculation of internal impedance. Numerical results of rectangular and square conductors by using the quasi-static VIE, modified VIE, accurate VIE, SIE, and PDE with Dirichlet boundary conditions are given.

1.2 Introduction to Acceleration of SDA for Shielded Microstrip Lines

1.2.1 Research motivation

The microstrip line is the most popular transmission line used in microwave integrated circuits (MICs) for designing components and interconnects due to its various advantages. They are relatively broadband in frequency. They provide circuits that are compact and light in weight. They are capable to reduce the losses and to control the coefficient of expansion. They can easily offer interfaces with other circuits leading to good compatibility with integrated hybrid circuits. And they are also used in the antenna design where they show good surface wave immunity gain, and bandwidth enhancement apart from the good mechanical integration [28]. A microstrip line may be designed on the different configuration of the substrate layers which could be single, double, or multilayered materials. Recently, the use of the multilayered substrates has been rapidly increased at high frequency due to the system-on-chip (SOC) requirement.

A microstrip line with a shielded box is a more realistic circuit configuration, by covering the basic microstrip configuration with metal top plates on the top and on the two sides. The main purposes of packaging are to provide mechanical strength, electromagnetic (EM) shielding, and heat dissipation in the case of high-power applications. Packaging must also protect the circuit from moisture, dust, salt spray, and other environmental contaminants. Moreover, microstrip transmission lines on the silicon can be considered as being a shielded environment in these following cases: first, in most packages and semiconductor backends, dummy metallization, ground planes and vias are typically placed around the signal interconnnects for both process optimization and electrical coupling reduction; second, in high density packaging, external electromagnetic interference (EMI) shielding could be used to limit interaction between components or a die may be flip-chip assembled above the power or ground plane of an underlaying package substrate [29].

The on-chip interconnect structure in modern VLSI circuits is a highly complicated EM system consisting of multiple layers of metal lines, vias, etc. embedded in multiple layers of lossy medium. Accurate EM modeling is very important for modern high-frequency circuit and chip design. The increasing demands on the speed and accuracy in EM simulation tools requires more efficient techniques to speed up the solving process. In order to increase the speed and accuracy, domain decomposition methods are being used in recent EM solvers like HFSS 13. The whole problem will be split into domains using the domain decomposition method and each domain would be analyzed using a problem specific approach on a separate core in the future version of EM solvers [30]. The second part of this dissertation mainly proposes a novel acceleration technique that can be used to speed up the solving process of spectral domain approach along with the method of moments (MoM) for the modeling of a generalized multiple metal lines and patches embedded in a multilayered shielded interconnect, as shown in Figure 1.2.

1.2.2 Literature review

The full wave spectral domain approach (SDA) along with MoM give reasonable accuracy of propagation constant for shielded microstrips with relative few unknowns. It is widely used to analyze the transmission line structures. However, the drawback of SDA is that the infinite summations of slowly convergent spectral domain series require tense computation and decrease the speed and efficiency. Therefore, several accelera-

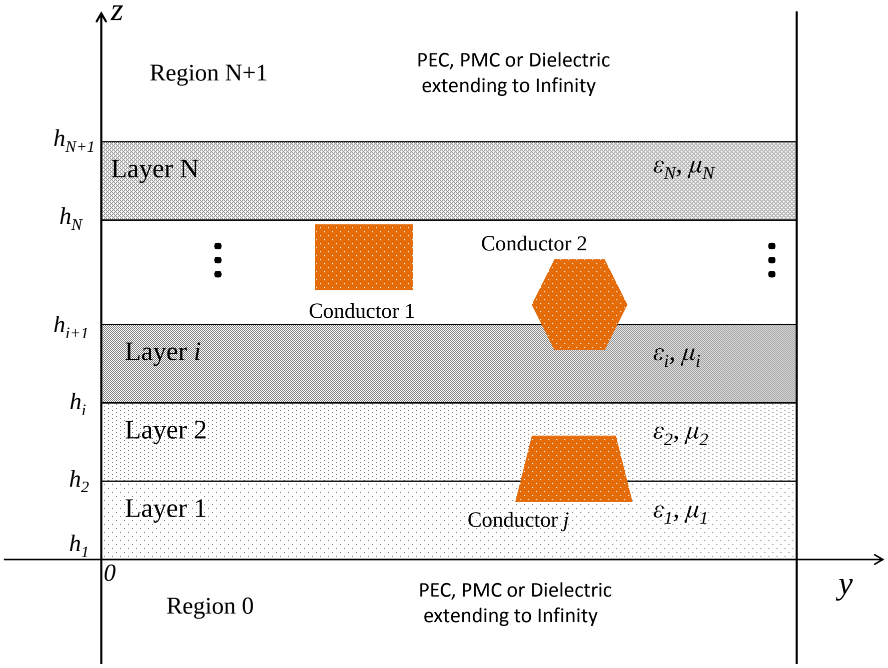

Figure 1.2 A generalized model for shielded multilayered interconnects with multiple arbitrary cross section metal lines in different layers

tion techniques must be applied to speed up the solving process. In order to accelerate the convergence of the spectral domain series summation, several techniques based on asymptotic expansion have been proposed in [31, 32]. The technique of [32] recasted the kernel functions in summation into three parts: one with exponential convergence, one with $1/n^k$ fast convergence, and one with closed form weakly singular terms. The mid-point summation (MPS) technique reported in [33] and a super convergent series (SCS) approach described in [34] have been applied to obtain fast convergence for summation of the infinite series in the form of sinusoidal functions divided by n^k and of $1/n^k$, after the spectral domain asymptotic extractions. Furthermore, two different fast convergent sine cosine series to accelerate the summation of the leading term after the asymptotic extraction to the Green's functions and the Bessel functions (basis functions) in the spectral domain are used in [35]. All these works depend on the asymptotic techniques such as leading term extraction which add the complexity to the derivation and programming.

The extrapolation methods have been used to solve the EM problem for many years. Some extrapolation methods have been reviewed for acceleration of the convergence of Sommerfeld-type integrals which arise in problems like scatterers embedded in planar multilayered media [36]. Moreover, several popular series transformation methods used in electromagnetic problems were introduced in [37], like the Shanks transformation [38] and Wynn's ϵ algorithm [39]. The Levin t transformation is better than the Shanks transformation, compared by Levin himself [40]. Blakemore *et al.* in [41] have found that the Levin v transformation is more efficient than Wynn's ϵ algorithm. Compared with other extrapolation methods mostly used in solving EM problem, the Levin's transformation is the best choice.

Dealing with the metal lines with finite thickness and conductivity is a big challenge in accurate modeling of multilayered interconnects. The skin depth approximation has been used to treat the real metal strips, such as surface impedance boundary condition (IBC), to determine propagation and attenuation constants when the thickness of strip is much larger than the skin depth [42,43]. The resistive boundary condition (R-card) have been used in [44] to solve for the propagation constant assuming the strip thickness to be much smaller than skin depth. The rigorous analysis of the propagation constant of multiple metal lines with arbitrary cross section in multilayered media is introduced in [45] by using boundary integral equation in conjunction with the MoM. The multilayered media dyadic spectral domain Green's functions are derived based on the transmission line network analog along the axis normal to the stratification, and mixed-potential integral equations (MPIE) are used to solve the arbitrarily shaped, three-dimensional objects embedded in such a medium [46]. Mostly recently, works of analyzing the propagation of bound and leaky modes in perfectly conducting open single and coupled microstrip lines with polygonal cross section is reported in [47].

1.2.3 Research work

In Chapter 3, the spectral domain approach with the MoM is used to solve for the propagation constant and effective permittivity of a single layer shielded microstrip. The infinite summations of slowly convergent spectral domain series are accelerated by using one of the most promising extrapolation method–the Levin's transformation. By using this proposed new acceleration technique, the asymptotic expansion for the spectral domain Green's functions and the Bessel functions (basis functions), which are the key part in many old acceleration techniques [31–35], is avoided. The new technique can obtain accurate results with relatively small number of terms. It can achieve the same accuracy as high order leading term extraction techniques does by using the same number of terms.

In Chapter 4, the proposed new technique in Chapter 3 is further extended to handle the multilayered shielded microstrip line structures. By recasting the summation kernel into a suitable form for the Levin's transformation, one can accelerate the solving process without doing the high order leading term extraction. This greatly reduces the complexity of solving the multilayered shielded microstrip to get the propagation constant and effective permittivity.

In Chapter 5, the finite thickness and finite conductivity issue of the metal strip lines are taken into account as the cross sections of the metal strip lines can be treated as arbitrary shape as shown in Figure 1.2. The two-dimensional PMCHWT formulation is derived from external and internal equivalent problems with both equivalent electric and magnetic currents $\mathbf{J}_s$ and $\mathbf{M}_s$ since it is free from internal resonance problem. The homogeneous dyadic Green's function is used to solve for the internal equivalent problem, and the layered medium spectral domain dyadic Green's function and transmission line Green's function are used to solve for the external equivalent problem. The subdomain current basis used in longitudinal direction is pulse basis, while the transverse current basis is chosen as triangular basis according to the physical property of the current distributions. The direct spatial domain integrations are calculated in the internal equivalent problem, while the spatial domain integrations are transfered to spectral domain summation in the external equivalent problem.

CHAPTER 2. CURRENT DISTRIBUTION AND IMPEDANCE OF INTERCONNECTS

In this chapter, a rigorous volume integral equation (VIE) is developed for the current distributions over two-dimensional conducting cylinders. For very low frequencies, it can be reduced to the widely-used quasi-static approximation. The different VIEs, surface integral equation (SIE), and partial differential equation (PDE) with Dirichlet boundary condition method are used to calculate the current distribution. A comparison between the numerical results applied to square and rectangular cross sections shows that the accurate VIE gives almost the same results as the SIE, but the VIE with quasi-static approximation for good conductor is not accurate enough for the current distribution as there is a constant ratio between the results calculated from the quasi-static VIE and SIE. Two more leading terms from the Hankel function have been added into the integral kernel to solve this problem. We also calculate the internal impedance by using the different VIEs and the PDE with Dirichlet boundary condition method. The different VIEs give the same internal impedance. The different results between VIE and PDE methods are due to the different boundary conditions.

2.1 Introduction

The quasi-static approximation is widely used in electromagnetic (EM) problems such as analysis of current distributions within conductors [24] and internal impedance of conductors [20,25]. It is relatively easy to develop the volume integral equation (VIE) for calculating the current distribution within a conductor with quasi-static approximation. The current distributions over conductors' cross sections can be calculated by method of moments (MoM) with pulse basis functions and Galerkin's method [20, 26]. Surface integral equation (SIE) can also be used to calculate the surface equivalent currents along the boundary of a conductor [48], and then get the current distributions within the conductor by using these surface equivalent currents to calculate the electric field everywhere inside the conductor [27]. Given the same excitation sources, the numerical results calculated from VIE and SIE should be the same, but we found there is a constant ratio between them.

In this chapter, we derive the accurate VIE rigorously for the current distributions within a conductor with arbitrary cross sections, and show the different partial differential equations (PDEs) obtained in quasi-static approximation and rigorous approaches require different Green's functions to get the solutions: logarithm and Hankel functions, respectively. By expanding the Hankel function for small arguments, two more leading terms should be added into the quasi-static VIE's integral kernel to cancel the constant ratio mentioned above. Numerical results of a square conductor by using the quasi-static VIE, accurate VIE, and SIE are given.

2.2 Volume Integral Equation (VIE) of the Current Distribution

The quasi-static approximation is widely used in practical engineering problems like analysis of current carrying conductors [24], and internal impedance of conductors [20,25]. The volume integral equations (VIE) for the current within a conductor are very easy to develop by using quasi-static approximation, and the current distribution over cross section can be calculated by use of method of moments (MoM) with pulse basis functions and Galerkin's method [20,48]. In this section, we derive the accurate VIE rigorously for the current distribution within a conductor with arbitrary cross sections. The different partial differential equations (PDEs) obtained in quasi-static approximation and rigorous approaches require different Green's functions to get the solutions: logarithm and Hankel function, respectively. By expanding the Hankel function for small arguments, two more leading terms should be added into the quasi-static VIE's integral kernel to cancel the constant ratio mentioned above. Then, the details of a standard MoM are described to solve the VIE.

2.2.1 Rigorous derivation for the VIE

Let's consider the case of a conductor with constitutive parameters permittivity ε_0, permeability μ_0, and conductivity σ surrounded by free space or any homogeneous medium. For time-harmonic case, the Maxwell's equations are:

$$\nabla \times \mathbf{E} = -j\omega \mathbf{B} \tag{2.1}$$

$$\nabla \times \mathbf{H} = \mathbf{J}_c + j\omega \mathbf{D} \tag{2.2}$$

$$\boldsymbol{\nabla} \cdot \mathbf{D} = \boldsymbol{\rho_e} \tag{2.3}$$

$$\boldsymbol{\nabla} \cdot \mathbf{B} = \mathbf{0} \tag{2.4}$$

By introducing the magnetic vector potential A, which is related to the magnetic flux density B in the following way:

$$\mathbf{B} = \nabla \times \mathbf{A} \tag{2.5}$$

Substituting this into (2.1), the Faraday law yields the electric-field intensity vector **E** in terms of **A** and the scalar potential function ϕ_e as:

$$\mathbf{E} = -\nabla \phi_e - j\omega \mathbf{A} \tag{2.6}$$

Then substituting (2.5) into (2.2), with $\mathbf{J}_c = \sigma \mathbf{E}$, using $\mathbf{B} = \mu_0 \mathbf{H}$ and $\mathbf{D} = \varepsilon_0 \mathbf{E}$, we can get:

$$\frac{1}{\mu_0} \nabla \times \nabla \times \mathbf{A} = (\sigma + j\omega\varepsilon_0)\, \mathbf{E} \tag{2.7}$$

Since $\nabla \times \nabla \times \mathbf{A} = \nabla(\nabla \cdot \mathbf{A}) - \nabla^2 \mathbf{A}$, substituting this into (2.7) along with (2.6), yields

$$\nabla^2 \mathbf{A} + k_0^2 \mathbf{A} = \mu_0 \left(\sigma \nabla \phi_e + j\omega\sigma \mathbf{A}\right) + \nabla \left(\nabla \cdot \mathbf{A} + j\omega\mu_0\varepsilon_0\phi_e\right) \tag{2.8}$$

where the free space wavenumber is defined as $k_0 = \omega\sqrt{\varepsilon_0\mu_0}$. By applying Lorentz gauge condition: $\nabla \cdot \mathbf{A} + j\omega\mu_0\varepsilon_0\phi_e = 0$, the above equation becomes

$$\nabla^2 \mathbf{A} + k_0^2 \mathbf{A} = -\mu_0 \mathbf{J} \tag{2.9}$$

where

$$\mathbf{J} = -j\omega\sigma \mathbf{A} + \mathbf{J}^{\text{imp}}. \tag{2.10}$$

$\mathbf{J}^{\text{imp}}$ is the impressed current defined as:

$$\mathbf{J}^{\text{imp}} = -\sigma \nabla \phi_e = \sigma \mathbf{E}^{\text{imp}}. \tag{2.11}$$

For the two-dimensional case, since the conductor is assumed to be infinite long in z-direction, which is the same direction as the current flows, the impressed $\mathbf{E}^{\text{imp}}$ field is along z-direction as shown in Figure 2.1, $\mathbf{J}$ and $\mathbf{A}$ have z-component only, $\mathbf{A} = \hat{z}A_z(x, y)$. Therefore we have:

$$\nabla^2 A_z(x, y) + k_0^2 A_z(x, y) = -\mu_0 J_z(x, y) \tag{2.12}$$

where

$$J_z(x, y) = J_z^{\text{imp}}(x, y) - j\omega\sigma A_z. \tag{2.13}$$

With the help of the two-dimensional scalar Green's function for wave equation, the solution to (2.12) for magnetic potential A_z is given by

$$A_z(\boldsymbol{\rho}) = \mu_0 \int_s G_0(\boldsymbol{\rho}, \boldsymbol{\rho}') J_z(\boldsymbol{\rho}') ds'. \tag{2.14}$$

with

$$G_0(\boldsymbol{\rho}, \boldsymbol{\rho}') = \frac{1}{4j} H_0^{(2)}(k_0|\boldsymbol{\rho} - \boldsymbol{\rho}'|). \tag{2.15}$$

where $H_0^{(2)}(x)$ is the second kind Hankel function of zero order, and s in (2.14) denotes the cross section of the conductor. Substituting (2.14) along with (2.15) into (2.13) yields the accurate volume integral equation (VIE) to be solved for the current distribution:

$$J_z(\boldsymbol{\rho}) + \frac{\omega\mu_0\sigma}{4}\int_s J_z(\boldsymbol{\rho}')H_0^{(2)}\left(k_0|\boldsymbol{\rho}-\boldsymbol{\rho}'|\right)ds' = J_z^{\mathrm{imp}}. \tag{2.16}$$

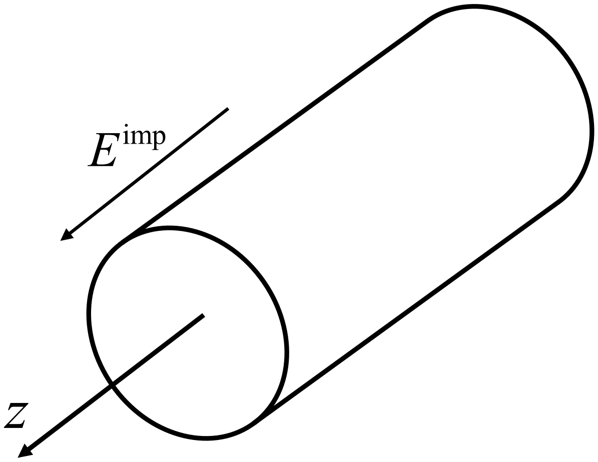

Figure 2.1 A two-dimensional conducting cylinder considering the field E^{imp} at the surface as the applied field

2.2.2 Quasi-static approximation for the VIE

The quasi-static case for a good conductor, simply ignores the displacement current so that (2.7) can be rewritten as follows [20]:

$$\frac{1}{\mu_0}\nabla\times\nabla\times\mathbf{A} = \mathbf{J} = \sigma\mathbf{E}. \tag{2.17}$$

Then the wave equation (2.12) is reduced to the Laplace's equation:

$$\nabla^2 A_z(x,y) = -\mu_0 J_z(x,y). \tag{2.18}$$

The solution to Equation (2.18) is known as:

$$A_z(\boldsymbol{\rho}) = \mu_0\int_s \tilde{G}_0(\boldsymbol{\rho},\boldsymbol{\rho}')J_z(\boldsymbol{\rho}')ds' \tag{2.19}$$

where $\tilde{G}_0$ stands for the logarithmic kernel

$$\tilde{G}_0(\boldsymbol{\rho}, \boldsymbol{\rho}') = -\frac{1}{2\pi} \ln(|\boldsymbol{\rho} - \boldsymbol{\rho}'|). \tag{2.20}$$

Therefore we obtain the VIE under the quasi-static approximation

$$J_z(\boldsymbol{\rho}) - \frac{j\omega\mu_0\sigma}{2\pi} \int_s J_z(\boldsymbol{\rho}') \ln\left(|\boldsymbol{\rho} - \boldsymbol{\rho}'|\right) ds' = J_z^{\text{imp}}. \tag{2.21}$$

The above quasi-static VIE was used for calculating current distribution in [24] and [20]. Please note that the sign is different for the second term in left hand side in [24] and [20]. The Hankel function can be replaced by leading term expansion, for small arguments

$$H_0^{(2)}(k_0R) = -j\frac{2}{\pi}\left[\ln(R) + \ln\left(\frac{\gamma k_0}{2}\right) + j\frac{\pi}{2} + \cdots\right] \tag{2.22}$$

where $R = |\boldsymbol{\rho} - \boldsymbol{\rho}'|$ and $\gamma = 1.781072418\ldots$. As the logarithmic function always applied to dimensionless quantities, we need keep at least one more term $\ln(\gamma k_0/2)$.

2.2.3 Method of moments

Numerical solution of the VIE is calculated by using the method of moments. The cross section of the conductor is divided into rectangular cells, as illustrated in Figure 2.2. The cells may be unequal in area $\Delta s_i = w_i t_i$. Since the Hankel function in (2.16) is replaced by its small arguments leading term expansion as (2.22), the integral kernel of (2.16) and (2.21) is logarithmic function and is integrated over a cell Δs_m:

$$\int_{\Delta s_m} J(x,y)dxdy \sim \int_{\Delta s_m}\int_s J(x',y') \ln\sqrt{(x-x')^2+(y-y')^2}dx'dy'dxdy + \int_{\Delta s_m} J_z^{\text{imp}} dxdy \tag{2.23}$$

when the cells are sufficiently small, the current density is considered uniform over each section and to be regarded as a constant in the integration. So, the equation (2.23) is then expressed as:

$$J(x_m,y_m)\Delta s_m \sim \sum_n J(x_n,y_n) \int_{\Delta s_m}\int_{\Delta s_n} \ln\sqrt{(x-x')^2+(y-y')^2}dx'dy'dxdy + J_z^{\text{imp}}\Delta s_m \tag{2.24}$$

The double integral in (2.24) is defined by the geometrical mean distance S_{mn} between two different cells m and n as reported in [20]:

$$\ln S_{mn} = \frac{\int_{\Delta s_m} \int_{\Delta s_n} \ln \sqrt{(x-x')^2 + (y-y')^2} dx'dy'dxdy}{\Delta s_m \Delta s_n} \tag{2.25}$$

Then equation (2.24) is further simplified as:

$$J(x_m, y_m) \sim \sum_n J(x_n, y_n) \Delta s_n \ln S_{mn} + J_z^{\text{imp}} \tag{2.26}$$

$m = 1, \ldots, N$ and $n = 1, \ldots, N$, where N is the total number of cells. From (2.26), we can obtain the final matrix form as (bold capital letters denoting the matrix variables here):

$$\mathbf{MJ} = \mathbf{J}_z^{\text{imp}} \tag{2.27}$$

We solve the matrix equation (2.27) for **J**, then we can calculate the spatial distributions of A by using the **J** solved:

$$A(x, y) = \frac{\mu_0}{2\pi} \sum_n J(x_n, y_n) \int_{\Delta s_n} \ln \sqrt{(x-x')^2 + (y-y')^2} dx'dy' \tag{2.28}$$

The $A(x, y)$ will be used in calculating the internal impedance by using the definition of Z_{PI}, which will be introduce in the following sections. The exact expression for $\ln S_{mn}$ is given by [20]:

$$\ln S_{mn} = -\frac{25}{12} + \frac{1}{2w_m w_n t_m t_n} \sum_{i=1}^{4} \sum_{j=1}^{4} (-1)^{i+j} f(q_i, r_j) \tag{2.29a}$$

$$f(q, r) = \left(\frac{q^2 r^2}{4} - \frac{q^4}{24} - \frac{r^4}{24} \right) \ln(q^2 + r^2) + \frac{q^3 r}{3} \tan^{-1}\left(\frac{r}{q}\right) + \frac{q r^3}{3} \tan^{-1}\left(\frac{q}{r}\right) \tag{2.29b}$$

where, with reference to Figure 2.2

$$\begin{aligned} q_1 &= l - \frac{w_m}{2} - \frac{w_n}{2} \\ q_2 &= l + \frac{w_m}{2} - \frac{w_n}{2} \\ q_3 &= l + \frac{w_m}{2} + \frac{w_n}{2} \\ q_4 &= l - \frac{w_m}{2} + \frac{w_n}{2} \end{aligned} \tag{2.29c}$$

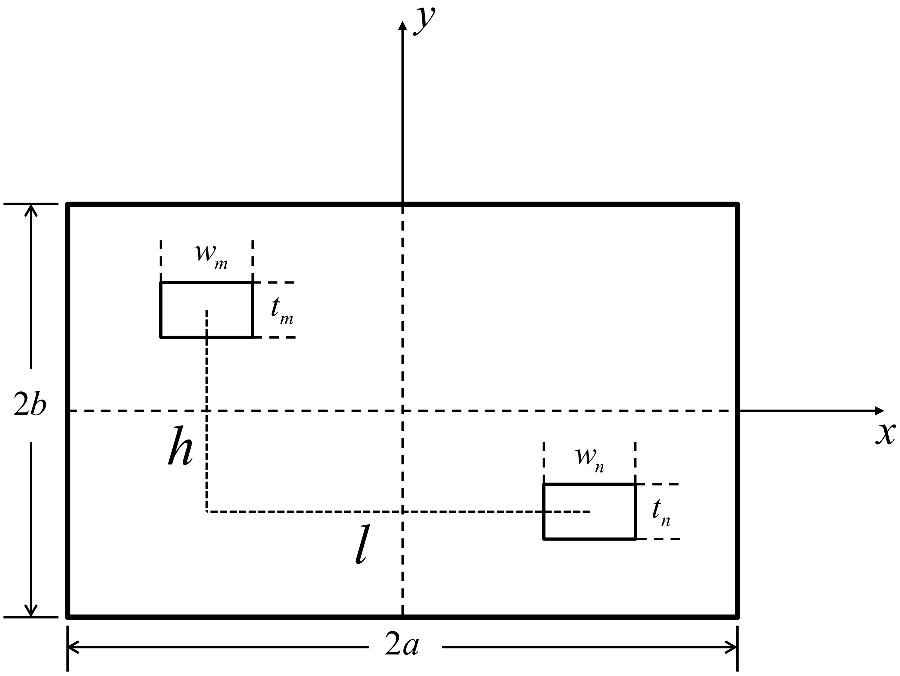

Figure 2.2 Schematic for discretization of rectangular cross-section and geometric mean distance evaluation.

and

$$
\begin{aligned}
r_1 &= h - \frac{t_m}{2} - \frac{t_n}{2} \\
r_2 &= h + \frac{t_m}{2} - \frac{t_n}{2} \\
r_3 &= h + \frac{t_m}{2} + \frac{t_n}{2} \\
r_4 &= h - \frac{t_m}{2} + \frac{t_n}{2}
\end{aligned} \tag{2.29d}
$$

For the case that $w_m = w_n = w$ and $t_m = t_n = t$, (2.29c) and (2.29d) become

$$\begin{aligned} q_1 &= l - w \\ q_2 &= l = q_4 \\ q_3 &= l + w \\ r_1 &= h - t \\ r_2 &= h = r_4 \\ r_3 &= h + t \end{aligned} \tag{2.30}$$

For square cells $w = t$, $\ln S_{mn} = \ln(0.44705w) = \ln(w) - 0.805$, as first proposed by Silvester [24].

2.3 Surface Integral Equation (SIE) of the Current Distribution

2.3.1 EFIEs for lossy dielectric cylinders

Let's consider a homogeneous conducting dielectric cylinder with an arbitrary cross section characterized by permittivity ε, permeability μ, and conductivity σ in the x-y plane surrounded by free space, illuminated by a transverse magnetic wave (TM-wave). The surface equivalent sources J_z and M_t are defined on the surface contour Γ. By considering the equivalent exterior and interior problem, the coupled EFIEs are used and specialized to the TM polarization to produce [26]

$$M_t(t) + jk_0\eta_0 A_z^{(0)} + \left(\frac{\partial F_y^{(0)}}{\partial x} - \frac{\partial F_x^{(0)}}{\partial y} \right)_{\Gamma^+} = E_z^{inc}(t) \tag{2.31}$$

$$-M_t(t) + jk_d\eta_d A_z^{(d)} + \left(\frac{\partial F_y^{(d)}}{\partial x} - \frac{\partial F_x^{(d)}}{\partial y} \right)_{\Gamma^-} = 0 \tag{2.32}$$

where

$$A_z^{(i)} = \int J_z(t') \frac{1}{4j} H_0^{(2)}(k_i R) dt' \tag{2.33}$$

$$\mathbf{F}_t^{(i)} = \int \hat{t}(t')M_t(t')\frac{1}{4j}H_0^{(2)}(k_iR)dt' \tag{2.34}$$

$$R = \sqrt{[x(t) - x(t')]^2 + [y(t) - y(t')]^2} \tag{2.35}$$

$\hat{t}$ is the unit vector tangent to the cylinder contour, and t is a parametric variable describing the cylinder surface. The Equation (2.31) is evaluated at an infinitesimal distance outside the surface contour (Γ^+), while Equation (2.32) is evaluated at an infinitesimal distance inside the surface contour (Γ^-).

The wavenumber of the free space and the conducting region are k_0 and k_d respectively; the intrinsic impedance of the free space and the conducting region are η_0 and η_d, respectively. k_d and η_d are given as $k_d = -j\sqrt{j\omega\mu(\sigma + j\omega\varepsilon)}$ and $\eta_d = \sqrt{j\omega\mu/(j\omega\varepsilon + \sigma)}$. MoM is used to solve the unknown J_z and M_t [26, 48]. We used pulse basis function and point matching method by discretizing the cylinder contour into flat strips. Once the surface equivalent sources J_z and M_t are calculated, we can use them to calculate the electric field everywhere inside the conducting cylinder [27]. Therefore, we have the following equation:

$$E(x, y) = \frac{k_d\eta_d}{4}\oint_\Gamma H_0^{(2)}(k_dR)J_zdt' + \frac{k_dj}{4}\oint_\Gamma \left(\frac{\Delta x}{R}\cos\phi + \frac{\Delta y}{R}\sin\phi\right) H_1^{(2)}(k_dR)M_tdt' \tag{2.36}$$

where Γ is the contour of the cylinder, $\Delta x = x(t) - x(t')$, and $\Delta y = y(t) - y(t')$; ϕ is the polar angle defining the outward normal vector.

2.3.2 Method of moments

The cylinder model is discretized into flat strips. We use pulse basis and delta testing functions to solve this problem, which means that the pulse basis functions are used to represent the unknowns J_z and M_t, and Equations (2.31) and (2.32) are tested in the center of each cell in the model. By using the method of moments, we obtain a matrix equation having a 2×2 block structure:

$$\begin{bmatrix} \mathbf{A} & \mathbf{B} \\ \mathbf{C} & \mathbf{D} \end{bmatrix} \begin{bmatrix} \mathbf{j} \\ \mathbf{k} \end{bmatrix} = \begin{bmatrix} \mathbf{E} \\ 0 \end{bmatrix} \tag{2.37}$$

where each entry in matrix equation (2.37) is an $N \times N$ matrix, whose off-diagonal elements are

$$A_{mn} = \frac{k_0 \eta_0}{4} \int_{\text{cell } n} H_0^{(2)}(k_0 R) dt' \tag{2.38}$$

$$B_{mn} = \frac{k_0}{4j} \int_{\text{cell } n} \left(\cos\phi_n \frac{\Delta x}{R_m} + \sin\phi_n \frac{\Delta y}{R_m} \right) H_1^{(2)}(k_0 R_m) dt' \tag{2.39}$$

$$C_{mn} = \frac{k_d \eta_d}{4} \int_{\text{cell } n} H_0^{(2)}(k_d R) dt' \tag{2.40}$$

$$D_{mn} = \frac{k_d}{4j} \int_{\text{cell } n} \left(\cos\phi_n \frac{\Delta x}{R_m} + \sin\phi_n \frac{\Delta y}{R_m} \right) H_1^{(2)}(k_d R_m) dt' \tag{2.41}$$

where

$$\Delta x = x_m - x(t') \tag{2.42}$$

$$\Delta y = y_m - y(t') \tag{2.43}$$

$$R_m = \sqrt{(\Delta x)^2 + (\Delta y)^2} \tag{2.44}$$

and ϕ_n is the polar angle defining the outward normal vector to the n^{th} strip in the model, as shown in Figure 2.3.

The diagonal matrix elements in matrix **A** cannot be approximated by using Equations (2.38) because the Hankel function is singular (infinite) if the source and observation cells are overlapped ($m = n$). We should use the leading term extraction technique to deal with this situation. For small arguments, the Hankel function can be expanded as a power series [49]

$$H_0^2(x) \approx \left(1 - \frac{x^2}{4}\right) - j\left\{\frac{2}{\pi}\ln\left(\frac{\gamma x}{2}\right) + \left[\frac{1}{2\pi} - \frac{1}{2\pi}\ln\left(\frac{\gamma x}{2}\right)\right]x^2\right\} + \cdots \tag{2.45}$$

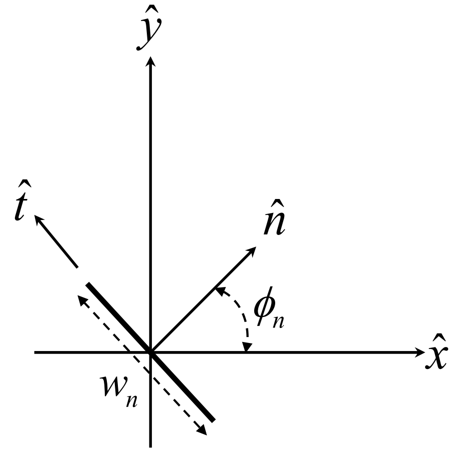

Figure 2.3 Schematic of a source cell with normal and tangent vectors

where

$$\gamma = 1.781072418\ldots \tag{2.46}$$

Since every cell is small enough to be considered flat, the first two leading terms in (2.45) are retained to produce

$$\begin{aligned} \int_{\text{cell } m} H_0^{(2)}(k_0 R)dt' &\approx 2\int_0^{w_m/2}\left[1 - j\frac{2}{\pi}\ln\left(\frac{\gamma k u}{2}\right)\right]du \\ &= w_m - \frac{2j}{\pi}w_m\left[\ln\left(\frac{\gamma k w_m}{4}\right) - 1\right] \end{aligned} \tag{2.47}$$

so that

$$A_{mm} \approx \frac{k_0\eta_0 w_m}{4}\left\{1 - \frac{2j}{\pi}\left[\ln\left(\frac{\gamma k_0 w_m}{4}\right) - 1\right]\right\} \tag{2.48}$$

The diagonal matrix elements in matrix **C** can be evaluated by following the exactly same process mentioned above, so that

$$C_{mm} \approx \frac{k_d\eta_d w_m}{4}\left\{1 - \frac{2j}{\pi}\left[\ln\left(\frac{\gamma k_d w_m}{4}\right) - 1\right]\right\} \tag{2.49}$$

The diagonal matrix elements in **B** are calculated by constructing the limit because the integral of (2.39) is evaluated in surface Γ^+, which is introduced in [26].

$$B_{mm} = \lim_{x\to x_m, y\to y_m} \frac{k_0}{4j}\int_{\text{cell } m}\left(\cos\phi_n \frac{\Delta x}{R} + \sin\phi_n \frac{\Delta y}{R}\right) H_1^{(2)}(k_0 R)dt' = \frac{1}{2} \tag{2.50}$$

and same process is used to estimated D_{mm}:

$$D_{mm} = -\frac{1}{2} \tag{2.51}$$

The off-diagonal matrix elements of matrix **A**, **B**, **C** and **D** can be calculated by using a n-point Gaussian quadrature rule.

2.4 Calculation of Internal Impedance

It is important to realize, not only different current distributions can influence the p.u.l. internal impedance Z_{in}, but also different definitions of impedance may influence the final result of Z_{in}.

2.4.1 The definition of Z_{PI} and Z_{VI}

From the energy considerations, the sum of the power dissipated in each subsection is equal to the total Joule losses; the total magnetic energy stored in the subsections equals to the energy within the conducting wire. Consequently, the internal impedance Z_{in} is defined as Z_{PI}

$$|I|^2 Z_{\mathrm{PI}} = \frac{1}{\sigma}\iint_s |J|^2 ds + j\omega \iint_s \mu_0 |H|^2 ds \tag{2.52}$$

The internal resistance and inductance can be calculated according to [20]:

$$r_i = \frac{\int_s |J|^2 ds}{\sigma |I|^2} \tag{2.53}$$

$$l_i = \frac{\int_s |\nabla \times \mathbf{A}|^2 ds}{\mu_0 |I|^2}. \tag{2.54}$$

The internal impedance can also be defined as the Thevenin impedance, which is obtained as the ratio of the open-circuit voltage at the terminals to the short-circuit current through the terminals [25]. In [25], the Thevenin theorem was applied to calculate Z_{in} in a series expression by relating the voltage drop over a small section Δz to the longitudinal current through this small section. We can simply call this definition Z_{VI}:

$$Z_{\mathrm{VI}} = -\frac{\partial V/\partial z}{I_{in}} \tag{2.55}$$

I_{in} is different from the total current I. In order to use the Z_{VI} definition to calculate the internal impedance, one must get rid of the part of current that is related to the external magnetic field. The external magnetic field will vanish if and only if A_z outside the interconnect were constant or, hence, zero, because on the reference at infinity $A_z = 0$. This is the reason that why the Dirichlet boundary condition $A_z = 0$ should be applied in the PDE method to determine the current I_{in}. We can also see that by means of this boundary condition $A_z = 0$, the proximity effect is avoided.

By using Z_{VI} definition, from the PDE with Dirichlet boundary condition method, we can get the following double summation expression for internal impedance [25] and [50]:

$$Z_{in}^{-1} = \frac{16\sigma}{ab}\sum_{m=1}^{\infty}\sum_{n=1}^{\infty}\frac{\left(\frac{(m-0.5)\pi}{a}\right)^2 + \left(\frac{(n-0.5)\pi}{b}\right)^2}{\left(\frac{(m-0.5)\pi}{a}\right)^2\left(\frac{(n-0.5)\pi}{b}\right)^2\left[\left(\frac{(m-0.5)\pi}{a}\right)^2 + \left(\frac{(n-0.5)\pi}{b}\right)^2 + j\omega\mu_0\sigma\right]} \tag{2.56}$$

We want to emphasize that different definitions of internal impedance decide or desire different boundary conditions leading to different current distributions. However, we can also use the Z_{PI} definition and the current distributions calculated from the PDE with Dirichlet boundary condition method to get the internal impedance. In fact, under the constant boundary value, we can demonstrate that these two different definitions will give the same result.

2.4.2 Different definitions but same boundary conditions

Since it is infinite long in z direction and field distributions invariance with z, also considering the TMz case, we only have E_z and H_t component. From Maxwell Equations (2.1) and (2.2) along with (2.6), only ignoring the displacement current, equations (2.1), (2.2) and (2.6) become:

$$\hat{x}\frac{\partial E_z}{\partial y} - \hat{y}\frac{\partial E_z}{\partial x} = -j\omega\mu\left(\hat{x}H_x + \hat{y}H_y\right) \tag{2.57}$$

$$\frac{\partial H_y}{\partial x} - \frac{\partial H_x}{\partial y} = \sigma E_z \tag{2.58}$$

$$E_z = -\frac{\partial \phi_e}{\partial z} - j\omega A_z \tag{2.59}$$

Here, the Z_{VI} definition (2.55) can be rewritten as $Z_{\text{VI}} = -\frac{\partial\phi_e/\partial z}{I}$. In this case, the current I can be expressed as two forms: $I = \oint_c H_t dl$ and $I = \iint_s \sigma E_z ds$. From Stokes' theorem, we know that if we only consider the conducting current, we should have the same current from these two forms of current I. Then, we have:

$$Z_{\text{VI}} = \frac{E_z + j\omega A_z}{I} = \frac{\iint_s (E_z + j\omega A_z)(\sigma E_z)^* ds}{\iint_s I(\sigma E_z)^* ds} = \frac{\sigma \iint_s (E_z E_z^* + j\omega A_z E_z^*) ds}{|I|^2} \tag{2.60}$$

The equation (2.60) is further simplified as:

$$Z_{\text{VI}} = \frac{\iint_s |J_z|^2 ds}{\sigma |I|^2} + j\omega \frac{\iint_s A_z(\sigma E_z^*) ds}{|I|^2} \tag{2.61}$$

And the second part of right hand side of (2.61) can be written using $\mathbf{H} = \frac{1}{\mu}\nabla \times \mathbf{A}$:

$$\iint_s A_z(\sigma E_z^*) ds = \iint_s A_z \left(\frac{\partial H_y^*}{\partial x} - \frac{\partial H_x^*}{\partial y}\right) ds = \mu \iint_s |H_t|^2 ds - p_{res} \tag{2.62}$$

Then, (2.61) is expressed as:

$$Z_{\text{VI}} = \frac{\iint_s |J_z|^2 ds}{\sigma |I|^2} + j\omega \left(\frac{\mu \iint_s |H_t|^2 ds}{|I|^2} - \frac{p_{res}}{|I|^2}\right) \tag{2.63}$$

where

$$
\begin{aligned}
p_{res} &= -\int_0^b \left(A_z H_y^* \Big|_{x=0}^{x=a} \right) dy + \int_0^a \left(A_z H_x^* \Big|_{y=0}^{y=b} \right) dx \\
&= \frac{1}{\mu} \int_0^b \left[A_z \left(\frac{\partial A_z^*}{\partial x} \right) \Big|_{x=0}^{x=a} \right] dy + \frac{1}{\mu} \int_0^a \left[A_z \left(\frac{\partial A_z^*}{\partial y} \right) \Big|_{y=0}^{y=b} \right] dx \qquad (2.64)
\end{aligned}
$$

From Equation (2.63), we can see that the internal resistances and inductances of Z_{VI} and Z_{PI} will be the same if p_{res} is zero. Then, from Equation (2.64), we can see that p_{res} is equal to zero if A_z equal to zero at the boundary, which agrees with the homogeneous Dirichlet boundary condition. Therefore, we demonstrate that based on constant boundary value condition, the different definitions (Z_{PI} vs. Z_{VI}) will give the same internal resistance and inductance. Thus, based on the PDE with Dirichlet boundary condition method, the Z_{PI} and Z_{VI} definitions will result the same internal impedance. A numerical result also confirm this property as illustrated in Figure 2.4: The internal resistance curve of PDE-Energy is calculated by using Z_{PI} definition while the dots of PDE-Thevenin is calculated by using Z_{VI} definition. They are both use the PDE with Dirichlet boundary condition method. However, the VIE method gives different current distribution and hence show difference internal resistance curve. Latter, more numerical results are shown to demonstrate that in some specific situations the boundary conditions (hence the current distributions) play a major role in determining the internal impedance, but not the definitions.

2.5 Numerical Results

Conductors with rectangular cross sections may be the most common and important shapes due to widely used of microstrip lines. The numerical solution is obtained by using the method of moments introduced in the above sections. To accelerate the calculations, we take advantages of two symmetric planes for the rectangular shape as shown in Figure 2.5, which reduces the original problem to only a quarter. Then we can combine

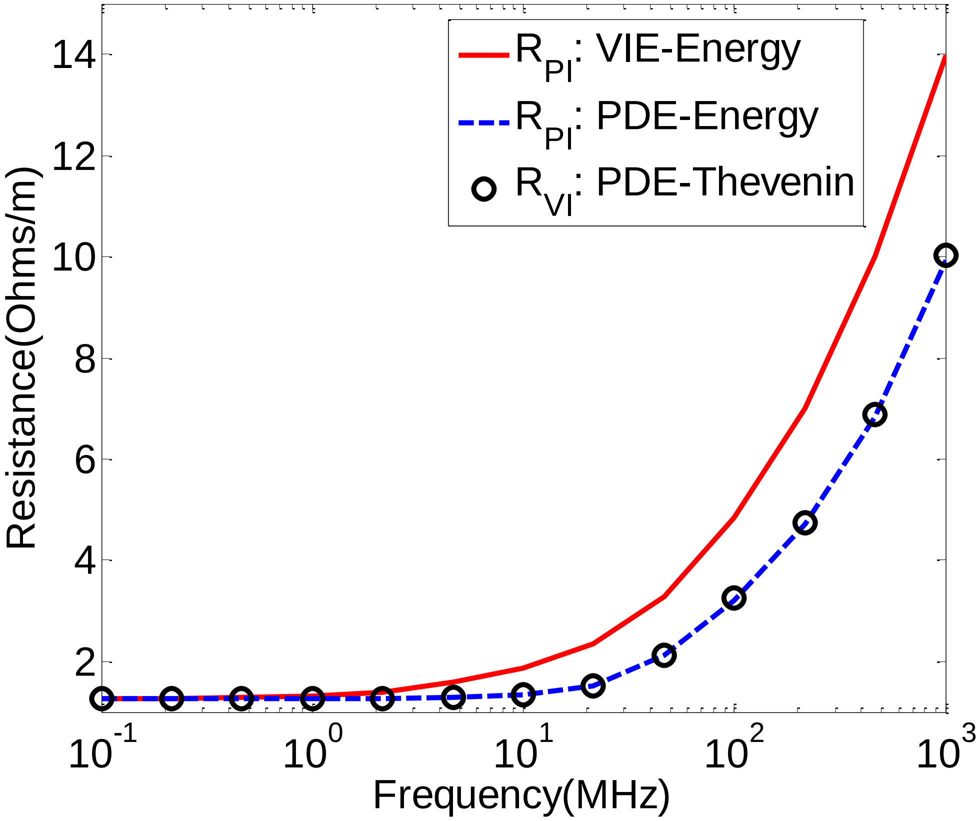

Figure 2.4 Internal resistance of a rectangular interconnect with dimensions 381 μm × 35.56 μm, $\sigma = 5.8 \times 10^7$ S/m at different frequencies.

four central-symmetric source sub-bars together as one source sub-bar.Therefore, if the original matrix has size of N, then the reduced matrix has size of $1/4\ N$. The modified program by using such kind of algorithm can significantly reduce the required memories and running time.

The structure chosen to illustrate the results is with rectangular and square cross sections, which are divided into rectangular or square sub-sections, where the current density is considered uniform over each sub-section as shown in Figure 2.2. The divided sub-sections may have different areas. The accurate VIE (2.16) and quasi-static VIE (2.21) are integrated over a sub-section, as described in the above subsections. For the VIE, there are m cells on the width, n cells on the thickness, giving a total of $m \times n$

sub-sections. The observation points for electric fields using in (2.36) are positioned just as the center points of the $m \times n$ sub-sections.

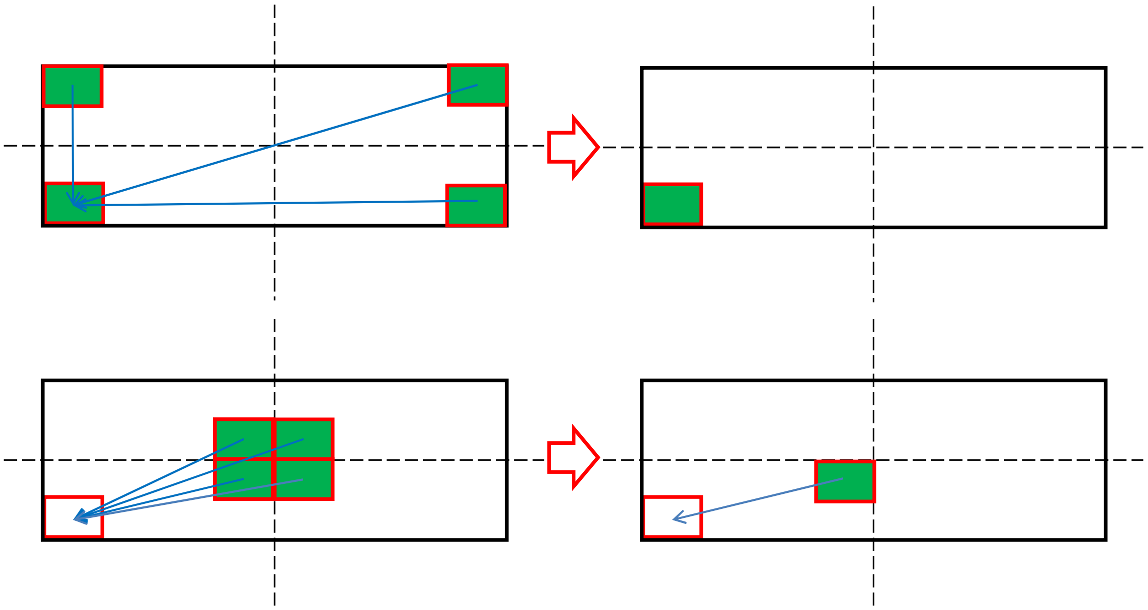

Figure 2.5 Schematic diagram of the fast algorithm for VIE-MoM matrix

2.5.1 Validation

First, we do some validations by comparing the numerical results from our methods with the results from published literature. Since we consider SIE as the accurate solution to current distribution and use the results calculated from SIE as reference to analyze the different VIEs, we must validate the results from our SIE method. Figure 2.6 shows the normalized electric current distribution along perfect electric conductor (PEC) square cylinder surface. It shows good agreement between our numerical results and the results from [51] and [52]. Figure 2.7 shows the normalized electric and magnetic current distribution along dielectric rectangular cylinder surface. We can see that except the corner singularity (point B and C), our data and reference data from [27] and [53] show very good agreements. Figure 2.8 shows several typical curves for normalized electric current distribution along PEC square cylinder surface with different dimensions ($ka = 1, 5, 10$). One should note that there are strong singularities in each corner (point B and C).

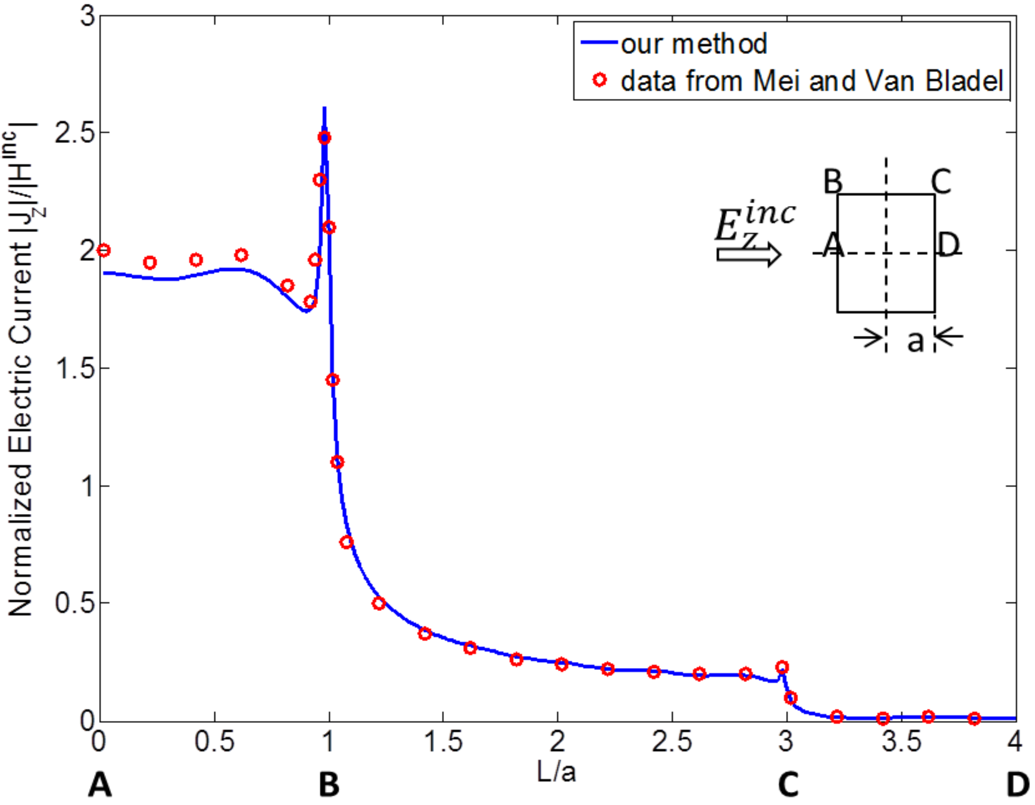

Figure 2.6 Normalized surface electric current distribution along PEC square cylinder surface with dimension $ka = 10$; the number of cells for each side is 50.

2.5.2 Current distribution from VIE, SIE and PDE

The first case is an isolated square copper interconnect wire with lengths 5 μm with a conductivity of $\sigma = 5.76 \times 10^7$ S/m, at 1 GHz (the skin depths is 2.1 μm). Figure 2.9 presents the 3-D volume current distributions calculated from accurate VIE, one-term

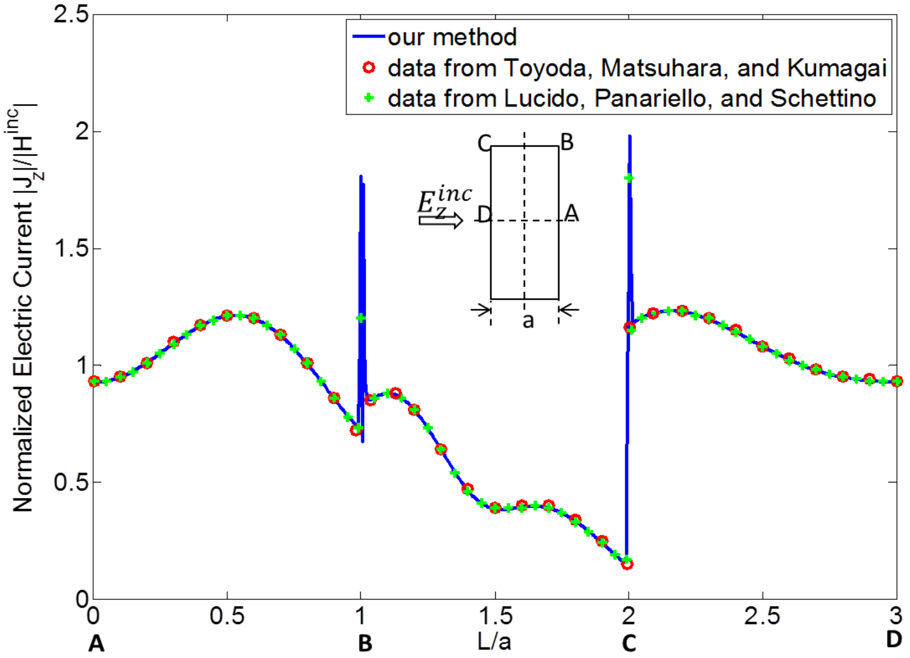

(a) Normalized electric current

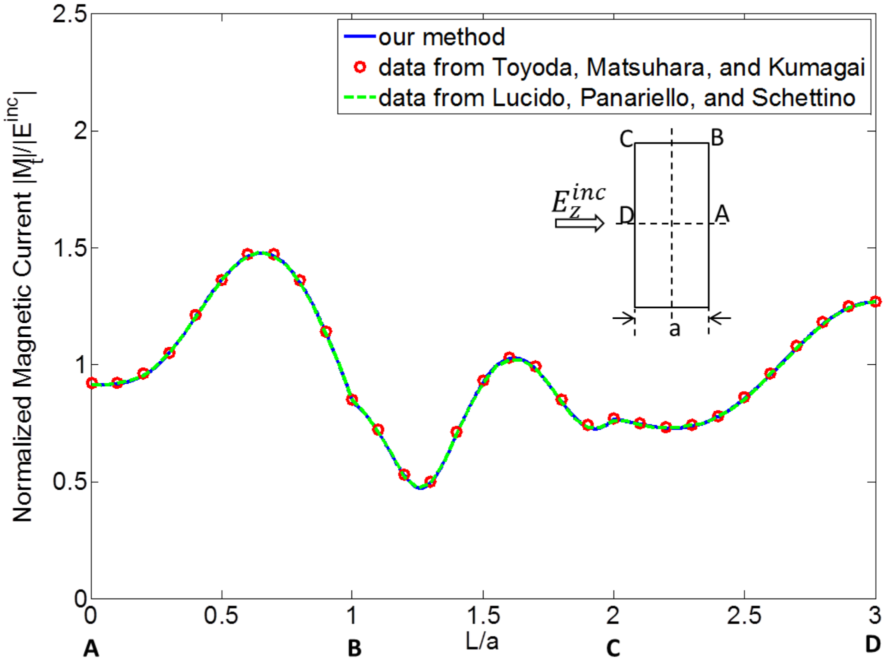

(b) Normalized magnetic current

Figure 2.7 Normalized electric and magnetic current distributions along dielectric rectangular cylinder surface with $a = 3\lambda/(1.414\pi)$, $b = 2a$, $\varepsilon_r = 2$; the number of cells is 1200 for total four sides

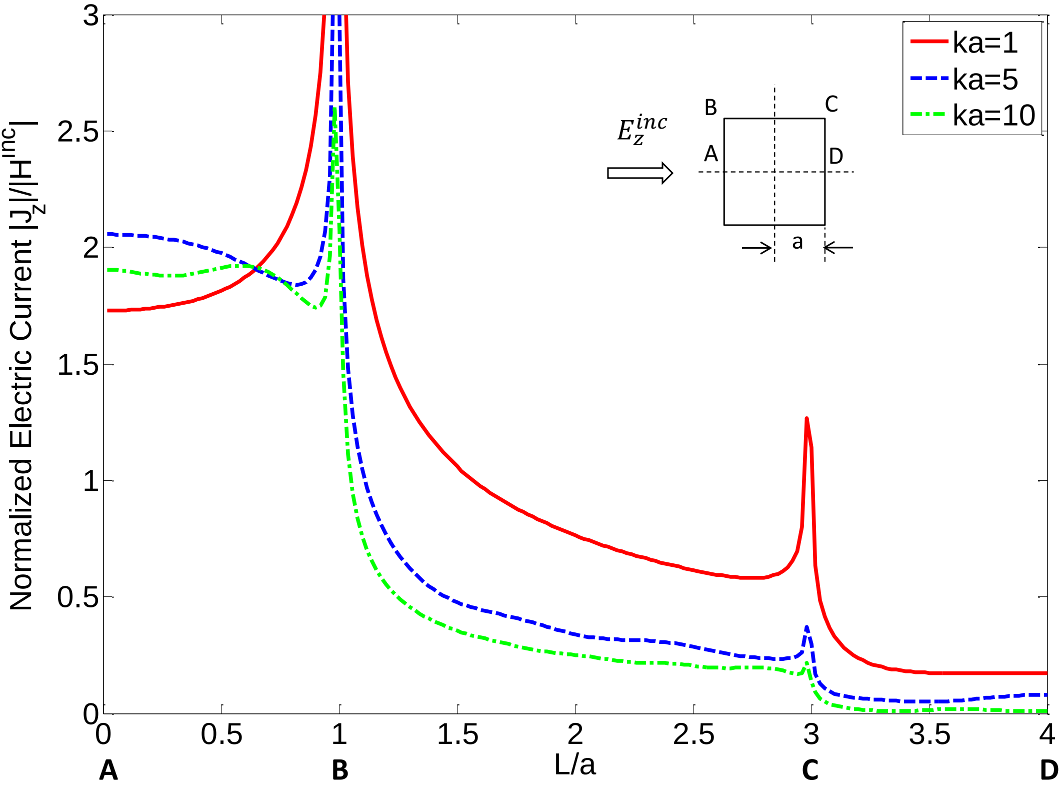

Figure 2.8 Normalized electric current distribution along PEC square cylinder surface with ka=1, 5, and 10; the number of cells is 50 for each side

added VIE, quasi-static VIE and SIE. Figure 2.9 gives us the first impression of the three-dimensional current distributions from different VIEs and SIE. The accurate VIE and SIE give nearly the same current distribution both in shape and in value. However the quasi-static VIE and one-term added VIE show similar shape but different values.

Cutting at the center of the current distributions over the square cross section, the magnitude of electric currents (normalized by σE_0), in Figure 2.10(a), is calculated by the quasi-static VIE, accurate VIE and SIE. It is more clear to see that the accurate VIE gives much better results than the quasi-static VIE, and agrees with SIEs results very well. Also note that the shape of the current distribution calculated from the quasi-static VIE are the same as that from the accurate VIE, because the major difference between two

Green's functions is a constant. Since the quasi-static VIE gives the current distribution in right shape, it still results in right resistance and internal inductance as shown in [24] and [20]. Figure 2.10(b) shows current distributions for the same square cylinder with 5 μm side length at 1 GHz, but compared the original quasi-static VIE, one term added, two terms added, and accurate VIE. It shows that if only one more leading term is added to the quasi-static VIE, the result is still not accurate enough. However, adding two more leading terms gives more accurate result, which agrees with the accurate VIE very well.

Figure 2.11 depicts the relative root-mean-square (RMS) error for the quasi-static VIE and the accurate VIE of square cylinder with different dimensions at the same frequency. As the dimension of the square cylinder reduces, δ/a increases (δ is the skin depth and a is the side length), the relative RMS error of the quasi-static VIE goes down, which means that at very low frequencies, the quasi-static VIE approaches to both the accurate VIE and SIE.

The second case is an isolated rectangular copper interconnect wire with dimensions 381 μm × 35.56 μm, $\sigma = 5.76 \times 10^7$ S/m, at 100 MHz. Figure 2.12 presents the quarterly 3-D volume current distributions calculated from accurate VIE and PDE with Dirichlet boundary condition methods separately. The current distribution calculated using PDE is almost uniform near the boundary of the cross section, while the current distribution calculated using VIE shows the non-uniformity. This difference is due to the different boundary conditions. Although this PDE with Dirichlet boundary condition method works for the circular cross section [19], it fails to consider the nature of rectangular interconnects which should show non-constant distribution on the edge.

2.5.3 Internal impedance

Let's first look at the low frequency behavior of the internal impedance. The internal resistance and inductance of an isolated rectangular interconnect with dimensions 50 μm × 20 μm and conductivity 4.1×10^7 S/m, at low frequency (e.g., 100 kHz) are

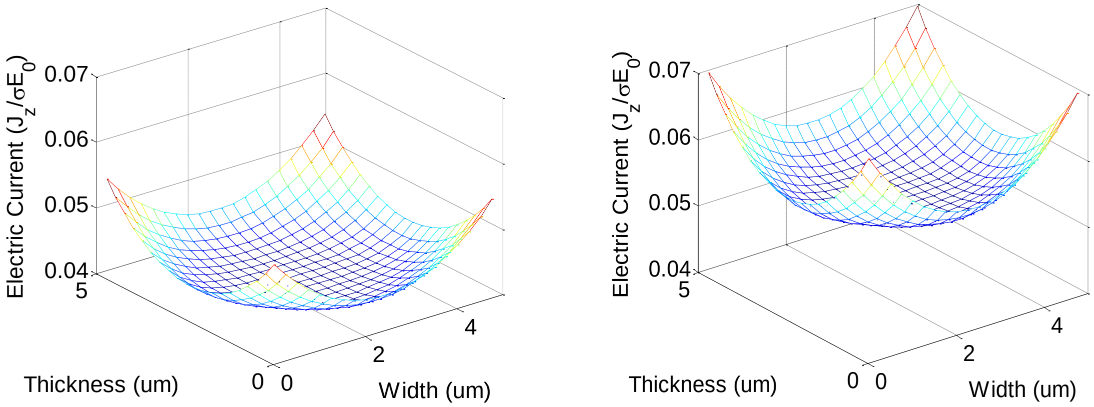

(a) Quasi-static VIE (b) One-term added VIE

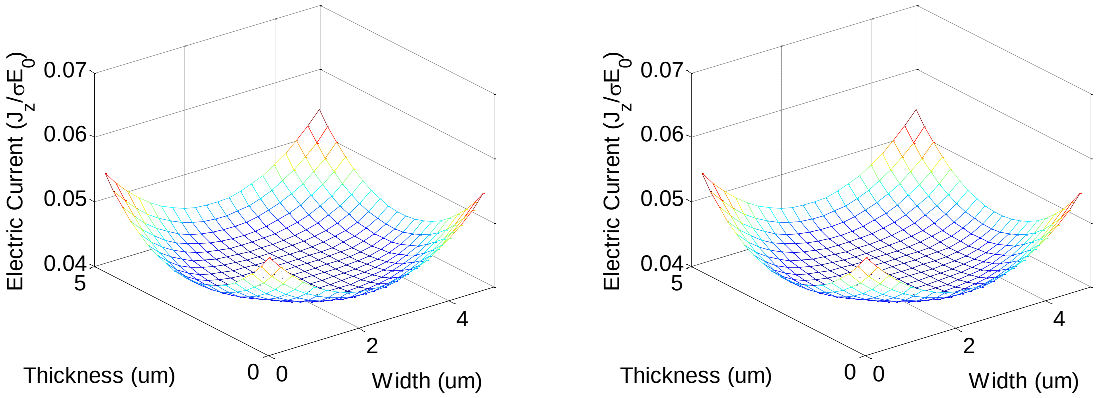

(c) Accurate VIE (d) SIE

Figure 2.9 3D current distribution of a 5 μm square interconnect with conductivity 5.76×10^7 S/m, at 1 GHz.

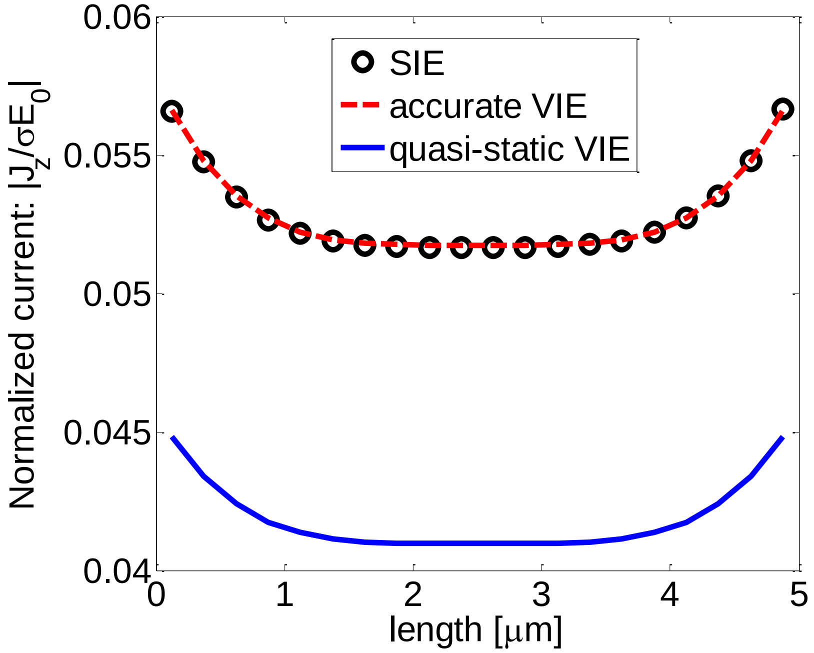

(a) SIE, accurate VIE and quasi-static VIE

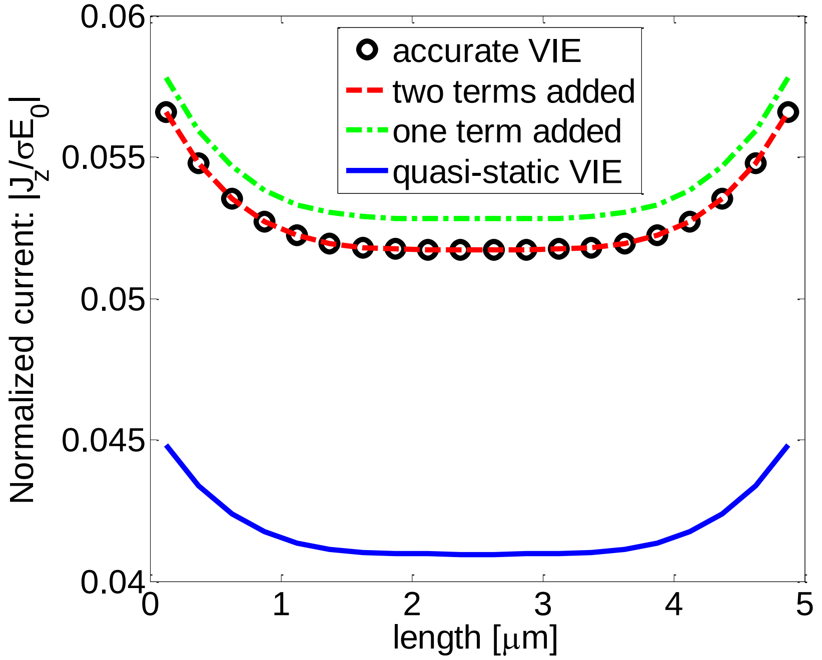

(b) Accurate, one term added, two terms added and quasi-static VIE

Figure 2.10 Center cutting current distribution of a 5 μm square interconnect with conductivity 5.76×10^7 S/m, at 1 GHz.

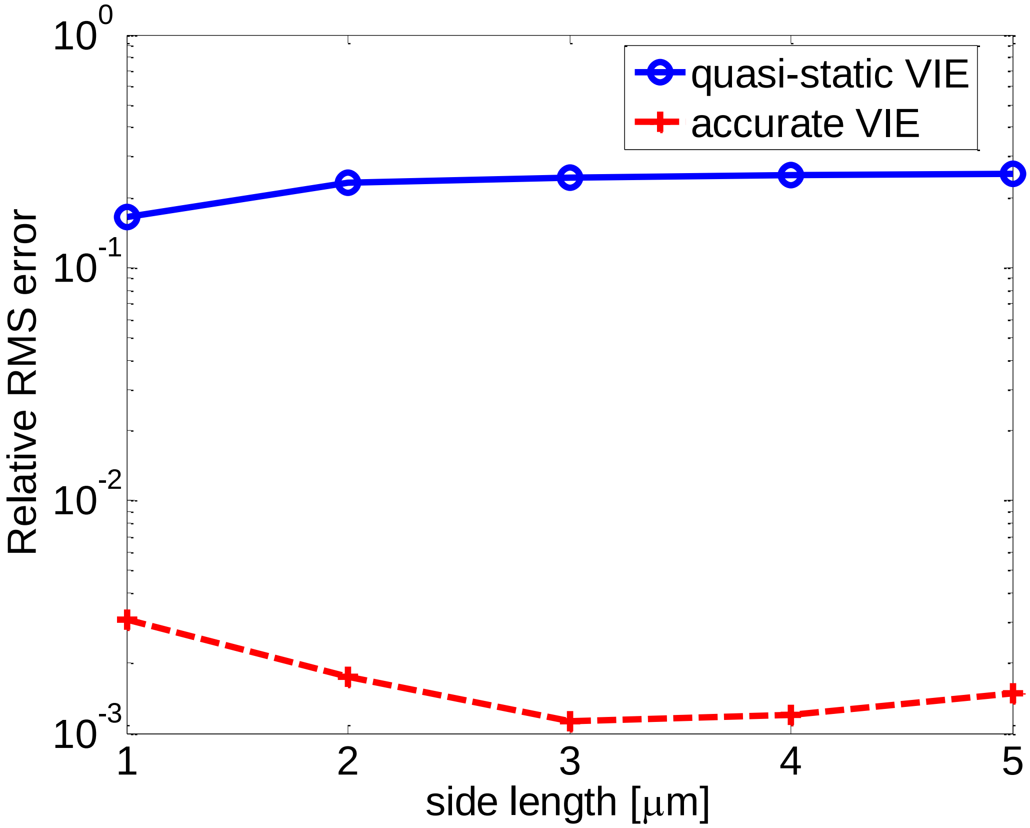

Figure 2.11 Relative RMS error of the quasi-static VIE and accurate VIE of current distribution comparing with solutions of the SIE at 1 GHz, with conductivity 5.76×10^7 S/m, the side length is from 1 μm to 5 μm.

investigated. The results from different methods are compared with DC values shown in Table 2.1 and Table 2.2. Leading term extraction was applied to series summation in PDE-Thevenin method. For the VIE method, the number of cells was 100 × 40. The DC p.u.l. internal resistance for such a rectangular interconnect is well known and given by:

$$R_{\mathrm{dc}} = \frac{1}{\sigma S} \tag{2.65}$$

At low frequencies, the current distributions calculated by VIE and PDE methods should be close. The close current distributions lead to almost the same internal resistance but different internal inductance.

From Table 2.1, it is observed that all the three methods give nearly the same resis-

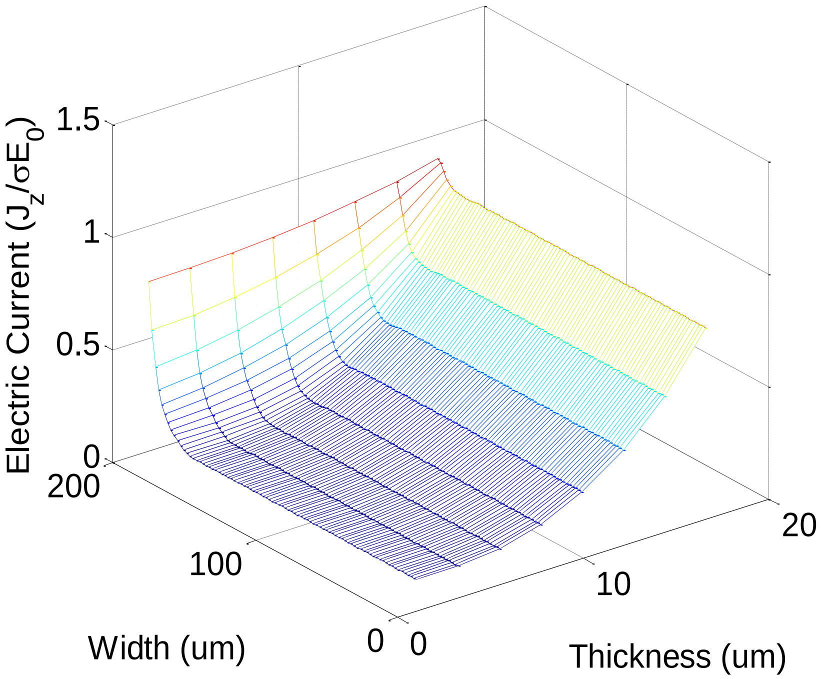

(a) PDE

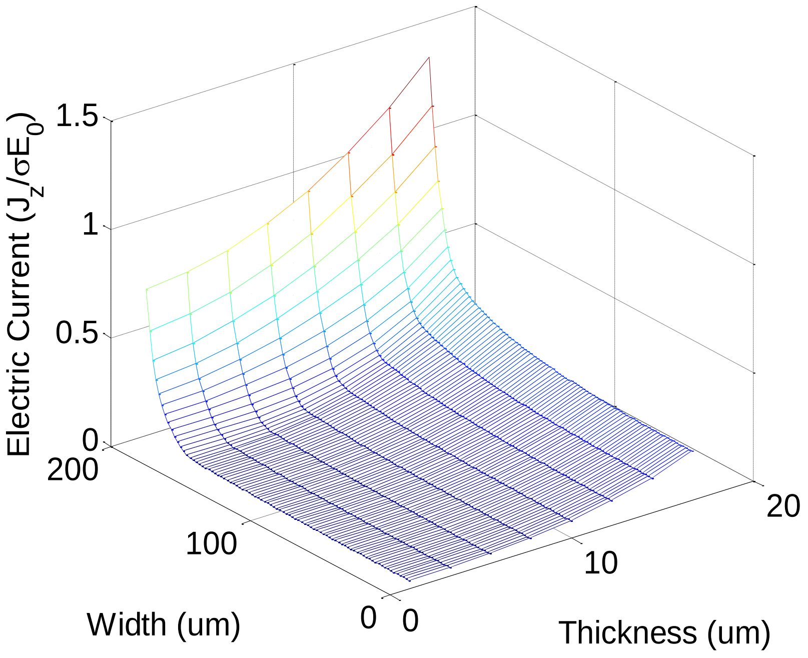

(b) Accurate, one term added, two terms added and quasi-static VIE

Figure 2.12 Quarterly current distribution of a rectangular interconnect with dimensions 381 μm × 35.56 μm, $\sigma = 5.8 \times 10^7$ S/m, at 100 MHz.

Table 2.1 Internal resistance at 100 kHz

Methods	Internal resistance (Ω/m)
VIE-Z_{PI}	24.39026
PDE-Z_{PI}	24.39025
PDE-Z_{VI}	24.39025
DC value from (2.65)	24.39024

tance value. The reason comes from two parts: one is that the difference between current distributions due to different methods almost vanishes at very low frequencies; the other one is that these two different definitions will always give the same resistance when the current distribution is calculated from PDE method with homogenous Dirichlet boundary condition. Two different DC internal inductances are listed in Table 2.2. The one from [25] used an approximate formula, which is considered not accurate enough. The one from [54] was calculated from a closed-form expression, which was obtained with a polynomial fit and considered more accurate than the former one. From Table 2.2, we can see that the different current distributions but not the definitions cause the different internal inductances. The current distribution calculated from VIE method is more accurate than that calculated from PDE method.

Table 2.2 Internal inductance at 100 kHz

Methods	Internal resistance (nH/m)
VIE-Z_{PI}	39.4229
PDE-Z_{PI}	31.3361
PDE-Z_{VI}	31.3361
DC value from [25]	31.3361
DC value from [54]	39.4177

We also calculate the frequency dependent internal resistance of the same structure from the different current distributions which are obtained by using quasi-VIE, accurate VIE, and PDE with Dirichlet boundary condition method. From Figure 2.13, we can see that the accurate VIE and quasi-VIE give the same internal resistance, because the difference between the current distributions is only the value not the shape. Also, we can see that the DC resistances of VIE method and PDE method converge to the same value, which means that when the frequency is low enough, skin effect is not dominant, the current distributions of VIE and PDE are close. The main reason for the difference between VIE and PDE methods shown in relative high frequency is the different current distributions over the cross section, hence the different boundary conditions (constant vs. non-constant). By using PDE method, the internal resistance becomes rapidly increasing when the smallest dimension of the block (35.56 μm) gets larger than about two skin depths (around 14 MHz as shown in Figure 2.13). The reason is that only skin effect plays a role in determining the current distribution. While by using VIE method, the calculation of the current distribution additionally consider the influence of the non-uniformity on the boundary. Therefore, the internal resistance becomes rapidly increasing as soon as the largest dimension (381 μm) of the interconnect becomes a few skin depths long, which happens at much lower frequencies than PDE method (around 1 MHz also shown in Figure 2.13).

Figure 2.14 shows the frequency dependent internal resistance of different shapes of cross sections conducting cylinders by using VIE and PDE methods. The square cross section has 40 μm side length. The two rectangular cross section cases are 20 μm × 80 μm and 10 μm × 160 μm, respectively. As we can see, all curves converge to the same DC p.u.l. internal resistance as predicted from Equation (2.65). Because the cross sections of these three cases have the same area but different shapes. The difference between these two methods (VIE and PDE) of square cross section is the smallest, while the "rect2" (10 μm × 160 μm) shows the biggest difference. The larger ratio between

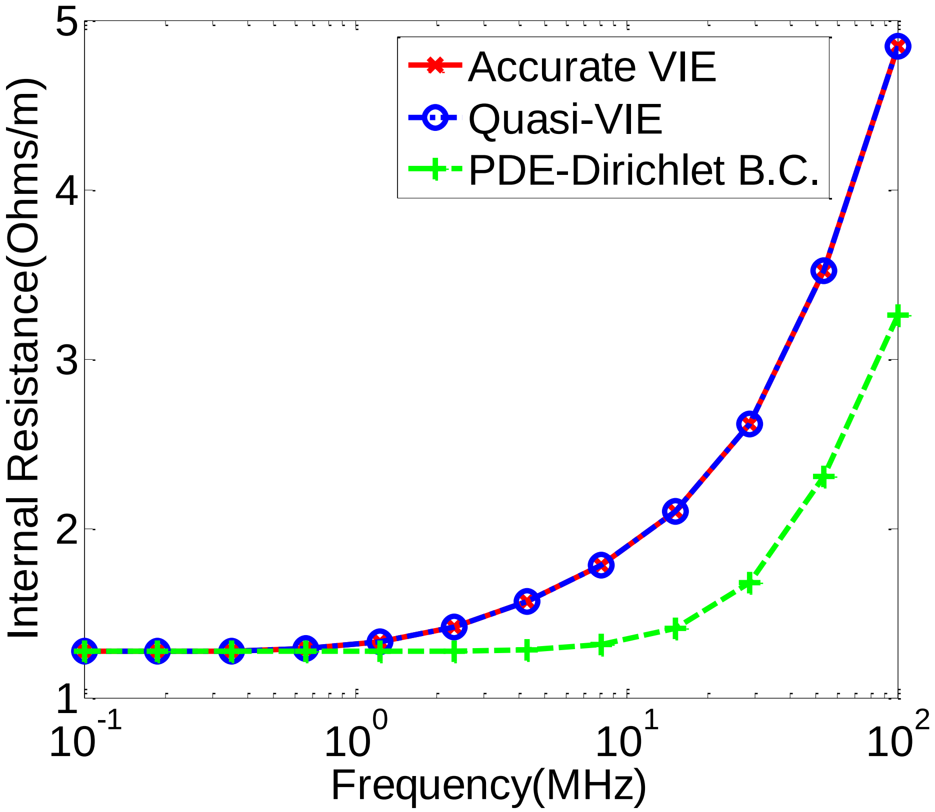

Figure 2.13 Frequency dependent internal resistance of a rectangular interconnect with dimensions 381 μm × 35.56 μm, $\sigma = 5.8 \times 10^7$ S/m), calculated from different current distributions by using different methods.

two sides of rectangular shape gives larger difference between VIE and PDE methods. For the limiting case, the VIE and PDE methods will give the same internal resistance if the cylinder has a circular cross section.

2.6 Summary

We develop a rigorous volume integral equation (VIE) without any approximation for the calculation of the current distribution over two-dimensional conducting cylinder with arbitrary cross section. We also find that there is a constant ratio between the quasi-static VIE and surface integral equation (SIE). Furthermore, we find that two

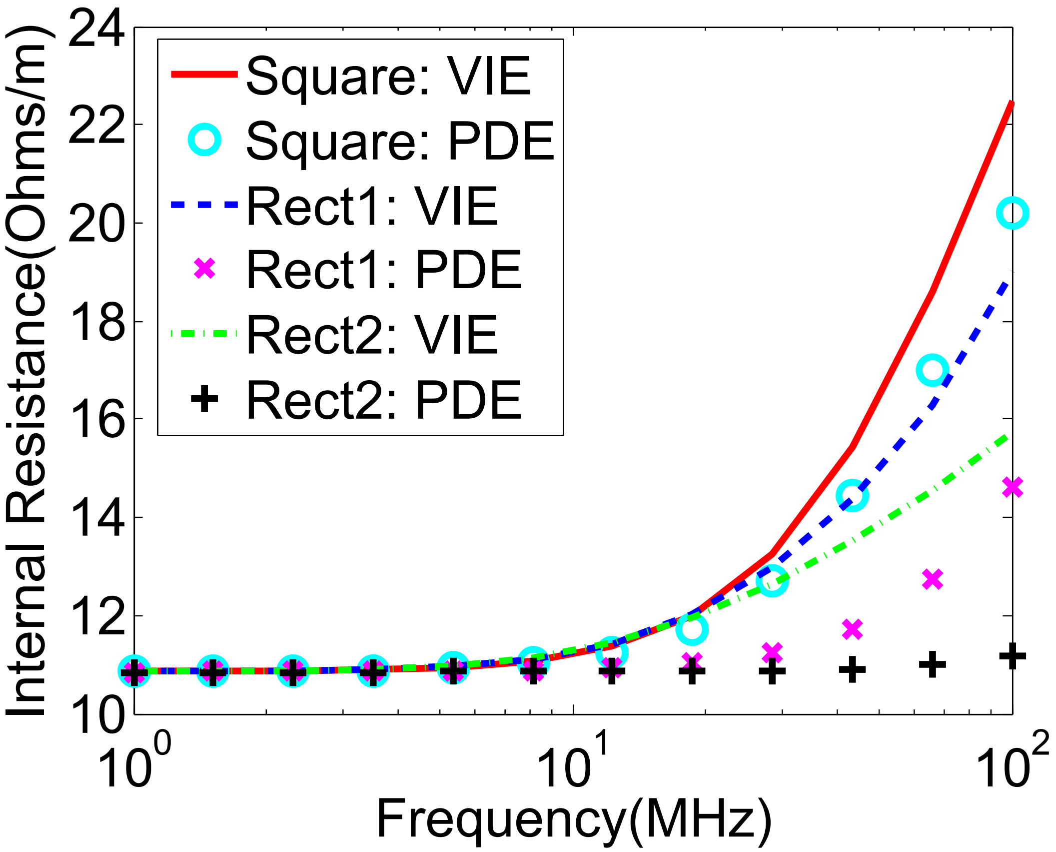

Figure 2.14 Frequency dependent internal resistance of different shapes of rectangular interconnects calculated from VIE and PDE methods.

more leading terms from the Hankel function should be added into the integral kernel to solve this problem. The current distributions calculated from different integral equations (quasi-static VIE, rigorous VIE, and SIE) are compared. The quasi-static VIE is not accurate enough for the current distribution, however this does not affect the calculation of internal impedance.

We also compare different definitions (Z_{PI} vs. Z_{VI}) and boundary conditions for calculation of the internal impedance. We demonstrate that based on constant boundary value condition, the different definitions (Z_{PI} vs. Z_{VI}) will give the same internal resistance and inductance. The main reason for the difference between VIE and partial differential equation (PDE) methods shown in relative high frequencies is the different current distributions over the cross section, hence the different boundary conditions (constant vs. non-constant). At low frequency range, the skin effect can be ignored and the current distributions of VIE and PDE are close, hence give almost the same results. Especially, the DC resistances of VIE method and PDE method converge to the same value. The larger ratio between two sides of rectangular shape gives larger difference in internal resistance by using VIE and PDE methods. As the limiting case, the VIE and PDE methods will give the same internal resistance if the cross section of the cylinder is circular.

CHAPTER 3. NOVEL ACCELERATION OF SPECTRAL DOMAIN APPROACH FOR SHIELDED MICROSTRIP LINES BY USING LEVIN'S TRANSFORMATION AND SUMMATION-BY-PARTS

A novel approach, which uses the Levin transformations or the hybrid of the Levin transformations and summation-by-parts, is presented for the acceleration of the slowly convergent series that asymptotically behave as $1/n^k$ and sinusoidal functions divided by n^k. This approach does not need the asymptotic expansion for the Green's functions and the Bessel functions, which saves the work for finding the asymptotic expansion coefficients. This approach has been applied to the acceleration of the infinite series summation in the shielded microstrip problem solved by the spectral domain approach (SDA) for obtaining accurate solutions of the propagation constant. Effective criteria of calculating the number of terms used in direct summation before applying the Levin transformations have been developed in this application. This approach can be easily extended to handle the multilayered shielded microstrip structure, which will be considered in next chapter.

3.1 Introduction

The spectral domain approach (SDA), since the outlines and notation of this specific technique were first given by [55], has been applied to various planar transmission line structures. For example, this approach can easily give very accurate results for the propagation constant (β) for shielded microstrip lines. It can lead to a very simple method, named as spectral domain immitance approach [56], for deriving the dyadic Green's functions for generalized multilayered transmission lines. It is also easy to incorporate the effect of finite thickness and conductivity by using surface integral equations [46]. However, the most significant drawback of SDA is its high computational cost due to the slow convergence of the spectral infinite summation involved in the calculation of the elements in the Galerkin matrix [31]. In order to speed up the calculation of the matrix elements, several acceleration techniques have been proposed in recent decades [31–35]. Most of them used the asymptotic techniques either in spatial domain or spectral domain, and recasted matrix elements into various rapidly convergent series. The technique in [32] recasted the kernel functions in summation into three parts: one with exponential convergence, one with $1/n^k$ fast convergence, and one with closed form weakly singular terms. The mid-point summation (MPS) technique reported in [33] and a super convergent series (SCS) approach described in [34] have been applied to obtain fast convergence for summation of the infinite series in the form of sinusoidal functions divided by n^k and in the form of $1/n^k$, after the spectral domain asymptotic extractions. Furthermore, two different fast convergent sine cosine series to accelerate the summation of the leading term after the asymptotic extraction to the Green's functions and the Bessel functions (basis functions) in the spectral domain are used in [35].

In this chapter, a new approach to speed up the SDA for computing the propagation constant for any mode of a generalized shielded microstrip is proposed. The proposed approach is versatile so that it can be used to speed up the SDA using a wide range of basis functions provided that the series asymptotically behave as sinusoidal functions divided by n^k or $1/n^k$, which is true for most cases. However, the new approach does not need to do the asymptotic approximation and leading term extractions. Instead, it uses two expansion coefficients P and Q [49] or Hankel functions to represent Bessel functions of the first kind, which are numerically solved by using two equations of Bessel functions without asymptotic approximation, and then applies an extrapolation method (the Levin transformations) [36] or the hybrid of the Levin transformations and summation-by-parts algorithm [57] to handle the infinite summations. Therefore, the new approach gets rid of the overhead of doing asymptotic expansion and leading term extraction. Some popular series transformation methods used in electromagnetic problems were introduced in [37], like the Shanks transformation [38] and Wynn's ϵ algorithm [39]. The Levin t transformation is better than the Shanks transformation, compared by Levin himself [40]. Blakemore *et al.* in [41] have found that the Levin v transformation is more efficient than Wynn's ϵ algorithm. Therefore, the Levin transformations are adopted in this work. Furthermore, in order to fully realize good convergence of the Levin transformations, the number of terms required in direct summation before applying the Levin transformations has been adaptively calculated. The new approach can obtain accurate results with relatively small number of terms. It can achieve the same accuracy as high order MPS or SCS does by using the same number of terms. In addition, it is much simpler to understand and much easier to implement, since it does not need to do the leading term extraction, which is the most laborious part of MPS and SCS. A practical application of this new approach to rapidly obtain accurate results of β for shielded microstrips using SDA has been shown.

3.2 Shielded Microstrip

Shielded microstrip transmission line is a member of the family of planar microwave transmission lines. it belongs to the most common planar transmission lines. Figure 3.1 shows a cross section of a shielded microstrip. The region 2 consists of air. The region 1 is filled by a dielectric material with relative permittivity and permeability ε_r and μ_r, respectively. This structure is uniform and infinite along the z axis. The thin metal casing and the thin metal strip are assumed to be perfect electric conductors (PECs).

The metal strip at the center is considered as zero thickness PEC. The width of the metal strip is w and that of the box is $2a$.

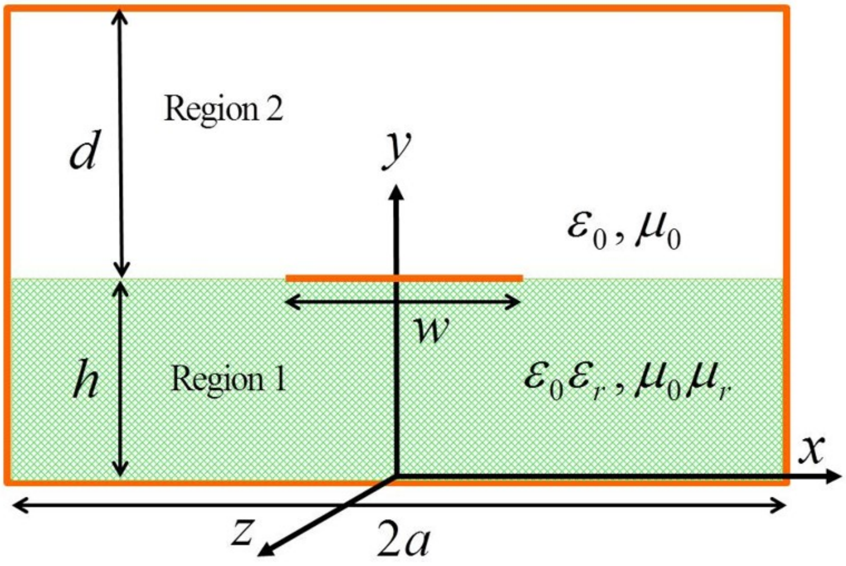

Figure 3.1 Single layer shielded interconnect with one signal strip.

3.3 Spectral Domain Approach (SDA)

It is well known that the microstrip structure cannot support pure transverse electromagnetic (TEM) waves. The solutions for microstrip lines are hybrid modes which are expressed in terms of a superposition of infinite TE^z and TM^z modes or TE^y and TM^y modes [58]. For the TE^z and TM^z modes all the field components can be expressed as two z-components of vector potentials [59]. The following derivation follows the same procedure as [29] and [60].

3.3.1 Vector potentials

The z dependency of the electric and magnetic field has the form of $e^{-j\beta z}$. The vector potential for TM^z mode is

$$A_{zi}(x, y, z) = -\frac{\omega\varepsilon_i\mu_i}{\beta}\Phi_i^{(e)}(x, y)e^{-j\beta z} \tag{3.1}$$

and the vector potential for TE^z mode is

$$F_{zi}(x,y,z) = -\frac{\omega\varepsilon_i\mu_i}{\beta}\Phi_i^{(h)}(x,y)e^{-j\beta z} \tag{3.2}$$

They satisfy homogeneous Helmholtz equation in source free region ($y \neq h$),

$$\nabla_t^2\Phi_i^{(p)}(x,y) + (k_i^2 - \beta^2)\Phi_i^{(p)}(x,y) = 0 \tag{3.3}$$

where $k_i^2 = \omega^2\varepsilon_i\mu_i$, $i = 1, 2$, and $p = e, h$.

The z-components of transverse electric (TE) and transverse magnetic (TM) modes can be written in terms of $\Phi_i^{(p)}(x,y)$ as

$$E_{zi}(x,y,z) = j\frac{k_i^2 - \beta^2}{\beta}\Phi_i^{(e)}(x,y)e^{-j\beta z} \tag{3.4}$$

$$H_{zi}(x,y,z) = j\frac{k_i^2 - \beta^2}{\beta}\Phi_i^{(h)}(x,y)e^{-j\beta z} \tag{3.5}$$

The transverse components can be written in terms of $\nabla_t\Phi_i^{(p)}(x,y)$ as

$$\mathbf{E}_{ti}(x,y,z) = \nabla_t\Phi_i^{(e)}(x,y)e^{-j\beta z} - \frac{\omega\mu_i}{\beta}\hat{z} \times \nabla_t\Phi_i^{(h)}(x,y)e^{-j\beta z} \tag{3.6}$$

$$\mathbf{H}_{ti}(x,y,z) = \nabla_t\Phi_i^{(h)}(x,y)e^{-j\beta z} + \frac{\omega\varepsilon_i}{\beta}\hat{z} \times \nabla_t\Phi_i^{(e)}(x,y)e^{-j\beta z} \tag{3.7}$$

or in their scalar form as:

$$E_{xi}(x,y) = \frac{\partial\Phi_i^{(e)}}{\partial x} + \frac{\omega\mu_i}{\beta}\frac{\partial\Phi_i^{(h)}}{\partial y} \tag{3.8}$$

$$E_{yi}(x,y) = \frac{\partial\Phi_i^{(e)}}{\partial y} - \frac{\omega\mu_i}{\beta}\frac{\partial\Phi_i^{(h)}}{\partial x} \tag{3.9}$$

$$H_{xi}(x,y) = \frac{\partial\Phi_i^{(h)}}{\partial x} - \frac{\omega\varepsilon_i}{\beta}\frac{\partial\Phi_i^{(e)}}{\partial y} \tag{3.10}$$

$$H_{yi}(x,y) = \frac{\partial\Phi_i^{(h)}}{\partial y} + \frac{\omega\varepsilon_i}{\beta}\frac{\partial\Phi_i^{(e)}}{\partial x} \tag{3.11}$$

All the fields and the potentials are defined from $x = -a$ to a and can be expanded as follows.

$$\tilde{f}(m) = \int_{-a}^{a} dx\, \tilde{f}(x)e^{j\alpha_m x} = \int_{-a}^{a} dx\, \tilde{f}(x)\left[\cos(\alpha_m x) + j\sin(\alpha_m x)\right] \tag{3.12}$$

$$f(x) = \frac{1}{2a}\sum_{m=-\infty}^{\infty}\tilde{f}(m)e^{-j\alpha_m x} = \frac{1}{2a}\sum_{m=-\infty}^{\infty}\tilde{f}(m)\left[(\cos\alpha_m x) - j\sin(\alpha_m x)\right] \tag{3.13}$$

where $\alpha_m = m\pi/a$. Using the boundary conditions and the properties of Fourier series [60] we can obtain that $m = (n - 1/2)$ for the even mode $(n = 1, 2, \ldots)$.

3.3.2 Fourier transform and general solutions

We define the Fourier series for the potentials $\Phi_i^{(e)}(x, y)$ and $\Phi_i^{(h)}(x, y)$ as follows:

$$\tilde{\Phi}_i^{(p)}(\alpha_n, y) = \int_{-a}^{a} dx\, \Phi_i^{(p)}(x, y) e^{j\alpha_n x} \tag{3.14}$$

$$\Phi_i^{(p)}(x, y) = \begin{cases} \frac{1}{a} \sum_{m=1}^{\infty} \tilde{\Phi}_i^{(p)}(\alpha_n, y) \cos(\alpha_n x) \\ -\frac{j}{a} \sum_{m=1}^{\infty} \tilde{\Phi}_i^{(p)}(\alpha_n, y) \sin(\alpha_n x) \end{cases} \tag{3.15}$$

where $i = 1, 2$, $p = e, h$ and $\alpha_n = (n - 1/2)\pi/a$.

By taking the Fourier transform of $\Phi_i^{(e)}(x, y)$ and $\Phi_i^{(h)}(x, y)$ with respect to x, the partial differential equation (3.3) can be reduced to ordinary differential equation. The wave equation (3.3) now becomes:

$$\left(\frac{d^2}{dy^2} - \gamma_i^2 \right) \tilde{\Phi}_i^{(p)}(\alpha_n, y) = 0 \tag{3.16}$$

where $\gamma_i^2 = \alpha_n^2 + \beta^2 - k_i^2$.

The general solutions of the wave equation (3.3) are of the form

$$\begin{aligned} \tilde{\Phi}_i^{(p)}(\alpha_n, y) &= A_i^{(p)}(\alpha_n) e^{\gamma_i y} + B_i^{(p)}(\alpha_n) e^{-\gamma_i y} \\ &= C_i^{(p)}(\alpha_n) \sinh(\gamma_i y) + D_i^{(p)}(\alpha_n) \cosh(\gamma_i y) \end{aligned} \tag{3.17}$$

The field components in the spectral domain can be expressed as

$$\tilde{E}_{zi}(\alpha_n, y) = j \frac{k_i^2 - \beta^2}{\beta} \tilde{\Phi}_i^{(e)}(\alpha_n, y) \tag{3.18}$$

$$\tilde{H}_{zi}(\alpha_n, y) = j \frac{k_i^2 - \beta^2}{\beta} \tilde{\Phi}_i^{(h)}(\alpha_n, y) \tag{3.19}$$

$$\tilde{E}_{xi}(\alpha_n, y) = -j\alpha_n \tilde{\Phi}_i^{(e)}(\alpha_n, y) + \frac{\omega\mu_i}{\beta} \frac{\partial}{\partial y} \tilde{\Phi}_i^{(h)}(\alpha_n, y) \tag{3.20}$$

$$\tilde{H}_{xi}(\alpha_n, y) = -j\alpha_n \tilde{\Phi}_i^{(h)}(\alpha_n, y) - \frac{\omega\varepsilon_i}{\beta} \frac{\partial}{\partial y} \tilde{\Phi}_i^{(e)}(\alpha_n, y) \tag{3.21}$$

The normal component $\tilde{E}_y$ and $\tilde{H}_y$ are not needed to solve the problem. And the factor $e^{-j\beta z}$ is dropped.

3.3.3 Boundary conditions

In order to find the unknowns in (3.17), we need to apply the boundary conditions. Considering PEC boundary conditions at $y = 0$ and $y = h + d$ we will get:

$$\begin{aligned}
E_{z1}(x,0) = 0 &\implies \tilde{E}_{z1}(\alpha_n, 0) = 0 \implies \tilde{\Phi}_1^{(e)}(\alpha_n, 0) = 0 \\
&\implies \tilde{\Phi}_1^{(e)}(\alpha_n, y) = A(\alpha_n)\sinh(\gamma_1 y) \qquad (3.22) \\
E_{z2}(x,h+d) = 0 &\implies \tilde{E}_{z2}(\alpha_n, h+d) = 0 \implies \tilde{\Phi}_2^{(e)}(\alpha_n, h+d) = 0 \\
&\implies \tilde{\Phi}_2^{(e)}(\alpha_n, y) = B(\alpha_n)\frac{\sinh[\gamma_2(h+d-y)]}{\sinh(\gamma_2 d)} \qquad (3.23) \\
E_{x1}(x,0) = 0 &\implies \tilde{E}_{x1}(\alpha_n, 0) = 0 \implies \frac{\partial}{\partial y}\tilde{\Phi}_1^{(h)}(\alpha_n, y)\bigg|_{y=0} = 0 \\
&\implies \tilde{\Phi}_1^{(h)}(\alpha_n, y) = C(\alpha_n)\cosh(\gamma_1 y) \qquad (3.24) \\
E_{x2}(x,h+d) = 0 &\implies \tilde{E}_{x2}(\alpha_n, h+d) = 0 \implies \frac{\partial}{\partial y}\tilde{\Phi}_2^{(h)}(\alpha_n, y)\bigg|_{y=h+d} = 0 \\
&\implies \tilde{\Phi}_2^{(h)}(\alpha_n, y) = D(\alpha_n)\frac{\cosh[\gamma_2(h+d-y)]}{\cosh(\gamma_2 d)} \qquad (3.25)
\end{aligned}$$

Now, we have four unknowns $A(\alpha_n)$, $B(\alpha_n)$, $C(\alpha_n)$, and $D(\alpha_n)$, so we need four more boundary conditions to solve for them. The tangential electric fields are continuous because no surface magnetic currents $\mathbf{M}_s$ occur on the interface.

$$\begin{aligned}
&\tilde{E}_{z1}(\alpha_n, h) = \tilde{E}_{z2}(\alpha_n, h) \\
&\implies \frac{k_1^2 - \beta^2}{\beta}\tilde{\Phi}_1^{(e)}(\alpha_n, h) = \frac{k_2^2 - \beta^2}{\beta}\tilde{\Phi}_2^{(e)}(\alpha_n, h) \\
&\implies (k_1^2 - \beta^2)A(\alpha_n)\sinh(\gamma_1 h) = (k_2^2 - \beta^2)B(\alpha_n) \qquad (3.26)
\end{aligned}$$

$$\begin{aligned}
&\tilde{E}_{x1}(\alpha_n, h) = \tilde{E}_{x2}(\alpha_n, h) \\
&\implies -j\alpha_n\tilde{\Phi}_1^{(e)}(\alpha_n, h) + \frac{\omega\mu_1}{\beta}\frac{\partial}{\partial y}\tilde{\Phi}_1^{(h)}(\alpha_n, y)\bigg|_{y=h} = -j\alpha_n\tilde{\Phi}_2^{(e)}(\alpha_n, h) + \frac{\omega\mu_2}{\beta}\frac{\partial}{\partial y}\tilde{\Phi}_2^{(h)}(\alpha_n, y)\bigg|_{y=h} \\
&\implies j\alpha_n[A(\alpha_n)\sinh(\gamma_1 h) - B(\alpha_n)] = \frac{\omega}{\beta}[\gamma_1\mu_1 C(\alpha_n)\sinh(\gamma_1 h) + \gamma_2\mu_2 D(\alpha_n)\tanh(\gamma_2 d)]
\end{aligned}$$

(3.27)

The boundary condition for the magnetic field is written as:

$$\hat{y} \times (\mathbf{H}_2 - \mathbf{H}_1) = \mathbf{J}_s \tag{3.28}$$

And, the surface current $\mathbf{J}_s$ has both x- and z-components:

$$\mathbf{J}_s(x, y = h, z) = \left[\hat{x} J_x(x) + \hat{z} J_z(x)\right] e^{-j\beta z} \tag{3.29}$$

In spectral domain, equation (3.28) can be written as:

$$\hat{y} \times \left[\tilde{\mathbf{H}}_2(\alpha_n, h) - \tilde{\mathbf{H}}_1(\alpha_n, h)\right] = \hat{x}\tilde{J}_x(\alpha_n) + \hat{z}\tilde{J}_z(\alpha_n) \tag{3.30}$$

$$\begin{aligned} &\tilde{H}_{z2}(\alpha_n, h) - \tilde{H}_{z1}(\alpha_n, h) = \tilde{J}_x(\alpha_n) \\ &\Longrightarrow j\frac{k_2^2 - \beta^2}{\beta} D(\alpha_n) - j\frac{k_1^2 - \beta^2}{\beta} C(\alpha_n)\cosh(\gamma_1 h) = \tilde{J}_x(\alpha_n) \end{aligned} \tag{3.31}$$

and

$$\begin{aligned} &\tilde{H}_{x2}(\alpha_n, h) - \tilde{H}_{x1}(\alpha_n, h) = -\tilde{J}_z(\alpha_n) \\ &\Longrightarrow -j\alpha_n\Big[D(\alpha_n) - C(\alpha_n)\cosh(\gamma_1 h)\Big] + \frac{\omega}{\beta}\Big[\varepsilon_1\gamma_1 A(\alpha_n)\cosh(\gamma_1 h) + \varepsilon_2\gamma_2 B(\alpha_n)\Big] = -\tilde{J}_z(\alpha_n) \end{aligned} \tag{3.32}$$

Now we have four equations (3.26), (3.27), (3.31) and (3.32) so we can solve for the four unkowns A, B, C and D.

$$\begin{aligned} \tilde{E}_{x2}(\alpha_n, h) &= -j\alpha_n\tilde{\Phi}_2^{(e)}(\alpha_n, h) + \frac{\omega\mu_2}{\beta}\frac{\partial}{\partial y}\tilde{\Phi}_2^{(h)}(\alpha_n, y)\bigg|_{y=h} \\ &= -j\alpha_n B(\alpha_n) - \frac{\omega\mu_2}{\beta}\gamma_2\tanh(\gamma_2 d) D(\alpha_n) \\ &= G_{xx}(\alpha_n, \beta)\tilde{J}_x(\alpha_n) + G_{xz}(\alpha_n, \beta)\tilde{J}_z(\alpha_n) \end{aligned}$$

$$\begin{aligned} \tilde{E}_{z2}(\alpha_n, h) &= j\frac{k_2^2 - \beta^2}{\beta}\tilde{\Phi}_2^{(e)}(\alpha_n, h) = j\frac{k_2^2 - \beta^2}{\beta} B(\alpha_n) \\ &= G_{zx}(\alpha_n, \beta)\tilde{J}_x(\alpha_n) + G_{zz}(\alpha_n, \beta)\tilde{J}_z(\alpha_n) \end{aligned}$$

where G_{xx}, G_{xz}, G_{zx}, and G_{zz} are spectral domain Green's function which is first introduced in [61].

$$G_{xx}(\alpha_n,\beta)=\frac{j\eta_2}{k_2\Delta}\Big[\mu_r\gamma_1(\alpha_n^2-k_2^2)\tanh(\gamma_1 h)+\gamma_2(\alpha_n^2-k_1^2)\tanh(\gamma_2 d)\Big] \tag{3.33}$$

$$G_{xz}(\alpha_n,\beta)=G_{zx}(\alpha_n,\beta)=\frac{j\eta_2\alpha_n\beta}{k_2\Delta}\Big[\mu_r\gamma_1\tanh(\gamma_1 h)+\gamma_2\tanh(\gamma_2 d)\Big] \tag{3.34}$$

$$G_{zz}(\alpha_n,\beta)=\frac{j\eta_2}{k_2\Delta}\Big[\mu_r\gamma_1(\beta^2-k_2^2)\tanh(\gamma_1 h)+\gamma_2(\beta^2-k_1^2)\tanh(\gamma_2 d)\Big] \tag{3.35}$$

$$\Delta=\left[\gamma_1\tanh(\gamma_1 h)+\varepsilon_r\gamma_2\tanh(\gamma_2 d)\right]\left[\gamma_1\coth(\gamma_1 h)+\mu_r\gamma_2\coth(\gamma_2 d)\right] \tag{3.36}$$

where $\varepsilon_r=\varepsilon_1/\varepsilon_2$ and $\mu_r=\mu_1/\mu_2$.

3.3.4 Method of moments

Now we have two spectral domain equations with two unknowns

$$G_{xx}(\alpha_n,\beta)\tilde{J}_x(\alpha_n)+G_{xz}(\alpha_n,\beta)\tilde{J}_z(\alpha_n)=\tilde{E}_{x2}(\alpha_n,h) \tag{3.37}$$

$$G_{zx}(\alpha_n,\beta)\tilde{J}_x(\alpha_n)+G_{zz}(\alpha_n,\beta)\tilde{J}_z(\alpha_n)=\tilde{E}_{z2}(\alpha_n,h) \tag{3.38}$$

The electric fields and currents at the interface $y=h$ are followed by PEC boundary condition:

$$E_{x1}=E_{x2}=E_{z1}=E_{z2}=\begin{cases}0 & |x|<w/2\\ \text{unknown} & |x|>w/2\end{cases}$$

There is no current outside PEC strip

$$J_x(x)=J_z(x)=\begin{cases}\text{unknown} & |x|<w/2\\ 0 & |x|>w/2\end{cases}$$

Therefore the product of the tangential field component and the surface current alway vanish on the whole $y = h$ plane:

$$E_{x2}(x)J_x(x) = 0 \tag{3.39}$$

$$E_{z2}(x)J_z(x) = 0 \tag{3.40}$$

The unknown current $\tilde{J}_x(\alpha_n)$ and $\tilde{J}_z(\alpha_n)$ are be expanded in terms of basis function $\tilde{J}_{xi}(\alpha_n)$ and $\tilde{J}_{zi}(\alpha_n)$:

$$\tilde{J}_x(\alpha_n) = \sum_{i=1}^{M_x} a_i \tilde{J}_{xi}(\alpha_n) \tag{3.41}$$

$$\tilde{J}_z(\alpha_n) = \sum_{i=1}^{M_z} b_i \tilde{J}_{zi}(\alpha_n) \tag{3.42}$$

$J_{xi}(x)$ is a real odd function, $J_{zi}(x)$ is a real even function for the dominant mode and other even modes. According to the properties of Fourier transform, $\tilde{J}_{xi}(\alpha_n)$ is a purely imaginary and odd function,$\tilde{J}_{zi}(\alpha_n)$ is a purely real and even function.

The Parseval's theorem says that

$$\sum_{n=1}^{\infty} \tilde{f}(n)\tilde{g}^*(n) = \frac{1}{2a}\int_{-a}^{a} f(x)g^*(x)dx \tag{3.43}$$

where superscript stars indicate complex conjugation. So we have

$$\sum_{n=1}^{\infty} \tilde{E}_{x2}(\alpha_n, h)\tilde{J}_{xm}(\alpha_n) = -\frac{1}{2a}\int_{-\infty}^{\infty} E_{x2}(x, h)J_{xm}(x)dx = 0 \tag{3.44}$$

$$\sum_{n=1}^{\infty} \tilde{E}_{z2}(\alpha_n, h)\tilde{J}_{zm}(\alpha_n) = \frac{1}{2a}\int_{-a}^{a} E_{z2}(x, h)J_{zm}(x)dx = 0 \tag{3.45}$$

or

$$\sum_{n=1}^{\infty} \tilde{E}_{x2}(\alpha_n, h)\tilde{J}_{xm}(\alpha_n) = 0, m = 1, 2, \ldots, M_{\mathrm{x}} \tag{3.46}$$

$$\sum_{n=1}^{\infty} \tilde{E}_{z2}(\alpha_n, h)\tilde{J}_{zm}(\alpha_n) = 0, m = 1, 2, \ldots, M_{\mathrm{z}} \tag{3.47}$$

Equations (3.46) and (3.47) can be written it in matrix form as:

$$\begin{bmatrix} K^{xx} & K^{xz} \\ K^{zx} & K^{zz} \end{bmatrix} \begin{bmatrix} A \\ B \end{bmatrix} = \begin{bmatrix} 0 \\ 0 \end{bmatrix}$$

where

$$K_{ij}^{pq} = \sum_{n=1}^{\infty} \tilde{J}_{pi}(\alpha_n) G_{pq}(\alpha_n, \beta) \tilde{J}_{qj}(\alpha_n) = \sum_{n=1}^{\infty} F_{ij}^{pq} \tag{3.48}$$

where $F_{ij}^{pq} = \tilde{J}_{pi}(\alpha_n) G_{pq}(\alpha_n, \beta) \tilde{J}_{qj}(\alpha_n), \quad p = x, z$ and $q = x, z.$ and A and B are vectors corresponding to the coefficients:

$$\begin{bmatrix} A \\ B \end{bmatrix} = \begin{bmatrix} a_1 \\ \vdots \\ a_{M_x} \\ b_1 \\ \vdots \\ b_{M_z} \end{bmatrix} \tag{3.49}$$

The determinant of the matrix should be zero for a homogeneous system to have a non trivial solution.

$$D(\beta, \omega) = \det \begin{bmatrix} K^{xx} & K^{xz} \\ K^{zx} & K^{zz} \end{bmatrix} = 0 \tag{3.50}$$

Finally, the propagation constant β, for each frequency point ω can be obtained by solving $\det[K] = 0$.

3.4 Basis Functions for Currents

There are multiple choices of current basis, which can be divided as two different kinds: entire domain and sub-domain. The most significant advantage of using entire domain basis functions is the fast convergence.

3.4.1 Basis choices

It is widely accepted that rate of convergence (here, the convergence refers to the convergence of final results, like the effective dielectric constant) may be speeded up by applying basis functions whose behaviors reflect the physical distribution of the expanded field or current. However, slow convergence may be associated with the basis set that satisfies the current singularity at the strip edge when we calculate a single element of the whole matrix, because its Fourier transform contains Bessel functions.

It is true that some simple assumption of purely longitudinal current distribution that does not take care of the singularity will also give acceptable accuracy, as in [55] and [62]. But one drawback is that the accuracy is not high (only about 2 significant digits), while choosing the current basis functions satisfying the edge condition can easily lead to very high accuracy (like 12 significant digits in [32]). In [63], the author states,"Instead, designers must make do with approximate results, for example, [62], which are achieved under the assumption of a uniform purely longitudinal current distribution and the accuracy of which can only be estimated. Therefore, it is one of the goals of this paper to demonstrate how the frequency dependent properties of single and coupled microstrip lines can be calculated rigorously, accurately and with further reduced computer time and storage requirements". In this chapter, we want to show that an accurate description of the current or field near the edge is necessary to evaluate frequency dependent parameters such as the characteristic impedance, and computations can be carried out very efficiently if the basis function satisfy the edge condition.

The other thing is that the good accuracy of uniform current distribution or even higher order approximation is dependent on frequency and constructive parameters (w/h, w/a, and ε_r) [64]. In [62], the author states, "The inaccuracy of the quasi-static results at high frequencies is evident", and "the numerical results presented here have been shown to be in agreement with those of other investigators at low frequencies. Considerable departure from the quasi-static results has been shown to occur with increasing frequency".

Above all, explicit satisfaction of the edge condition might not be necessary if we only need roughly accurate results and limited to certain cases (frequency and constructive parameters like w/h, w/a, and ε_r). By choosing basis functions satisfying the appropriate edge conditions, rate of convergence of final results will be speeded up, the matrix size will be significantly reduced, and the overall computing time will be saved. The only deficiency that may be associated with the use of basis functions that satisfies the current singularity at the strip edge is that the Fourier transforms of its elements contain Bessel functions which converge slowly and could be a disadvantage from the series summation point of view.

3.4.2 Chebyshev polynomials

The basis functions for electric currents on the metal strip are chosen such that $J_{xi}(x)$ is a real odd function and $J_{zi}(x)$ is a real even function for the dominant mode and other even modes. From the properties of Fourier transforms, $\tilde{J}_{xi}(\alpha_n)$ is a purely imaginary and odd function, $\tilde{J}_{zi}(\alpha_n)$ is a purely real and even function. The Fourier transform for the Chebyshev polynomial along with the weighting function to take care of the edge singularity for the longitudinal current and the zero at the edges for the transverse current is the Bessel's function.

The even mode $J_z(x)$ is an even function, therefore it should be expanded by using the even order Chebyshev polynomials of the first kind including a term to incorporate the edge singularities [59].

$$J_z(x) = \sum_{n=1}^{M_z} I_{zn} \frac{T_{2n-2}(2x/w)}{\sqrt{1-(2x/w)^2}} \tag{3.51}$$

where $T_{2n}(u)$ satisfies recursive relation [65]

$$\begin{aligned} T_0(u) &= 1 \\ T_1(u) &= u \\ T_2(u) &= 2u^2 - 1 \\ T_n(u) &= 2uT_{n-1}(u) - T_{n-2}(u) \end{aligned} \tag{3.52}$$

The transverse current J_x is proportional to ω, so as frequency decreases it will become very small compared to J_z, so J_x is normalized with $k_0 w$ [66]. $J_x(x)$ is an odd function so it is expanded by using odd order Chebyshev polynomials of the second kind including a term to make sure that it vanishes at the edges.

$$J_x(x) = j\sqrt{1-(2x/w)^2}\sum_{n=1}^{M_{\mathrm{x}}} I_{xn}U_{2n-1}(2x/w) \tag{3.53}$$

where U_{2n-1} satisfies

$$\begin{aligned} U_0(u) &= 1 \\ U_1(u) &= 2u \\ U_2(u) &= 4u^2-1 \\ U_n(u) &= 2uU_{n-1}(u) - U_{n-2}(u) \end{aligned} \tag{3.54}$$

The Fourier transforms of the unknown current $\tilde{J}_x(\alpha_n)$ and $\tilde{J}_z(\alpha_n)$ are expanded in terms of basis functions $\tilde{J}_{xi}$ and $\tilde{J}_{zi}$:

$$\tilde{J}_x(\alpha_n) = \sum_{i=1}^{M_{\mathrm{x}}} a_i\tilde{J}_{xi}(\alpha_n)k_0 w \tag{3.55}$$

$$\tilde{J}_z(\alpha_n) = \sum_{i=1}^{M_{\mathrm{z}}} b_i\tilde{J}_{zi}(\alpha_n) \tag{3.56}$$

The Fourier transforms of the basis functions are reported in [29]:

$$\tilde{J}_x(\alpha_n) = \frac{w\pi}{\delta_n}\sum_{i=1}^{M_{\mathrm{x}}} I_{xi}i(-1)^i J_{2i}(\delta_n)k_0 w \tag{3.57}$$

$$\tilde{J}_z(\alpha_n) = \frac{w\pi}{2}\sum_{i=1}^{M_{\mathrm{z}}} I_{z(i-1)}(-1)^{i-1}J_{2(i-1)}(\delta_n) \tag{3.58}$$

where $J_n(z)$ is the Bessel function of the first kind and $\delta_n = \alpha_n w/2$.

3.5 Leading Term Extraction

3.5.1 Asymptotic approximation to Green's functions

As $\alpha_n \to \infty$, we keep the first two terms in Taylor expansion:

$$\gamma_1 = \sqrt{\alpha_n^2 + \beta^2 - k_1^2} \approx \alpha_n + \frac{\beta^2 - k_1^2}{2\alpha_n} \tag{3.59}$$

$$\gamma_2 = \sqrt{\alpha_n^2 + \beta^2 - k_2^2} \approx \alpha_n + \frac{\beta^2 - k_2^2}{2\alpha_n} \tag{3.60}$$

$$\begin{aligned}\tilde{\Delta} &\approx (\varepsilon_r\gamma_2 + \gamma_1)(\mu_r\gamma_2 + \gamma_1) = \varepsilon_r\mu_r\gamma_2^2 + (\varepsilon_r + \mu_r)\gamma_1\gamma_2 + \gamma_1^2 \\ &\approx \alpha_n^2(1+\varepsilon_r)(1+\mu_r) \\ &+ \frac{1}{2}(1+\varepsilon_r)\Big[(\beta^2 - k_1^2) + \mu_r(\beta^2 - k_2^2)\Big] + \frac{1}{2}(1+\mu_r)\Big[(\beta^2 - k_1^2) + \varepsilon_r(\beta^2 - k_2^2)\Big]\end{aligned} \tag{3.61}$$

Then, the Green's functions are approximated as:

$$G_{xx} \approx G_{xx0}\alpha_n w \left(1 - y_{xx}^2/\alpha_n^2\right) \tag{3.62}$$

$$G_{xz} \approx G_{xz0} \left(1 - y_{xz}^2/\alpha_n^2\right) \tag{3.63}$$

$$G_{zz} \approx \frac{G_{zz0}}{\alpha_n w} \left(1 - y_{zz}^2/\alpha_n^2\right) \tag{3.64}$$

where the expressions for the constants G_{xx0}, G_{xz0}, G_{zz0}, y_{xx}^2, y_{xz}^2, and y_{zz}^2 are given in [65]:

$$G_{xx0} = \frac{1}{1+\varepsilon_r} \tag{3.65}$$

$$G_{xz0} = \frac{\beta}{(1+\varepsilon_r)k_0} \tag{3.66}$$

$$G_{zz0} = \frac{(\beta^2 - k_1^2) + \mu_r(\beta^2 - k_2^2)}{k_0^2(1+\varepsilon_r)(1+\mu_r)} \tag{3.67}$$

$$y_{xx}^2 = \frac{\beta^2}{2} + \frac{\varepsilon_r k_1^2 + k_2^2}{2(1+\varepsilon_r)} \tag{3.68}$$

$$y_{xz}^2 = \frac{\beta^2}{2} + \frac{(k_2^2 - k_1^2)(1-\mu_r)}{2(1+\mu_r)} - \frac{\varepsilon_r k_2^2 + k_1^2}{2(1+\varepsilon_r)} \tag{3.69}$$

$$y_{zz}^2 = \beta^2 - k_2^2 + \frac{1}{2}\Big[\Big(\frac{k_2^2 - k_1^2}{1+\mu_r} + \frac{k_2^2 - k_1^2}{1+\varepsilon_r}\Big) - \frac{(\beta^2 - k_1^2)(\beta^2 - k_2^2)(1+\mu_r)}{(\beta^2 - k_1^2) + \mu_r(\beta^2 - k_2^2)}\Big] \tag{3.70}$$

3.5.2 Asymptotic expansion for the Bessel function

The series for the Bessel functions are given by [49]:

$$J_v(z) = \sqrt{\frac{2}{\pi z}}\left[P(v,z)\cos\chi - Q(v,z)\sin\chi\right] \tag{3.71}$$

$$Y_v(z) = \sqrt{\frac{2}{\pi z}}\left[P(v,z)\sin\chi + Q(v,z)\cos\chi\right] \tag{3.72}$$

where

$$P(v,z) = 1 - \frac{(\mu-1)(\mu-9)}{2!(8z)^2} + \cdots$$

$$Q(v,z) = \frac{\mu-1}{8z} - \frac{(\mu-1)(\mu-9)(\mu-25)}{3!(8z)^3} + \cdots$$

$$\chi = z - \left(\frac{1}{2}v + \frac{1}{4}\right)\pi$$

and with $\mu = 4v^2$. By using the asymptotic forms of the Green's functions and the Bessel function for large α_n, we can obtain the leading term of F_{ij}^{pq}, involving terms in the form of sinusoidal functions divided by α_n^k (n^k) and terms in the form of $1/\alpha_n^k$ $(1/n^k)$, which can be evaluated by using midpoint summation method (MPS) [33] or super convergent series (SCS) method [34].

3.6 The Extrapolation Methods and Summation-by-parts

The most popular extrapolation methods used in electromagnetic problems are Shanks and Levin's transformations. So, we briefly introduce them and compare them with emphasis on which one is suitable for the acceleration of SDA for shielded microstrip lines.

The infinite summation to be evaluated is presented as follows:

$$S = \sum_{i=1}^{\infty} u_i \tag{3.73}$$

and the partial sum is:

$$S_n = \sum_{i=1}^{n} u_i \tag{3.74}$$

3.6.1 The Shanks and Levin's transformations

The Shanks transformation belongs to non-linear series acceleration methods. The ε-algorithm, developed by Wynn [39], is a recursive algorithm for the Shanks transformation and is the most convenient way to compute the Shanks transformation:

$$\varepsilon_{k+1}^{(n)} = \varepsilon_{k-1}^{(n+1)} + \frac{1}{\varepsilon_k^{(n+1)} - \varepsilon_k^{(n)}} \tag{3.75}$$

$$\varepsilon_{-1}^{(n)} = 0, \quad \varepsilon_0^{(n)} = S_n \tag{3.76}$$

where n and k are the indices for the terms and the order of the transformation respectively $(n, k = 0, 1, 2, \ldots)$. Note that only the even order transformations are used, while the odd order ones are intermediate values. Namely, if $S_0, \ldots, S_{2k}$ are known, $\varepsilon_{2k}^{(0)}$ is the best approximation of S, while if $S_0, \ldots, S_{2k+1}$ are know, $\varepsilon_{2k}^{(1)}$ should be used.

The generalized Levin's transformation is introduced in [36,40], and is most efficiently computed by the W algorithm of Sidi [67,68], which is also a recursive formula:

$$L_k(S_n) = \frac{S_n/\omega_n}{\delta^k(1/\omega_n)} \tag{3.77}$$

$$\delta^{k+1}(u_n) = \frac{\delta^k(u_{n+1}) - \delta^k(u_n)}{(n+k+1)^{-1} - n^{-1}}, \quad \delta^0(u_n) = u_n \tag{3.78}$$

where $n, k = 0, 1, 2, \ldots$. Therefore, if $S_0, \ldots, S_k$ are known, $L_k(S_0)$ is the best approximation of S. Different choices of numerical remainder estimates ω_n lead to different versions of Levin transformations: if $\omega_n = u_n$, the t transformation is obtained; if $\omega_n = nu_n$, one will get the u transformation; and $\omega_n = u_n u_{n+1}/(u_n - u_{n+1})$ will lead to the v transformation.

An explicit representation of the generalized Levin transformation is reported as [69]:

$$S_n^{(k)} = \frac{\sum\limits_{m=0}^{k} \frac{S_{n+m}}{\omega_{n+m}} \pi_n^{(k,m)}}{\sum\limits_{m=0}^{k} \frac{1}{\omega_{n+m}} \pi_n^{(k,m)}} \tag{3.79}$$

where:

$$\pi_n^{(k,m)} = \prod_{\substack{r=0 \\ r\neq m}}^{k} \frac{1}{x_{n+r} - x_{n+m}}, \quad S_n^{(0)} = S_n \tag{3.80}$$

$x_n = 1/(n+1)$, and k being the order of extrapolation. Theoretically, if $S_n, S_{n+1}, \ldots, S_{n+k}$ are known, $S_n^{(k)}$ is the best approximation of S. But due to machine accuracy limit, the extrapolation order cannot be too high. And, different choices of remainder estimates ω_n will give different versions of the Levin transformations [40]. For example, the t transformation is obtained if $\omega_n = u_n$, the u transformation is characterized by $\omega_n = nu_n$, and $\omega_n = u_n u_{n+1}/(u_n - u_{n+1})$ will lead to the v transformation.

It has been found that the direct application of the conventional Levin transformations to Fourier series (sinusoidal functions) is not appropriate [70, 71]. A simple way to overcome this issue is to apply the accelerators to complex Fourier series and then take real and imaginary parts of the results [71]. Therefore, we can apply the Euler's formula and have the following transform:

$$\sum_{n=1}^{\infty} \frac{\sin(nx)}{n^k} = \Im\left(\sum_{n=1}^{\infty} \frac{e^{jnx}}{n^k}\right) \tag{3.81}$$

$$\sum_{n=1}^{\infty} \frac{\cos(nx)}{n^k} = \Re\left(\sum_{n=1}^{\infty} \frac{e^{jnx}}{n^k}\right) \tag{3.82}$$

where x is real. Then, instead of applying the Levin transformations directly to the series on the left hand sides of (3.81) and (3.82), we can apply the Levin transformations

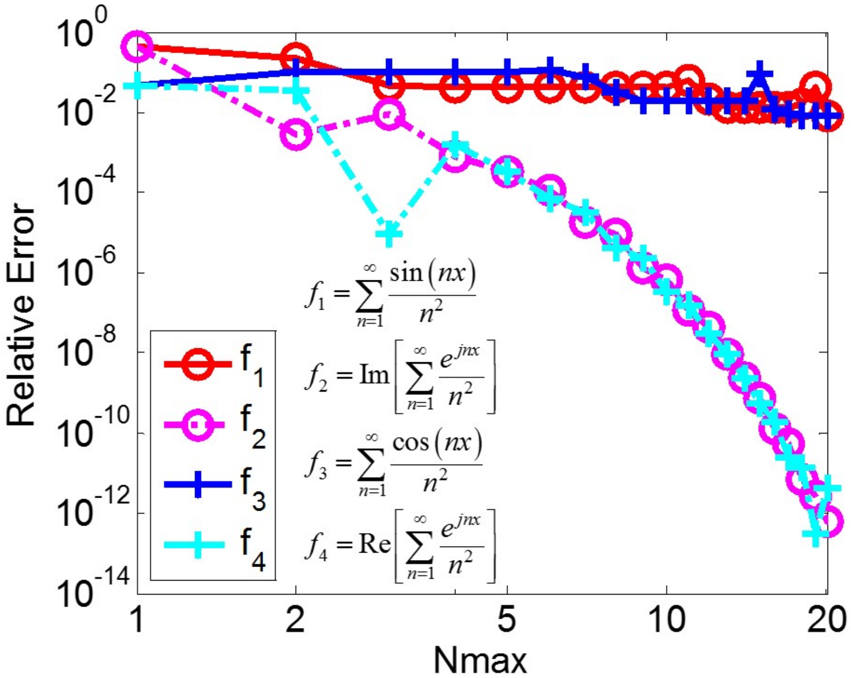

Figure 3.2 Comparison of the sinusoidal and exponential functions in the Levin v transformation.

to the series with exponential form first, and then take the imaginary or real part to get the final results. The advantage of this strategy is illustrated by Figure 3.2 to evaluate $\sum_{n=1}^{\infty}\sin(nx)/n^2$ and $\sum_{n=1}^{\infty}\cos(nx)/n^2$, for $x = 1/2$. The v transformation is adopted here, and other choices mentioned above will show similar behavior. The reference value is calculated by using the Riemann Zeta function [72].

Figure 3.2 shows that directly using sine or cosine function in the Levin v transformation fails to give accurate results, but using exponential function and taking the real or imaginary part after using the Levin v transformation exhibits very good performance. The reason can be heuristically explained by observing (3.79): No matter what kind of the Levin transformations, the remainder estimates ω serves as a denominator, and exponential form with its constant amplitude will have less singular behaviors than the sinusoidal form. Furthermore, a modified Levin transformation reported in [73] can be successfully used to accelerate the Fourier series.

The asymptotic performance of the slowly convergent series in SDA is in the form of sinusoidal functions divided by n^k or in the form of $1/n^k$, which are alternating series and monotonic series, respectively.

For the purpose of comparison between the Shanks and Levin's transformations, the results, relative error versus the number of terms used, obtained from different extrapolation methods are given in Figure 3.3. The reference values are calculated by using Riemann Zeta functions [72]. It is observed that the Shanks transformation and all three versions of Levin transformations work well for alternating series, like sinusoidal functions divided by n^k. However, only the Levin u and v transforms work well for both alternating and monotonic series, and these two transforms perform similarly. Therefore, we only implement the Levin v transformation to accelerate the series in SDA to calculate the β of a shielded microstrip line.

3.6.2 Summation-by-parts

The summation-by-parts algorithm is reported in [57]. The key idea is that to find the efficient evaluation of the infinite remainder R_N:

$$R_N = \sum_{n=N}^{\infty} \tilde{G}_n f_n \tag{3.83}$$

where $\tilde{G}_n$ represents the spectral domain Green's function, which is a slow varying function, and f_n which is a highly oscillatory (sinusoidal in our problem) function. The key point for us to change the form of R_N is that we want the partial sums of f_n have closed formulas in R_N. And we obtain the summation-by-parts form of R_N as:

$$R_N = \sum_{n=N}^{\infty} \tilde{G}_n^{(0)} f_n^{(0)} = \sum_{i=1}^{\infty} \tilde{G}_N^{(1-i)} f_{N-1}^{(+i)} \tag{3.84}$$

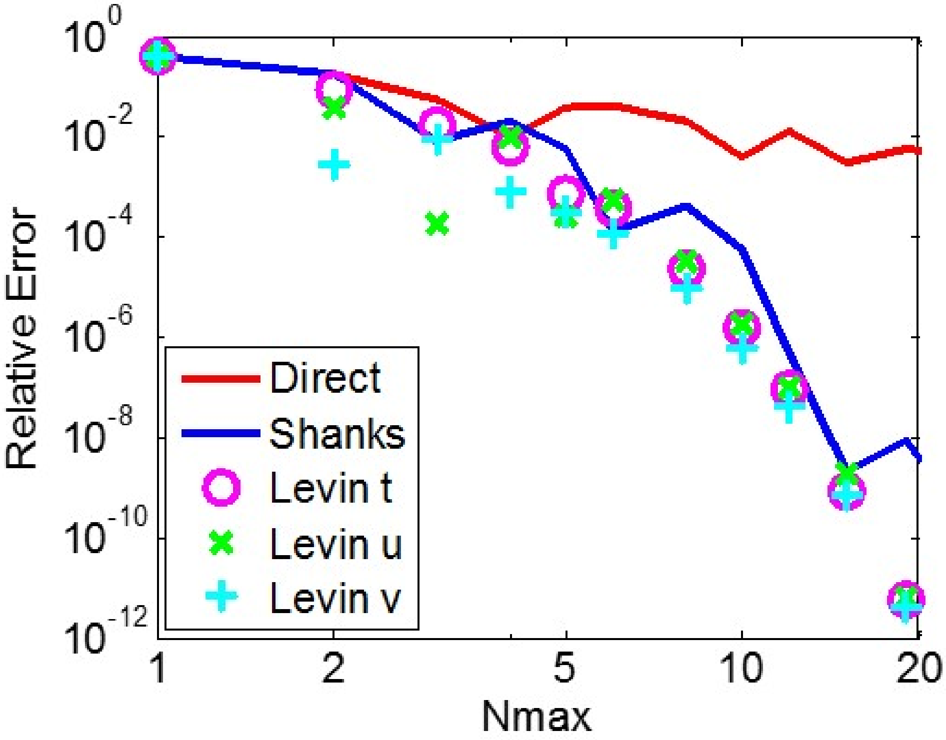

(a) $\sum_{n=1}^{\infty} \frac{\sin(nx)}{n^2}$

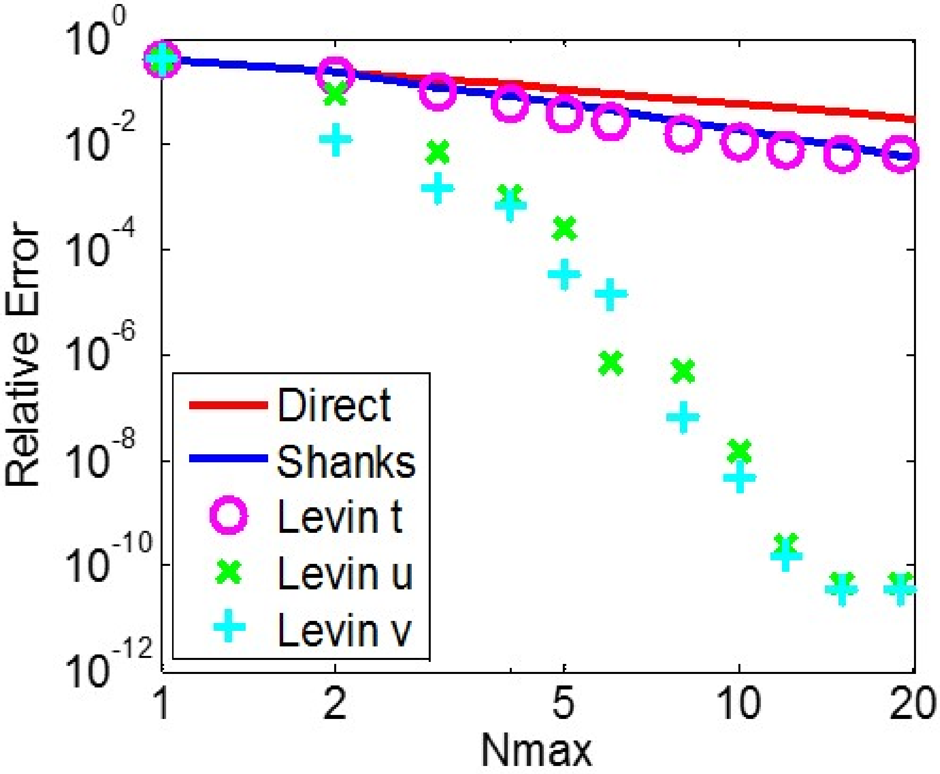

(b) $\sum_{n=1}^{\infty} \frac{1}{n^2}$

Figure 3.3 Relative error for the infinite summation for two different kinds of convergent series.

where the successive sums of f_n and differences of $\tilde{G}_n$ is in the following form [57]:

$$\begin{aligned} \tilde{G}_n^{(0)} &= \tilde{G}_n \\ \tilde{G}_n^{(-i)} &= \tilde{G}_{n+1}^{(1-i)} - \tilde{G}_n^{(1-i)} \end{aligned} \tag{3.85}$$

$$\begin{aligned} f_n^{(0)} &= f_n \\ f_n^{(+i)} &= \sum_{k=n+1}^{\infty} f_k^{(i-1)} \end{aligned} \tag{3.86}$$

In general case, $f_n = e^{j(nz+\alpha)}$, the series $f_n^{(+i)}$ can be easily evaluated analytically, thus obtaining:

$$f_n^{(+i)} = \sum_{k=n+1}^{\infty} f_k^{(i-1)} = \frac{e^{j[nz+\alpha+i(\pi+z)/2]}}{2^i\left[\sin(z/2)\right]^i} \tag{3.87}$$

For special cases, $f_n = \cos(nz+\alpha)$ or $f_n = \sin(nz+\alpha)$, $f_n^{(+i)}$ can be obtained by using Euler's formula:

$$f_n^{(+i)} = \frac{\cos\left[nz+\alpha+i(\pi+z)/2\right]}{2^i\left[\sin(z/2)\right]^i} \tag{3.88}$$

$$f_n^{(+i)} = \frac{\sin\left[nz+\alpha+i(\pi+z)/2\right]}{2^i\left[\sin(z/2)\right]^i} \tag{3.89}$$

Also, the author in [57] mentioned that the summation-by-parts algorithm is less efficient for very small values of z since (3.87) starts to show a divergence behavior, as indicated by the sine function in the denominator.

3.7 New Acceleration Approach without Asymptotic Approximation

In order to use midpoint summation method or super convergent series method, efforts has to be paid to do high order leading term extraction and errors are introduced due to the asymptotic approximation after the truncation. However, after we separate the series into two parts: one part asymptotically behaves as sinusoidal function divided by n^k and the other asymptotically behaves as $1/n^k$; we can apply the Levin transformations or summation-by-parts to evaluate them.

3.7.1 Summation kernel recasting

We cannot simply apply the Levin's transformation to the F_{ij}^{pq} in (3.48), since F_{ij}^{pq} contains two different types of convergent series. We need to separate them and recast the summation kernel into a suitable form to be applied in the Levin's transformation.

We have known that the P and Q in (3.71) and (3.72) are in the form of large argument asymptotic expansions; however, if we treat P and Q as two unknowns and (3.71) and (3.72) as two equations, P and Q are solved as the following:

$$P(v,z) = \sqrt{\frac{\pi z}{2}}\big[J_v(z)\cos\chi + Y_v(z)\sin\chi\big] \tag{3.90}$$

$$Q(v,z) = \sqrt{\frac{\pi z}{2}}\big[-J_v(z)\sin\chi + Y_v(z)\cos\chi\big] \tag{3.91}$$

Then, without any asymptotic approximation of the Green's functions and Bessel functions, F_{ij}^{pq} in (3.48) can be expressed as PQ representation:

$$F_{ij}^{pq}(\alpha_n)(-1)^{i+j} = \frac{2G_{pq}}{\pi\delta_n(\alpha_n w)^{\delta_{px}}(\alpha_n w)^{\delta_{qx}}}\left(T_1^{pq} + T_2^{pq} + T_3^{pq}\right) \tag{3.92}$$

where

$$T_1^{pq} = P(v_{pi},\delta_n)P(v_{qj},\delta_n) + Q(v_{pi},\delta_n)Q(v_{qj},\delta_n)$$

$$T_2^{pq} = \big[P(v_{qj},\delta_n)Q(v_{pi},\delta_n) + P(v_{pi},\delta_n)Q(v_{qj},\delta_n)\big]\cos(n\phi+\theta)$$

$$T_3^{pq} = \big[P(v_{pi},\delta_n)P(v_{qj},\delta_n) - Q(v_{pi},\delta_n)Q(v_{qj},\delta_n)\big]\sin(n\phi+\theta)$$

$$v_{pi} = 2(i-\delta_{pz}), \quad v_{qj} = 2(j-\delta_{qz}).$$

$$\delta_{pq} = \begin{cases} 1, & p = q \\ 0, & p \neq q \end{cases}$$

with $\phi = \pi w/a$ and $\theta = -\phi/2$.

Similarly, we can represent the Bessel functions of the first kind using Hankel functions without any approximation as:

$$J_v(z) = \frac{H_v^{(1)}(z) + H_v^{(2)}(z)}{2} \tag{3.93}$$

Then, F_{ij}^{pq} can be written as Hankel representation:

$$F_{ij}^{pq}(\alpha_n)(-1)^{i+j} = \frac{G_{pq}}{4(\alpha_n w)^{\delta_{px}}(\alpha_n w)^{\delta_{qx}}}\left(T_1^h + T_2^h + T_3^h\right) \tag{3.94}$$

where

$$T_1^h = H_{v_{pi}}^{(1)}(\delta_n)H_{v_{qj}}^{(2)}(\delta_n) + H_{v_{qj}}^{(1)}(\delta_n)H_{v_{pi}}^{(2)}(\delta_n)$$

$$T_2^h = H_{v_{pi}}^{(1)}(\delta_n)H_{v_{qj}}^{(1)}(\delta_n)$$

$$T_3^h = H_{v_{pi}}^{(2)}(\delta_n)H_{v_{qj}}^{(2)}(\delta_n)$$

The series that arise from (3.92) and (3.94) have either of the forms $\sum\limits_{n=1}^{\infty} a_n$, or Fourier series $\sum\limits_{n=1}^{\infty} [a_n \cos(n\phi) + b_n \sin(n\phi)]$, where $a_n \sim 1/n^k$ and $b_n \sim 1/n^k$ for $n \to \infty$. The part in the form of $\sum\limits_{n=1}^{\infty} a_n$ can be evaluated by using the Levin transformations, and the part in the form of $\sum\limits_{n=1}^{\infty} [a_n \cos(n\phi) + b_n \sin(n\phi)]$ can be evaluated by using the Levin transformations or summation-by-parts. For a nonsymmetrical structure, the only difference in the formula is that the Fourier transforms of the basis functions will contain $\sin(\alpha_n c)$ or $\cos(\alpha_n c)$, in which c represent the distance from the center of the metal strip to the vertical axis. By using Euler's formula, one can convert sine and cosine functions to exponential functions, and then follows the similar procedures to apply the Levin transformations.

The Figure 3.4 shows that applying the Levin's transformation to the original summation kernal F_{ij}^{pq} (denoted as ${K_{ZZ}}^1$ in Figure 3.4) will fail. We must recast the summation kernal to the suitable form (like Hankel representation, which is denoted as ${K_{ZZ}}^2$ in Figure 3.4) in order to be successfully applied in the Levin's transformation.

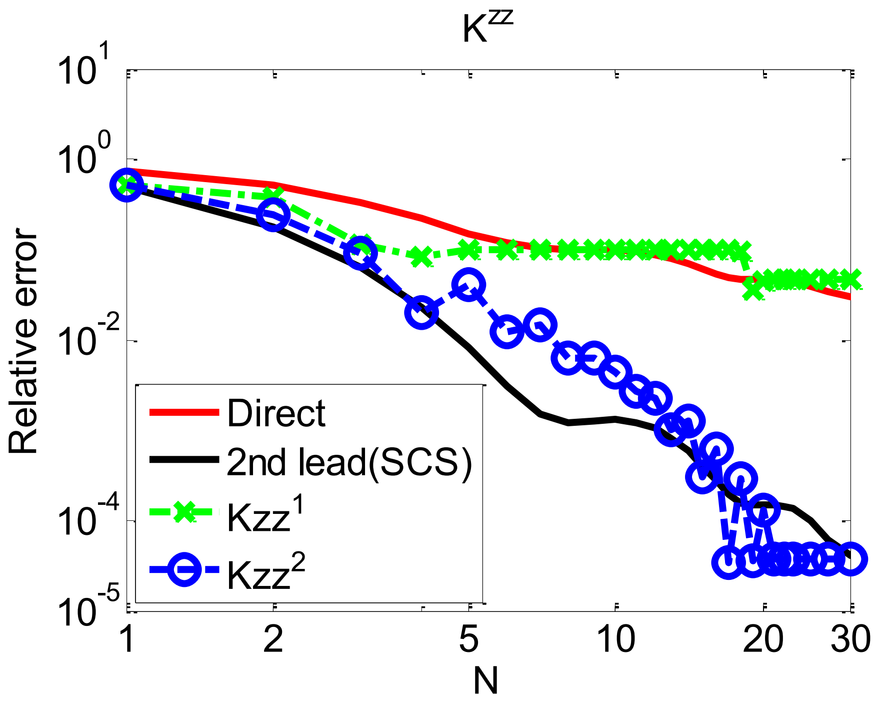

Figure 3.4 Convergence performance comparison of matrix element K_{11}^{zz} by using original representation of F_{ij}^{pq} and Hankel representation of F_{ij}^{pq} in the Levin's transformation

3.7.2 Extrapolation delay for the Levin's transformation

It is well known that the asymptotic form of the Bessel functions of the first kind for small arguments is expressed as [58]:

$$J_v(z) \simeq \frac{1}{v!}\left(\frac{z}{2}\right)^v \quad z \to 0,\ v > 0 \tag{3.95}$$

whose value decreases more and more rapidly as the order v becomes larger and larger. Therefore, if the orders of the Bessel functions of the first kind in (3.90) and (3.91) are big, the calculated P and Q will suffer a large error due to the machine accuracy limit. Thus, we need to do direct summation by using certain number of the original term F_{ij}^{pq} in (3.48), and then apply the novel approach by using the term F_{ij}^{pq} in (3.92) or (3.94). We call this extrapolation delay and define it as follows:

$$K_{ij}^{pq} = \sum_{n=1}^{N_d} F_{ij}^{pq} + \sum_{n=N_d+1}^{\infty} F_{ij}^{pq} \quad p = x, z \text{ and } q = x, z \tag{3.96}$$

where N_d is the number of original terms F_{ij}^{pq} used in direct summation. If $N_d > 0$, we first do the direct summation and then apply the Levin transformations to the remainder. If $N_d = 0$, we don't need the direct summation and apply the Levin transformation from the very beginning. The number of original terms used in direct summation in (3.96) calculated from the first criterion, denoted as N_{d_1}, can be estimated from the first maximum point of the Bessel functions of the first kind, which is also the first real zero of the first derivative of the Bessel functions of the first kind. The asymptotic expansion of the first real zero of the first derivative of the Bessel functions of the first kind is given as [49]:

$$j'_{v,z} \sim v + 0.8086 v^{1/3} + \ldots \tag{3.97}$$

However, as we observe, if the maximum order between v_{pi} and v_{qj} is picked, the obtained N_{d_1} will far exceed the actually terms needed in extrapolation delay. Based on our numerical tests, it is safe to keep one term in (3.97) and pick the minimum order between

v_{pi} and v_{qj}. Then, since we know that $z = \delta_n = \pi w(n-1/2)/(2a)$ in this problem, we can simply obtain N_{d_1} as:

$$N_{d_1} = \left\lceil \frac{2a}{\pi w} \min(v_{pi}, v_{qj}) \right\rceil \tag{3.98}$$

As mentioned above, the first term in the right-hand side of (3.92) and (3.94) is in the asymptotic form of $1/n^k$, which exhibits monotonic convergence and is evaluated by the Levin transformations. However, we also need to quantify after how many terms it will asymptotically decrease as $1/n^k$, from which we can determine the second criterion to calculate the number of terms used in direct summation, denoted as N_{d_2}. If we look at the first term in the right hand side of (3.92) and (3.94), it is shown that they have the same form as a sum of two products of Bessel functions as follows:

$$P_{v_1}P_{v_2} + Q_{v_1}Q_{v_2} = (-1)^{\frac{v_1+v_2}{2}} \frac{\pi z}{2} \left(J_{v_1}J_{v_2} + Y_{v_1}Y_{v_2}\right) \tag{3.99}$$

$$H_{v_1}^{(1)}H_{v_2}^{(2)} + H_{v_2}^{(1)}H_{v_1}^{(2)} = 2\left(J_{v_1}J_{v_2} + Y_{v_1}Y_{v_2}\right) \tag{3.100}$$

Then, by using $J_v(z) = M_v \cos\theta_v$ and $Y_v(z) = M_v \sin\theta_v$ in [49], we rewrite $J_{v_1}J_{v_2} + Y_{v_1}Y_{v_2}$ as:

$$J_{v_1}J_{v_2} + Y_{v_1}Y_{v_2} = M_{v_1}M_{v_2}\cos\left(\theta_{v_1} - \theta_{v_2}\right) \tag{3.101}$$

where

$$M_{v_1}M_{v_2} = \frac{2}{\pi z}\left[1 + \frac{1}{2}\frac{\mu_1 - 1}{(2z)^2} + \cdots\right]^{\frac{1}{2}} \left[1 + \frac{1}{2}\frac{\mu_2 - 1}{(2z)^2} + \cdots\right]^{\frac{1}{2}} \sim \frac{1}{z}$$

$$\theta_{v_1} - \theta_{v_2} = \frac{1}{2}(v_2 - v_1)\pi + \frac{\mu_2 - \mu_1 - 2}{8z} + \cdots \sim \frac{\xi}{z}$$

With the asymptotic expansion of $\theta_{v_1} - \theta_{v_2}$, $\cos(\theta_{v_1} - \theta_{v_2})$ can be simplified as the asymptotic form of $\cos(\xi/z)$, where $\xi = (v_2^2 - v_1^2)/2$. So, when the argument z keeps increasing, $\cos(\xi/z)$ will approach to 1. We choose the last zero point of $\cos(\xi/z)$ as the break-point, only after which does the series show regular monotonic convergence in the form of $1/n^k$. We apply direct summation first, and then apply the Levin transformations to the remaining monotonically convergent series. The number of terms used in direct summation N_{d_2} can be found from the last zero of $\cos(\xi/z)$ as solving $\xi/z = \pi/2$. Also, we have known that the first leading term of $P_{v_1}P_{v_2} + Q_{v_1}Q_{v_2}$ and $H^{(1)}_{v_1}H^{(2)}_{v_2} + H^{(1)}_{v_2}H^{(2)}_{v_1}$ are $(-1)^{\frac{v_1+v_2}{2}}4/(\pi\delta_n)$ and 1, respectively. If we use their first leading term and evaluate the difference by using the Levin transformations, we can further reduce the number of terms used in direct summation, which is found from the second zero to the last of $\cos(\xi/z)$ as solving $\xi/z = 3\pi/2$. Finally, with $z = \delta_n = \pi w(n-1/2)/(2a)$, we obtain N_{d_2} as:

$$N_{d_2} = \left\lceil \frac{2a}{\pi w}\frac{|v_{pi}^2 - v_{qj}^2|}{3\pi} \right\rceil \tag{3.102}$$

In order to guarantee the desired accuracy, we need to choose the larger one between N_{d_1} and N_{d_2}:

$$N_d = \max(N_{d_1}, N_{d_2}) \tag{3.103}$$

3.8 Numerical Results

The new approach was numerically validated using a shielded microstrip with parameters $\varepsilon_r = 11.7$, $\mu_r = 1$, $f = 4$ GHz, $h = 3.17$ mm, $w = 3.04$ mm, $2a = 37.74$ mm, $d = 50$ mm in [32].

Figure 3.5-3.8 show the comparisons of the convergence in evaluating matrix elements K^{zz}_{11}, K^{xz}_{11}, K^{xx}_{11} and K^{zz}_{32} using different approaches: Direct means the direct summation of series in (3.48), n^{th} lead+SCS refers to n^{th} order leading term extraction with SCS method [34], LE (PQ) stands for the PQ representation (3.92) with the Levin v transformation, LE (Hankel) represents the Hankel representation (3.94) with the Levin v transformation, LE (PQ)+SBP means the PQ representation (3.92) with the hybrid of the Levin v transformation and summation-by-parts, and 1^{st} lead+LE (Hankel) refers to first leading term extraction of the Hankel representation (3.94) with the Levin v transformation. The result using four leading term extraction SCS with $N_{\max} = 10^4$ is used as a reference. It shows that by uisng the criteria of N_d in (3.98), (3.102), and (3.103), we can guarantee that the performances of new approach match that of the higher order leading term extraction of SCS, or even better.

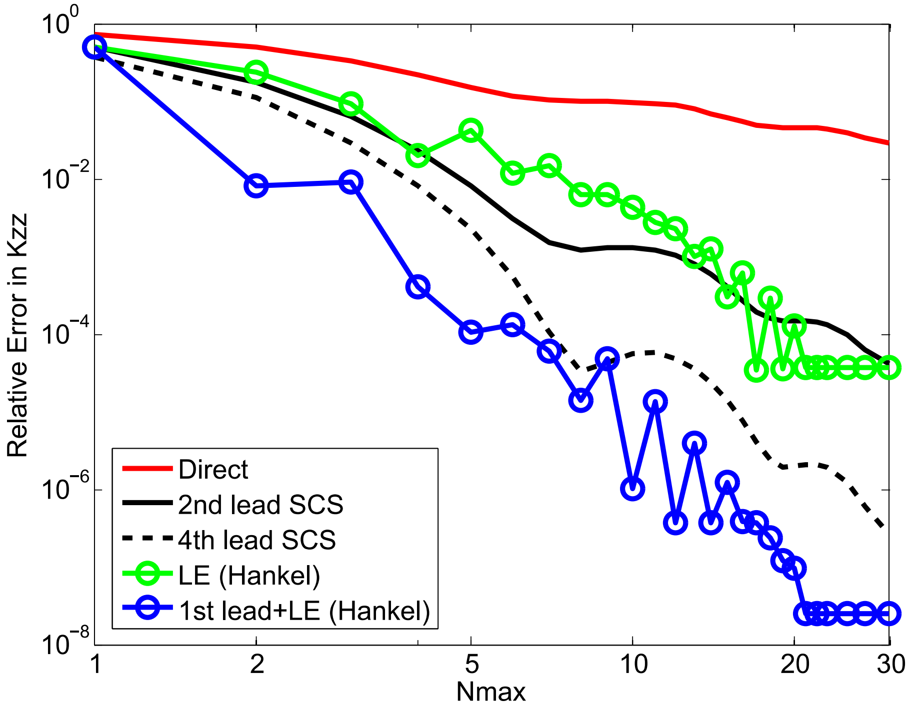

Figure 3.5 Convergence of the matrix element K_{11}^{zz}, compared among novel approaches and other methods; with $N_d = 0$, $\beta = 5k_0$.

Figure 3.5 shows the convergence of K_{11}^{zz}, where $v_{pi} = v_{qj} = 0$. According to (3.98) and (3.102), $N_{d_1} = N_{d_2} = 0$; therefore $N_d = 0$. It shows that LE (Hankel) method performs as good as the 2^{nd} lead SCS method, and 1^{st} lead+LE (Hankel) method performs as good as the 4^{th} lead SCS method. In Figure 3.6 and 3.7, We can see that the new approaches perform even better than the SCS method, due to the reason that when the orders of the Bessel functions of the first kind are higher, the error from asymptotic approximation of the Bessel functions will ruin the performance of SCS more heavily when using relative small $N_{\max}$. Also, in order to get the better convergence, it is necessary and important to use the extrapolation delay and the criteria proposed in (3.98), (3.102), and (3.103).

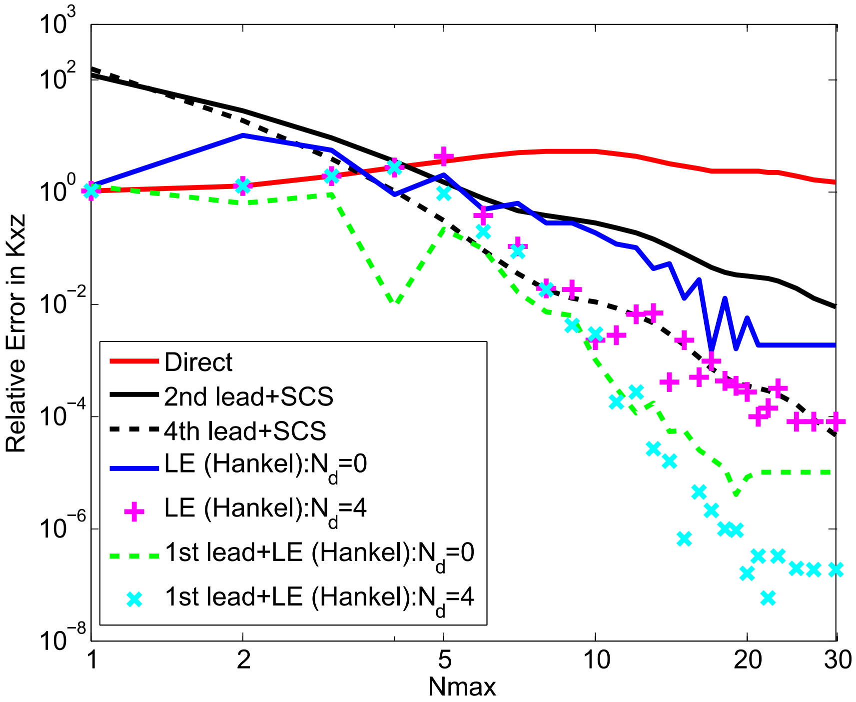

Figure 3.6 Convergence of the matrix element K_{11}^{xz}, compared among novel approaches and other methods; with $N_d = 0$, $\beta = 5k_0$.

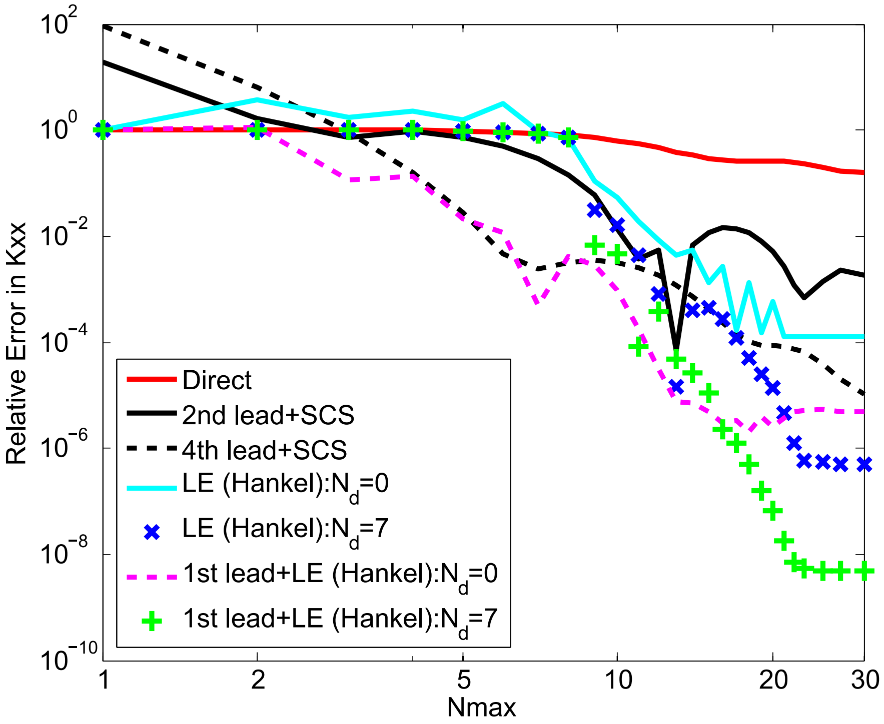

Figure 3.7 Convergence of the matrix element K_{11}^{xx}, compared among novel approaches and other methods; with $N_d = 0$, $\beta = 5k_0$.

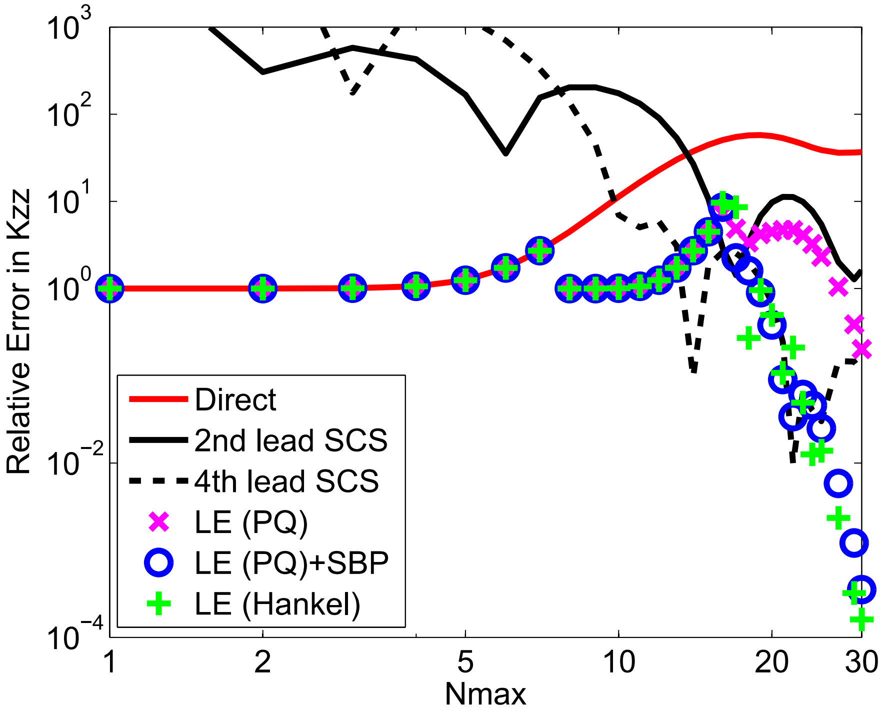

Figure 3.8 Convergence of the matrix element K_{zz}^{32}, compared among novel approaches and other methods; with $N_d = 0$, $\beta = 5k_0$.

The comparison of the Levin v transformation with two different representations is given in Figure 3.8. Here, $v_{pi} = 4$ and $v_{qj} = 2$ for K_{32}^{zz} case. Therefore $N_{d_1} = 7$, $N_{d_2} = 5$, then $N_d = 7$. The performance of LE (Hankel) and LE (PQ)+SBP methods are almost the same and both are better than LE (PQ) method. This can be explained by two facts: first, the summation-by-parts algorithm is stabler than extrapolation method for evaluating series in the form of sinusoidal function divided by n^k when the orders of the Bessel functions are high in the series to be evaluated; second, the Hankel representation (3.94) is better than the PQ representation (3.92) for the Levin transformations in evaluating the series in the form of sinusoidal function (or complex exponential function) divided by n^k, because the Hankel functions asymptotically perform as the complex exponential functions, hence are better than the asymptotic performance of P and Q. Furthermore, the Hankel representation (3.94) is simpler in formula and easier in coding. Therefore, it is recommended in implementation.

Figure 3.9 shows the relative error of $\varepsilon_{\text{reff}}$, which is defined as β^2/k_0^2 and k_0 is the propagation constant in the free space, calculated with and without extrapolation delay: $N_d = 0$ represents without extrapolation delay; adaptive N_d represents with extrapolation delay, and N_d is calculated adaptively according to different orders of the Bessel functions of the first kind by using the criteria (3.98), (3.102), and (3.103). It shows that if extrapolation delay is not applied, the Levin transformations will fail to give the accurate solution. This comparison demonstrates that extrapolation delay is necessary and important in successfully applying the Levin transformations, and the criteria (3.98), (3.102), and (3.103) proposed above to calculate the N_d are proper.

The comparison of the relative error of $\varepsilon_{\text{reff}}$ by using different approaches is shown in Figure 3.10: n^{th} lead+MPS refers to n^{th} order leading term extraction with mid-point summation (MPS) method; others are the same as above. Adaptive N_d is used here. A result accurate to 12 significant digits ($\varepsilon_{\text{reff}} = 8.81004157493$) in [32] is taken as a reference. Since the results are similar whether using an odd number of leading term or

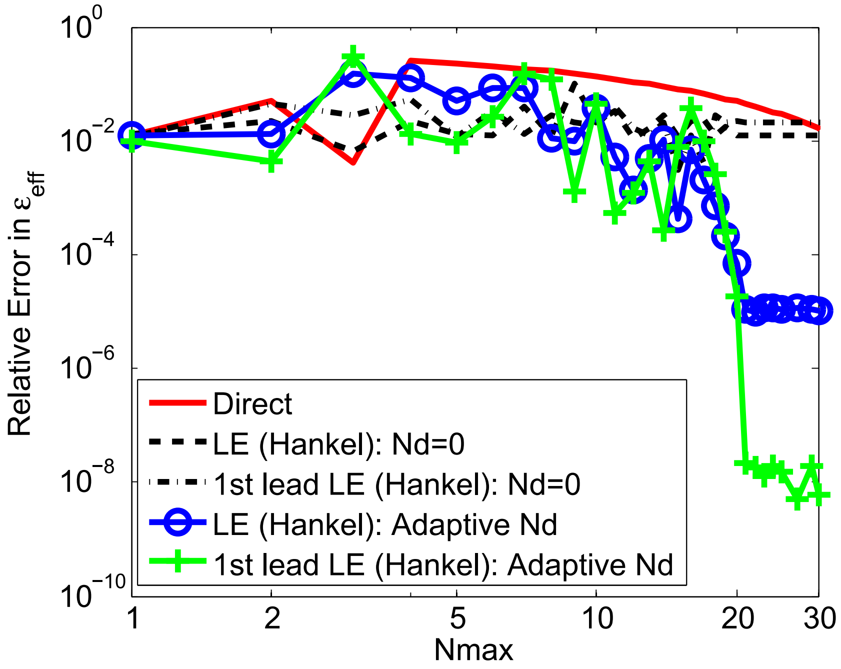

Figure 3.9 Convergence of $\varepsilon_{\text{reff}}$ using the Levin v transformation with the Hankel representation, with and without N_d; $M_x = 3$, $M_z = 4$.

the next even number of leading term in MPS or SCS, we only compare with even number of leading term (2^{nd} and 4^{th} order leading term extraction) in MPS and SCS. Compared with MPS [33] and SCS [34], the new approaches will achieve the same accurate result or even more accurate results than high order leading term extraction with just a few number of terms. It is observed that by using the new approaches, with only 20 terms used, results accurate to 5 significant digits can be obtained without any asymptotic techniques and results accurate to 8 significant digits can be obtained with only first leading term extraction. Figure 3.11 shows that the overall performance of LE (Hankel) and LE (PQ)+SBP methods are almost the same.

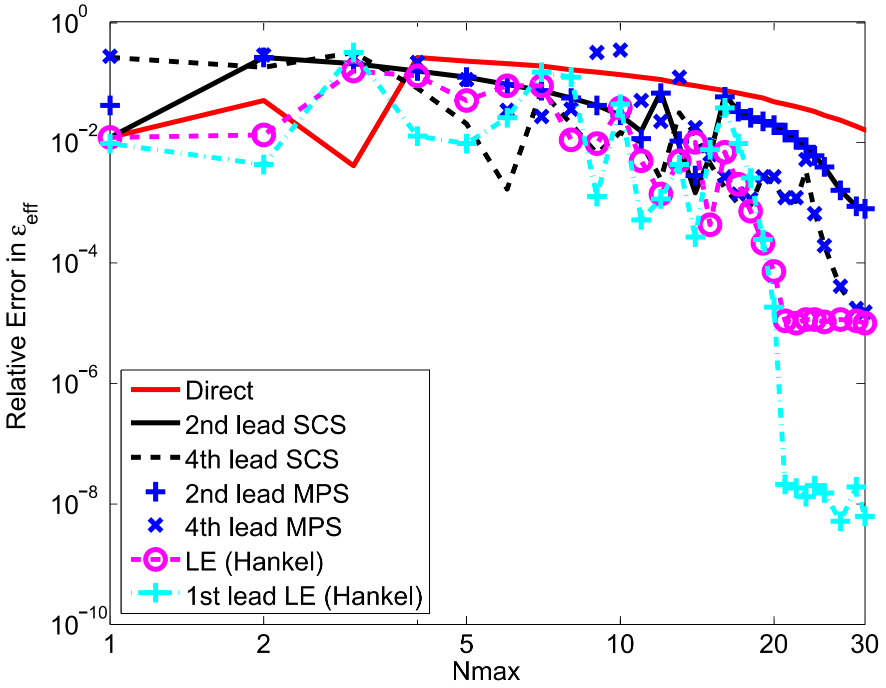

Figure 3.10 Convergence of $\varepsilon_{\text{reff}}$ compared among novel approaches and former approaches, with adaptive N_d; $M_x = 3$, $M_z = 4$.

3.9 Summary

The most difficult and important part in applying SDA to solve the microstrip lines problem is the acceleration of the slowly convergent infinite summation series. We propose a novel acceleration method based on an extrapolation method–the Levin's transformation. In order to use the Levin's transformation, the summation kernel should be recasted into a suitable form and extrapolation delay must be applied. We also compare the Levin's transformation with another popular extrapolation method–Shank's transformation and find that Levin's transformation is capable for accelerating the summation in SDA. The novel acceleration method does not need to do the asymptotic expansion and leading term extraction so that the complexity is dramatically reduced. It can achieve results as accurate as that obtained by using high order leading term extraction in midpoint summation (MPS) or super convergent series (SCS) methods. Furthermore, the

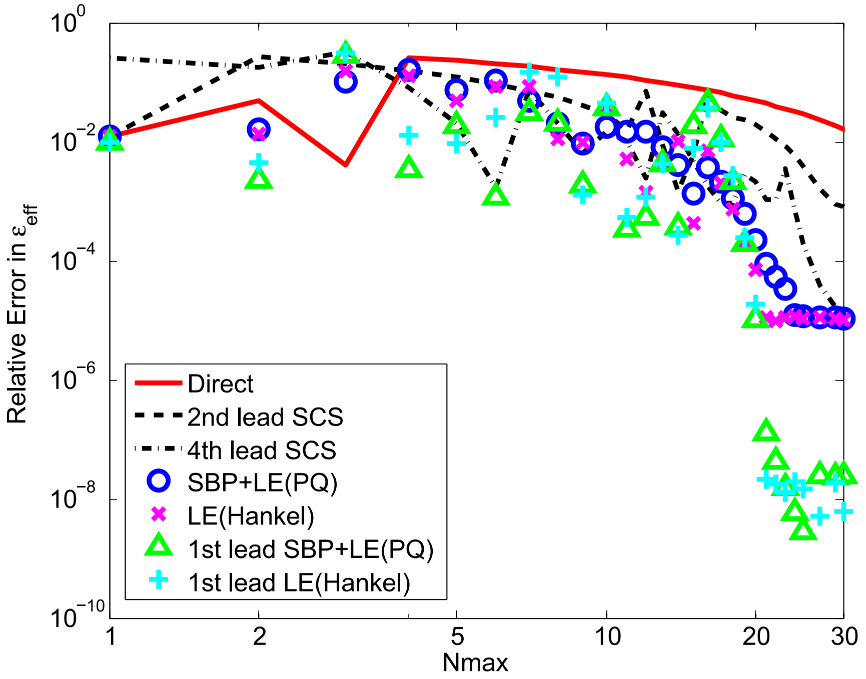

Figure 3.11 Convergence of $\varepsilon_{\text{reff}}$ compared between Levin's transformation and Summation-by-parts, with adaptive N_d; $M_x = 3$, $M_z = 4$.

accuracy can be further improved if we only do the first leading term extraction with the novel method.

CHAPTER 4. NOVEL ACCELERATION OF SPECTRAL DOMAIN IMMITANCE APPROACH FOR GENERALIZED MULTILAYERED SHIELDED MICROSTRIP LINES USING THE LEVIN'S TRANSFORMATION

In the previous chapter, the Levin's transformation and summation-by-parts algorithm have been applied to accelerate the convergence of infinite spectral domain series in spectral domain approach (SDA). The Levin's transformation based on novel acceleration approach is more powerful when it is used to deal with the multilayered and multiple strips structures, because the spectral domain Green's function and current basis functions are more complicated than that in the previous chapter.

Some extrapolation methods have been reviewed for acceleration of the convergence of Sommerfeld-type integrals which arise in problems like scatterers embedded in planar multilayered media [36]. Two different fast convergent sine cosine series, also known as two fast convergent series (FCS), are used to accelerate the summation of the leading term after the asymptotic extraction to the Green's functions and the basis functions in the spectral domain [35]. And, it has been extended to handle the shielded microstrip with multiple metal lines in the same layer over a layered substrate [74]. However, the higher order asymptotic approximation need lots of work to find the leading term coefficients, and it inevitably bring in errors due to asymptotic approximation of both the Green's function and the basis functions. A recent development on the use of the Levin's transformation to compute potentials and fields in multilayered media is reported in [75].

This chapter extends the novel approach in the previous chapter to speed up the spectral domain immitance approach (SDIA) of shielded microstrips with multiple metal strips in the same layer over mutilayered substrates by using one of the most promising extrapolation methods—the Levin's transformation [76]. It greatly saves the work for finding the asymptotic expansion coefficients. Using only the first leading term extraction, the overall acceleration performance is further improved. Convergence properties of SDIA by using this method match with or are even better than other acceleration techniques with high order leading term extraction. It can achieve the same accuracy as FCS with high-order leading term extraction and the method proposed in [31] by using the same number of terms. It is much simpler to understand and much easier to implement, because it does not require the laborious high order leading term extraction. Two practical cases of this technique to rapidly obtain accurate values of β for multilayered shielded microstrips have been reported.

4.1 Multilayered Shielded Microstrip Lines

Figure 4.1 shows a general multilayered shielded microstrip structure with M metal lines with a unique width w_i $(i = 1, \ldots, M)$ displaced by a distance c_i from the left wall located on $y = 0$ plane and extending infinitely in the z direction. The two side walls are perfect electric conductor (PEC) or perfect magnetic conductor (PMC). The m^{th} layer is defined by ε_m, μ_m and has a thickness D_m. The top and bottom cover layers can be PEC, PMC, or dielectric extending up to infinity.

4.2 Spectral Domain Immitance Approach

By using the spectral domain immitance approach (SDIA) [56] and the Galerkin method after expanding the spectral domain source currents as a linear combination of

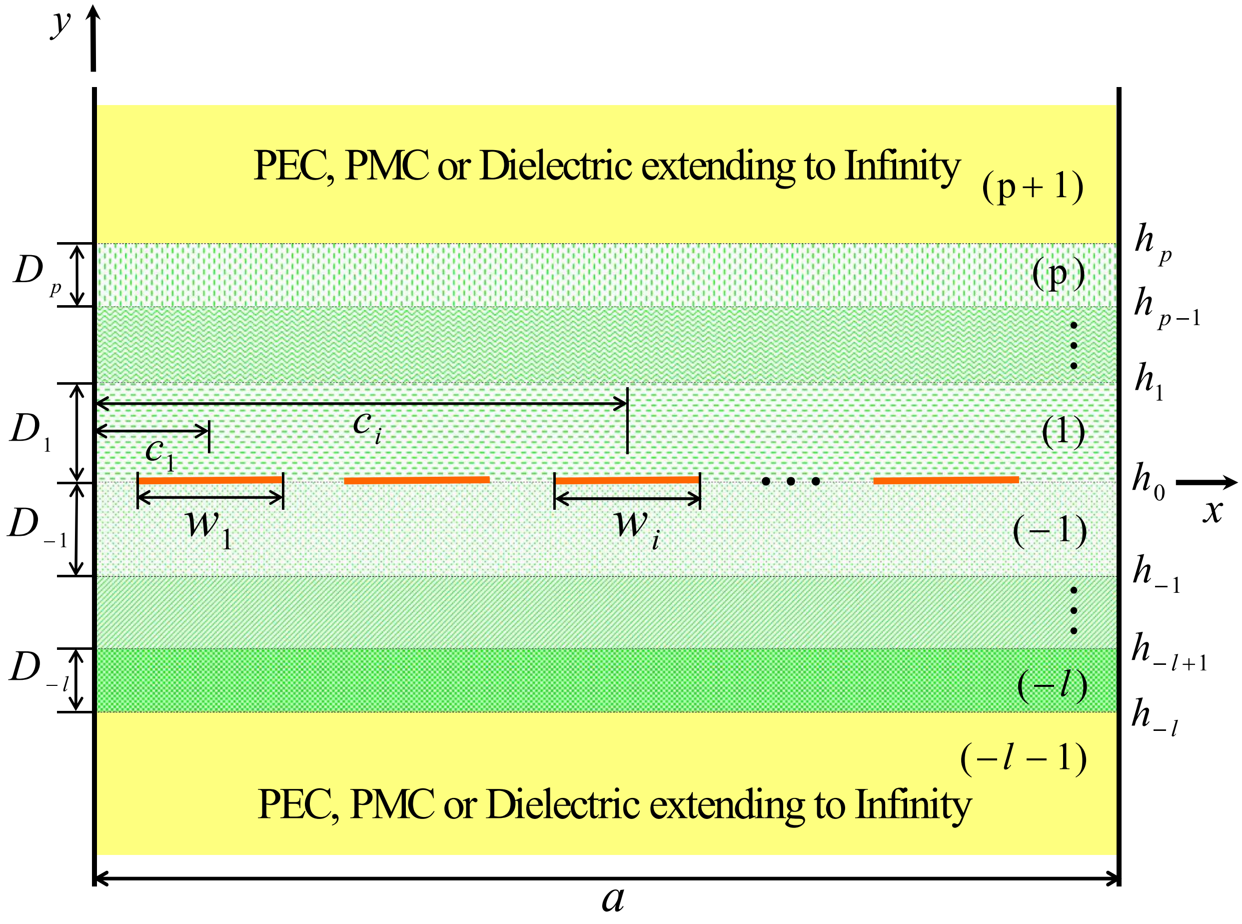

Figure 4.1 Shielded multilayered microstrip with multiple metal strips in one of the layers.

well chosen basis functions, the expansion coefficients a_i and b_i are the solutions of a homogeneous system of linear equations as the following:

$$\begin{bmatrix} K^{xx} & K^{xz} \\ K^{zx} & K^{zz} \end{bmatrix} \begin{bmatrix} A \\ B \end{bmatrix} = \begin{bmatrix} 0 \\ 0 \end{bmatrix} \tag{4.1}$$

where A and B are vectors which are proportional to the coefficients a_i and b_i, respectively. The propagation constant β can be obtained by solving $\det[K] = 0$. The key step is to develop a simple and quick method to generate the K matrix:

$$K^{pq}_{(u,i)(v,j)} = \sum_{n=1}^{\infty} F^{pq}_{(u,i)(v,j)} = \sum_{n=1}^{\infty} \tilde{I}^{p}_{u,i-\delta_{pz}} G_{pq}(n,\beta) \tilde{I}^{q}_{v,j-\delta_{qz}} \tag{4.2}$$

where $(p,q) \in (x,z)$, $\tilde{I}^{p}_{u,i-\delta_{pz}}$ refers to the p component of the i^{th} basis for the u^{th} metal line, and

$$\delta_{pq} = \begin{cases} 1, & p = q \\ 0, & p \neq q \end{cases} \tag{4.3}$$

The constant term at $n = 0$ in (4.2) is skipped here, and the expressions for the Green's functions are reported in [35]. A well-established natural set of basis functions is Chebyshev polynomials centered around the center of each metal line [59], as it is an entire domain basis and satisfy the edge condition.

$$\tilde{I}^{p}_{u,k}(n) = \frac{J_k(\alpha_n w_u)\left[e^{j\alpha_n c_u} - (-1)^k e^{-j\alpha_n c_u}\right]}{2(\alpha_n w_u)^{\delta_{px}}} \tag{4.4}$$

where J_k is the k^{th} order Bessel function of the first kind and $\alpha_n = n\pi/a$.

4.3 New Acceleration Approach for Spectral Domain Infinite Summation

4.3.1 Recasting the summation kernel

The original summation kernel cannot be applied in the Levin's transformation directly. Our starting point is to recast the Bessel functions of the first kind into Hankel functions without any approximation by using the equation (3.93), and the trigonometric functions into complex exponential functions by using the Euler's formula. Then, $F^{pq}_{(u,i)(v,j)}$ is recast as:

$$\bar{F}^{pq}_{(u,i)(v,j)} = \frac{G_{pq} C^{pq}_{(u,i)(v,j)}}{16(\alpha_n w_u)^{\delta_{px}} (\alpha_n w_v)^{\delta_{qx}}} (T_1 + T_2 + T_3) \tag{4.5}$$

where

$$T_1 = H^{(1)}_{i-\delta_{pz}}(z_u) H^{(1)}_{j-\delta_{qz}}(z_v) \tag{4.6}$$

$$T_2 = H^{(2)}_{i-\delta_{pz}}(z_u) H^{(2)}_{j-\delta_{qz}}(z_v) \tag{4.7}$$

$$T_3 = H^{(1)}_{i-\delta_{pz}}(z_u) H^{(2)}_{j-\delta_{qz}}(z_v) + H^{(1)}_{j-\delta_{qz}}(z_v) H^{(2)}_{i-\delta_{pz}}(z_u) \tag{4.8}$$

$$\begin{aligned} C^{pq}_{(u,i)(v,j)} &= \left[e^{j\alpha_n (c_u + c_v)} + (-1)^{i+j-\delta_{pz}-\delta_{qz}} e^{-j\alpha_n (c_u + c_v)} \right] \\ &- \left[(-1)^{j-\delta_{qz}} e^{j\alpha_n (c_u - c_v)} + (-1)^{i-\delta_{pz}} e^{-j\alpha_n (c_u - c_v)} \right] \end{aligned} \tag{4.9}$$

and $z_u = \alpha_n w_u$. Now, the kernel is suitable to be applied in the Levin's transformation, because the series that arise from (4.5) have either the forms $\sum_{n=1}^{\infty} a_n$ and $\sum_{n=1}^{\infty} a_n e^{\pm jn\phi}$, where $a_n \sim 1/n^k$ for $n \to \infty$, ϕ is a constant, and k is an integer. Also, note that T_1 and T_2 are always complex conjugates, therefore we only need to compute one of them.

Further improvement can be achieved by using only the first leading term extraction of the Green's function G_{pq} and T_3. The leading terms of the Green's function and the coefficients are given in [35]. By using $J_i(z) = M_i \cos\theta_i$ and $Y_i(z) = M_i \sin\theta_i$ and their asymptotic forms in [49]

$$T_3 = \frac{4}{\pi \alpha_n \sqrt{w_u w_v}} \cos\left[\alpha_n (w_u - w_v) - \frac{\pi}{2}(i - j) + \ldots \right] \tag{4.10}$$

Let's denote $L = G_{pq} T_3 C^{pq}_{(u,i)(v,j)} / [(\alpha_n w_u)^{\delta_{px}} (\alpha_n w_v)^{\delta_{qx}}]$, then

$$\sum_{n=1}^{\infty} L = \sum_{n=1}^{\infty} (L - \hat{L}) + \sum_{n=1}^{\infty} \hat{L} \tag{4.11}$$

where $\hat{L}$ has two types of numerical series:

$$\hat{L} \sim \frac{1}{n^2} \left\{ \begin{array}{l} \sin[\alpha_n(w_u - w_v) \pm \alpha_n(c_u \pm c_v)] \\ \cos[\alpha_n(w_u - w_v) \pm \alpha_n(c_u \pm c_v)] \end{array} \right\} \tag{4.12}$$

which are alternative strongly convergent series, and can be calculated by using the Riemann Zeta function [72]. The difference series $L - \hat{L}$ converges very fast, and is very efficient to be evaluated using the Levin's transformation.

4.3.2 Extrapolation delay

The above subsections introduced how to recast the summation kernel into the form suitable to be applied in the Levin's transformation. However, the Levin's transformation fails in some cases unless we delay the extrapolation after direct summation, because of the error introduced as a result of cancellation of large numbers and the break point for the steady asymptotic behavior of the series. The asymptotic form of the Bessel functions of the first kind for small arguments is well known as [49]:

$$J_v(z) \simeq \frac{1}{v!}\left(\frac{z}{2}\right)^v \qquad z \to 0,\ v > 0 \tag{4.13}$$

and its value decreases more and more rapidly as the order v becomes larger and larger. At the very beginning, the value of series T_1 and T_2 are very large numbers. If the orders of the Hankel functions in (4.5) are big, the recasted series will suffer a large error at the very beginning terms due to large numbers cancellation. Thus, direct summation is applied before the Levin's transformation as introduced in [77]

$$K^{pq}_{(u,i)(v,j)} = \sum_{n=1}^{N_d} F^{pq}_{(u,i)(v,j)} + \sum_{n=N_d+1}^{\infty} \bar{F}^{pq}_{(u,i)(v,j)} \tag{4.14}$$

where N_d is the number of original terms F used in direct summation. If $N_d = 0$, we don't need the direct summation and apply the Levin transformation from the very beginning.

The asymptotic behavior of T_3 is an alternative convergent series as $\cos(nx)$ or $\sin(nx)$ over n. The break point for the steady asymptotic behavior can be roughly estimated from the first maximum point of the Bessel functions of the first kind (the first real zero of the first derivative). Its asymptotic expansion is given as [49]:

$$j'_{v,z} \sim v + 0.8086v^{1/3} + \dots \tag{4.15}$$

The error due to the cancellation of large numbers is also avoided if we choose the first maximum point as the starting point to apply the Levin's transformation. Therefore, the first N_d is

$$N_{d_1} \approx \frac{a}{\pi \min\left(w_u, w_v\right)} \max(i - \delta_{pz}, j - \delta_{qz}) \tag{4.16}$$

When $u = v$ or $w_u = w_v = w$ in (4.10), T_3 converges monotonically as $1/n$. In this situation, the asymptotic expansion of T_3 can be written as $\cos(\xi/z)$ [77], where $\xi = (v_i^2 - v_j^2)/2$, $v_i = i - \delta_{pz}$, $v_j = j - \delta_{qz}$, and $z = n\pi w/a$. The $\cos(\xi/z)$ will approach to 1 as $n \to \infty$. The last zero of $\cos(\xi/z)$ can be chosen as the breakpoint, only after which does the series T_3 show steady monotonic convergence in the form of $1/n$. Therefore, we obtain the second N_d

$$N_{d_2} \approx \frac{a}{\pi w} \frac{|(i - \delta_{pz})^2 - (j - \delta_{qz})^2|}{\pi} \tag{4.17}$$

Finally, we choose the larger one between N_{d_1} and N_{d_2}

$$N_d = \max(N_{d_1}, N_{d_2}) \tag{4.18}$$

4.4 Numerical Results

The new technique is validated by a single metal strip, three-layered shielded microstrip with parameters as shown in Figure 4.2 and a coupled metal strips, three-layered shielded microstrip with parameters as shown in Figure 4.3.

Figure 4.4 shows the relative error of $\varepsilon_{\text{reff}}$, defined as β^2/k_0^2, calculated with and without the extrapolation delay. Adaptive N_d means the number of terms used in direct summation is calculated adaptively in each matrix element using the criteria (4.16),

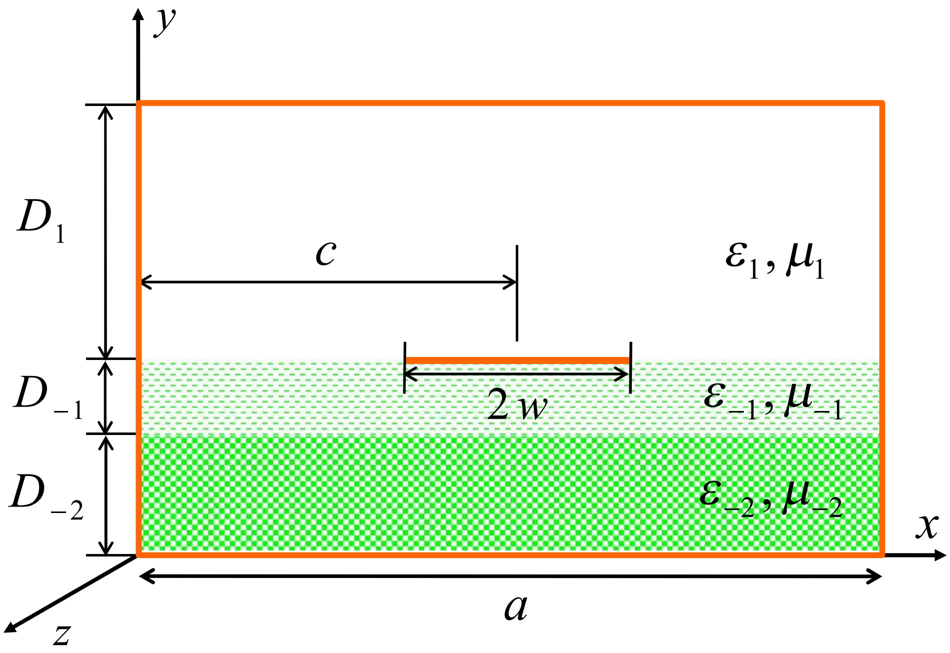

Figure 4.2 A three-layered shielded microstrip with parameters: $\epsilon_{r_{-2}} = \epsilon_{r_1} = 1$, $\epsilon_{r_{-1}} = 10.2$, $\mu_{r_i} = 1$, $D_{-2} = 6.35$ mm, $D_{-1} = D_1 = 0.635$ mm, $2w = 0.635$ mm, $a = 7.62$ mm, and $c = a/2$.

(4.17), and (4.18). This comparison demonstrates that extrapolation delay is necessary and important in successfully applying the Levin's transformation, and the criteria proposed to estimate the N_d are proper.

The comparison of the relative error of $\varepsilon_{\text{reff}}$ by using different approaches is shown in Figure 4.5. Adaptive N_d is used here. A result accurate to 9 significant digits ($\beta/k_0 = 1.58818126$) in [35] is taken as a reference. Since the results are similar whether using an odd number of leading term or the next even number of leading term with FCS, we only compare with even number of leading term (2^{nd} and 4^{th} order leading term extraction) in FCS. Compared with FCS [35], the new technique achieves the same or even more accurate results than the higher order leading term extraction with similar number of terms. It is observed that by using the new technique, with only 30 terms, results accurate to 5 significant digits can be obtained without any asymptotic techniques

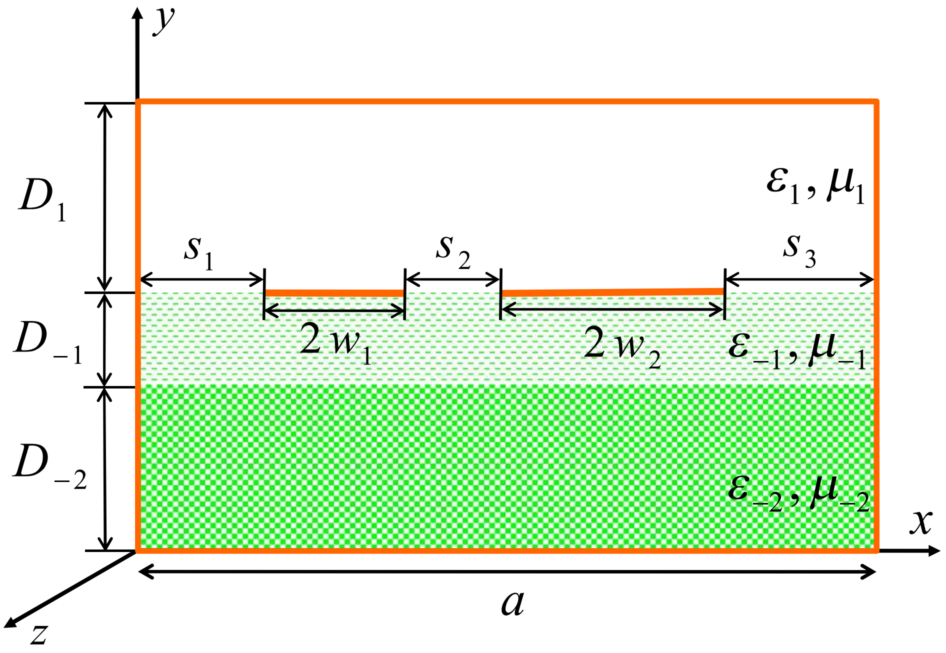

Figure 4.3 A three-layered shielded microstrip with two metal lines in the same layer and parameters: $\epsilon_{r_{-2}} = \epsilon_{r_1} = 1$, $\epsilon_{r_{-1}} = 2.2$, $\mu_{r_i} = 1$, $D_{-2} = D_{-1} = 0.254$ mm, $D_1 = 0.762$ mm, $a = 2.54$ mm, $S_2 = 0.0127$ mm, $S_1 : 2w_1 : S_2 : 2w_2 : S_3 = 89.5 : 20 : 1 : 40 : 49.5$.

and results accurate to 7 significant digits can be obtained with only first leading term extraction.

Finally, we compare our result (β/k_0 for the dominant mode) with the ones in [31] as shown in Table 4.1. Our data converge to the final values which are highlighted by boldface characters. Our results are very close, although not identical, to the ones in [31]. The convergence rate of our technique without any leading term extraction is better than their first order approximation method, although the final accuracy is limited to 5 digits. The convergence rate of our technique with only the first leading term extraction matches their second order approximation method, and achieves similar final accuracy.

With the help of the proposed technique, the complexity of the SDA and SDIA can be dramatically decreased because either asymptotic expansion is not involved or only

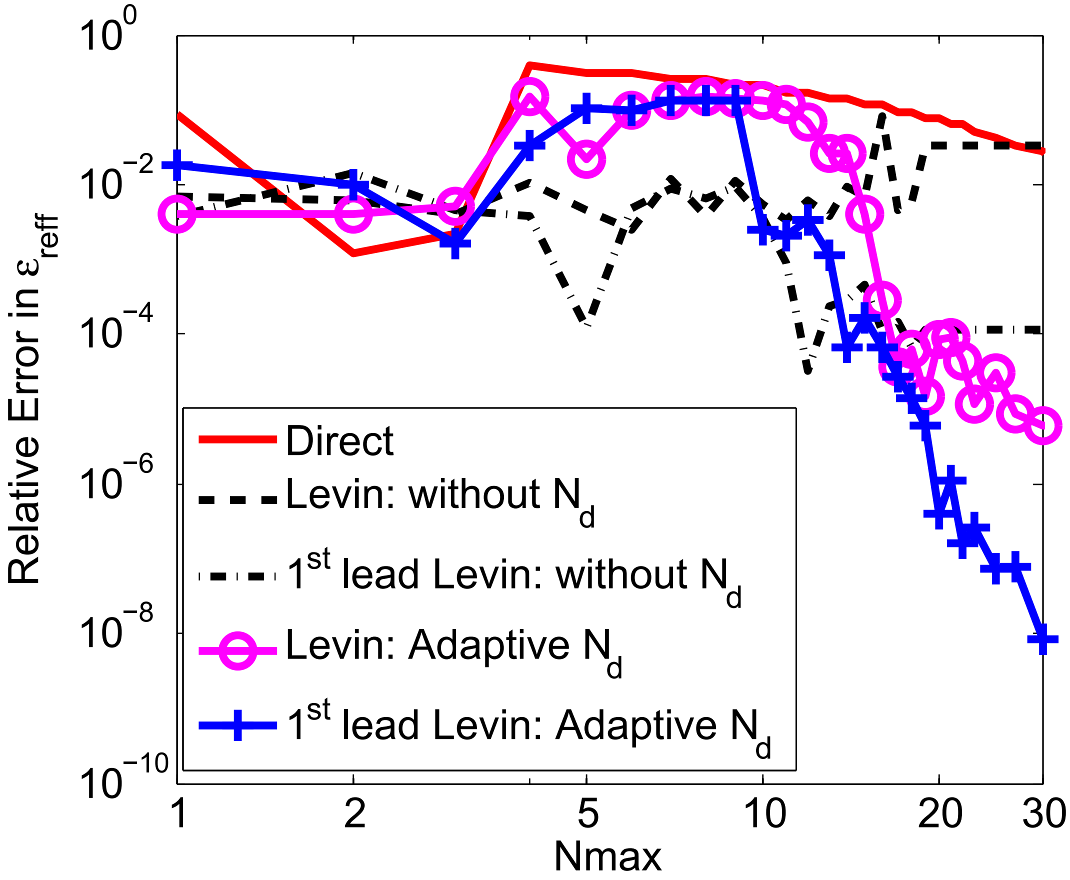

Figure 4.4 Convergence of $\varepsilon_{\text{reff}}$ using the Levin's transformation with and without extrapolation delay for the shielded microstrip with parameters as given in Figure 4.2 at 1 GHz; $M_x = 3$, $M_z = 4$.

first leading term extraction is needed. It achieves convergence rates as fast as or even faster than high order asymptotic extraction techniques. This technique shows more advantages when it is extended to deal with the case of multilayered substrates and multiple strips, for which the spectral domain Green's function and basis functions are more complicated. Due to its simplicity and easy implementation, this technique is a promising alternative to other cumbersome methods such as the asymptotic extraction techniques used in the past.

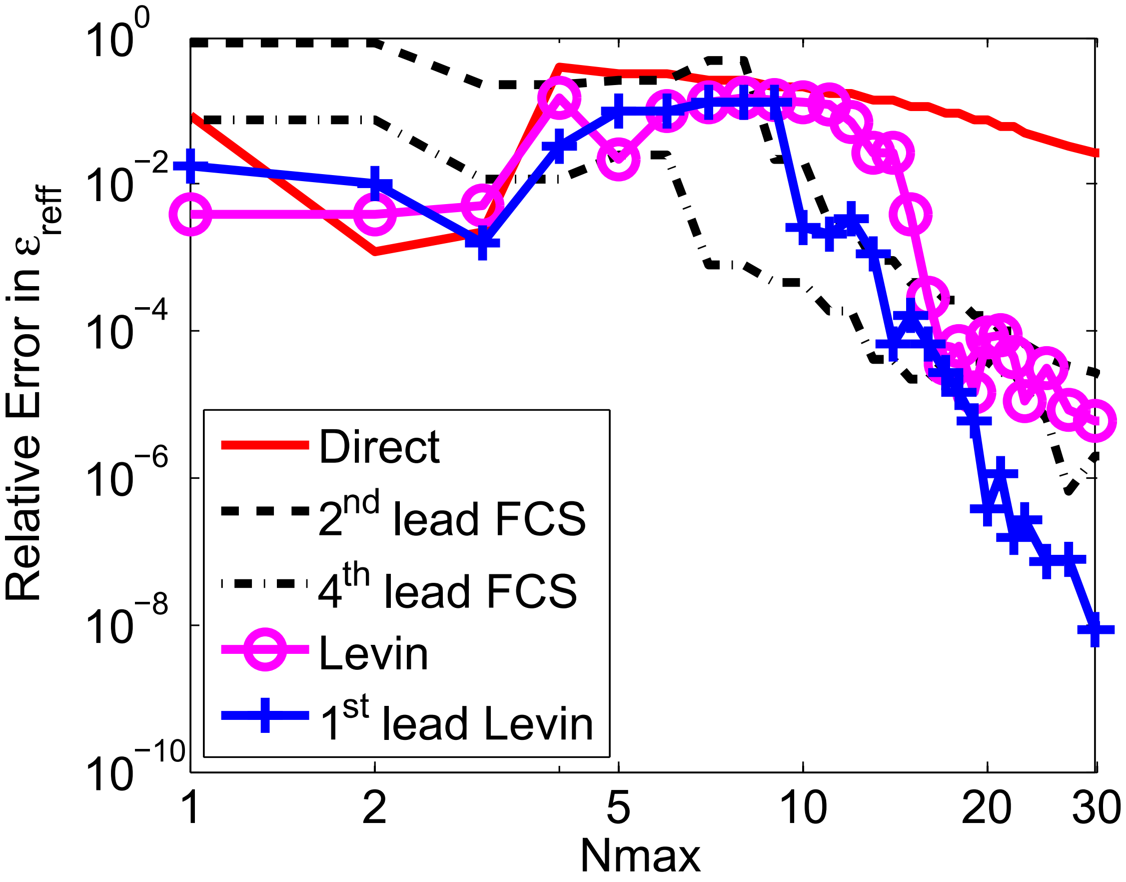

Figure 4.5 Convergence of $\varepsilon_{\text{reff}}$ compared with 2^{nd} and 4^{th} leading term extraction FCS method for the shielded microstrip with parameters as given in Fig. 4.2 at 1 GHz; $M_x = 3$, $M_z = 4$.

4.5 Summary

The acceleration method introduced in Chapter 3 is extended to handle the multiple metal strips and multilayered shielded microstrip structures. This technique shows more advantages when it is extended to deal with the multilayered and multiple strips case, for which the spectral domain Green's function and basis functions are more complicated. We recast the summation kernel into a suitable for the Levin's transformation, and do the extrapolation delay to ensure the successful application of the Levin's transformation. This technique is a promising alternative to other cumbersome methods based on the asymptotic extraction because of its simplicity and easy implementation.

Table 4.1 β/k_0 of the dominant mode in a coupled metal strips, three-layered shielded microstrip at 150 GHz and parameters as given in Figure 4.3

N	Levin	[31] (1st order)	1st lead Levin	[31] (2nd order)
5	1.2598679	1.2593177	1.2607169	1.2610062
10	1.2590489	1.2604623	1.2609279	1.2609137
20	1.2610138	1.2608074	1.2609112	1.2609104
30	1.2609057	1.2608630	**1.260910**1	1.2609103
40	1.2609261	———	———	———
50	**1.2609**277	———	——-	———
250	———	1.2609103	———	———

CHAPTER 5. APPROACHES TO HANDLE ARBITRARY CROSS SECTION AND FINITE CONDUCTIVITY OF MULTIPLE METAL LINES WITH MULTILAYERED SUBSTRATES

Most analyses of microstrip lines about its characteristics like propagation constant were based on the assumption of infinitely thin metal strip and infinite conductivity. However, microstrip lines are very attractive to achieve high-speed interconnections in monolithic microwave integrated circuits (MMIC). In this situation, the thickness of the metal strips cannot be neglected, because the metallization thickness is comparable to the skin depth and these strips are very close to each other. The strips often have a trapezoidal-like cross section due to the etching undercuts or electrolytical growth during fabrication. And actually, we can see a variety of complicated strip cross sections existing in MMIC interconnect structures. The microstrip lines would have different propagation characteristics from the previous ones of assuming zero metallization thickness or assuming finite metallization thickness but with infinite conductivity.

A rigorous analysis of the propagation characteristics of multiple metal strips with arbitrary cross sections and finite conductivity in multilayered shielded microstrip structure has been developed. A PMCHWT formulation is used in conjunction with the method of moments (MoM). Both the surface equivalent electric and magnetic currents are used to determine the fields inside and outside the metal strips, and the basis functions are chosen as pulse basis for longitudinal direction and triangular basis for transverse direction. The spatial domain integral is calculated in the equivalent internal problem with the spatial dyadic Green's functions, while the spectral domain summation is calculated in the equivalent external problem with the spectral domain dyadic Green's functions.

5.1 General Models of the Problem

A model of the mutilple metal lines with arbitrary cross section and finite conductivity in multilayered shielded microstrip is shown in Figure 5.1. The side walls are set to perfect electric conductor (PEC) or perfect magnetic conductor (PMC). The ith layer is defined by ε_i, μ_i, thickness d_i and $k_i = \omega\sqrt{\varepsilon_i \mu_i}$. All the layers are defined above $y-$axis, and are numbered from 1 to N. The parameters pertaining to layer i with boundaries at h_i and h_{i+1} are distinguished by a subscript i. The top and bottom cover layers can be PEC, PMC or dielectrics extending up to infinity. The real metal strips with arbitrary cross sections are located between region 0 and region $N+1$, and can be totally embedded in one certain layer or embedded cross different layers. The wave is assumed to propagate along the x direction.

5.2 2D PMCHWT Formulations

By using the surface equivalence principle and introducing the equivalent surface electric current $\mathbf{J}_s$ and magnetic current $\mathbf{M}_s$, we can define the external and internal problems. In the external problem, the electromagnetic fields outside the dash contours are calculated from the equivalent sources as illustrated in Figure 5.2. In the internal problem, the electromagnetic fields inside the dash contours are calculated from the equivalent sources in Figure 5.3.

Then, by using both external and internal surface equivalences, we obtain the electric field integral equations (EFIEs) and magnetic field integral equations (MFIEs):

$$\hat{n} \times \mathbf{E}^i = -\frac{1}{2}\mathbf{M}_s - \hat{n} \times \mathbf{E}_l^s \left(\mathbf{J}_s, \mathbf{M}_s\right) \tag{5.1}$$

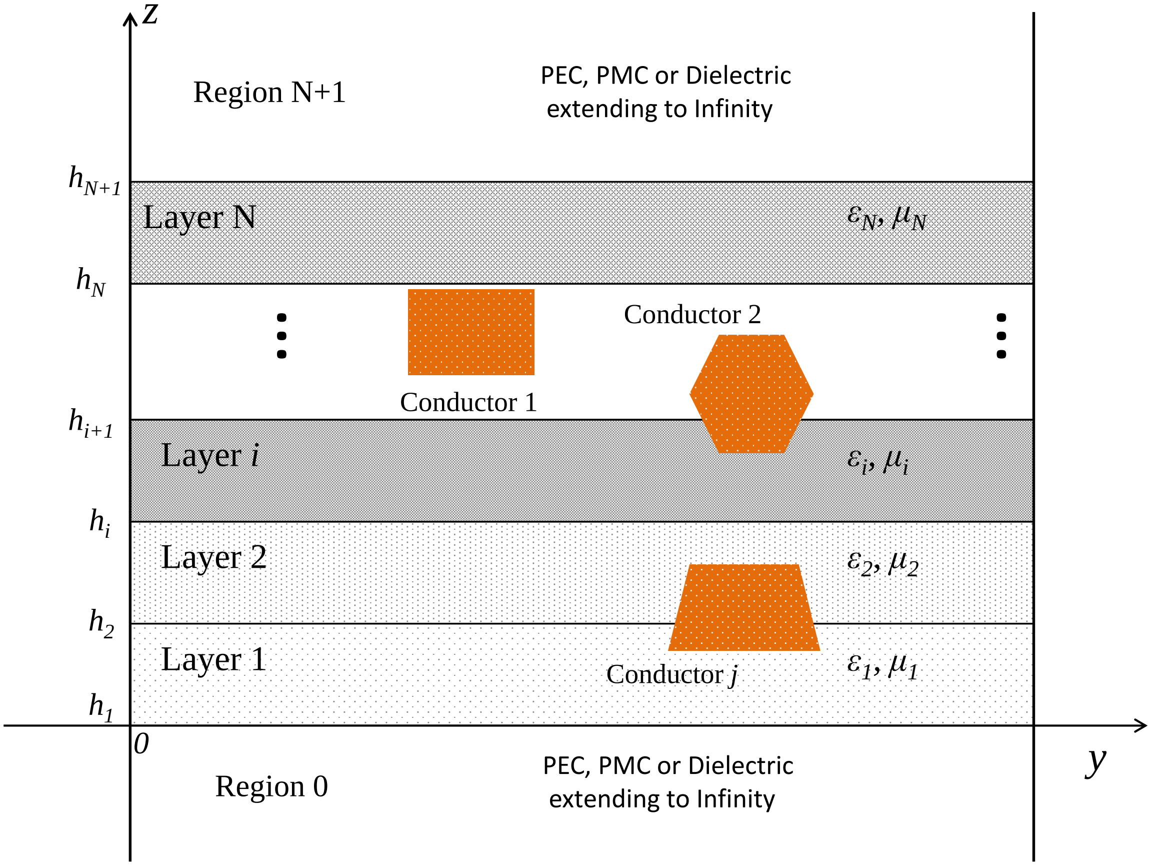

Figure 5.1 Shielded multilayered microstrip with multiple arbitrary cross-section metal strips.

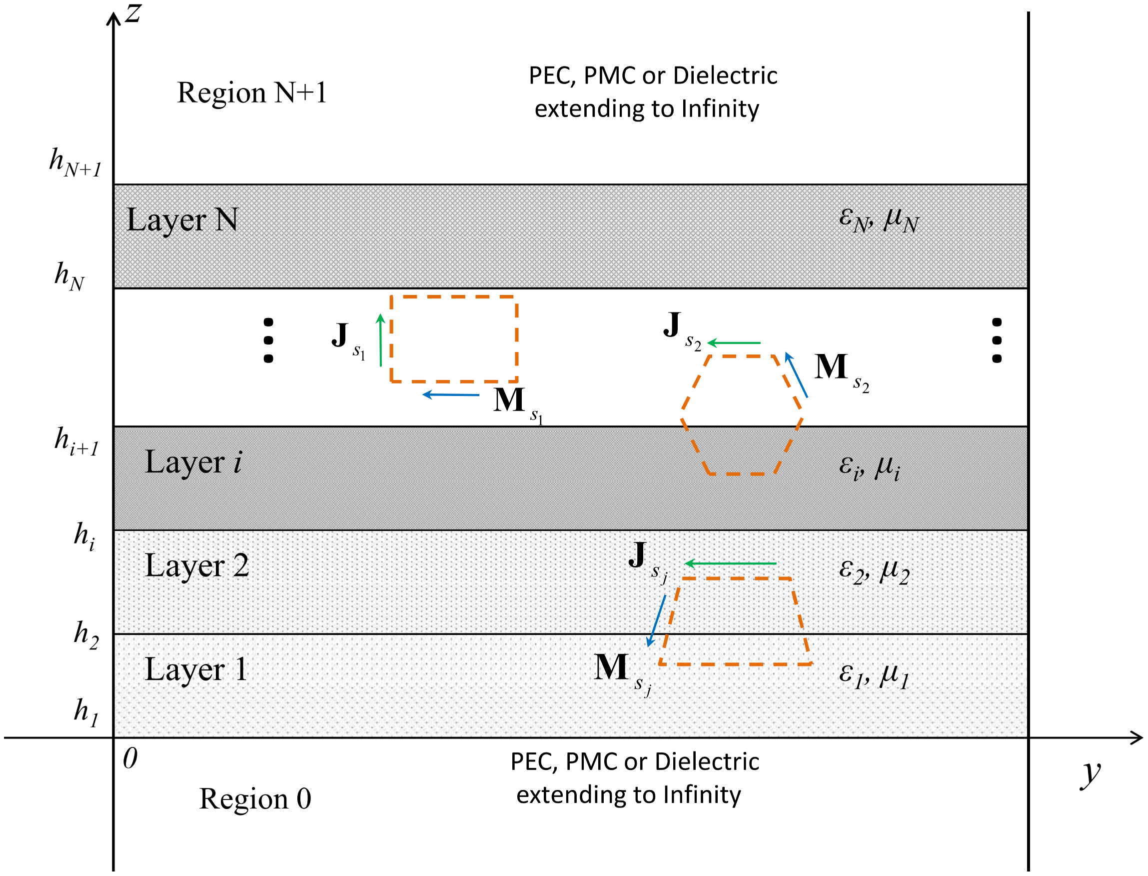

Figure 5.2 External equivalent problem

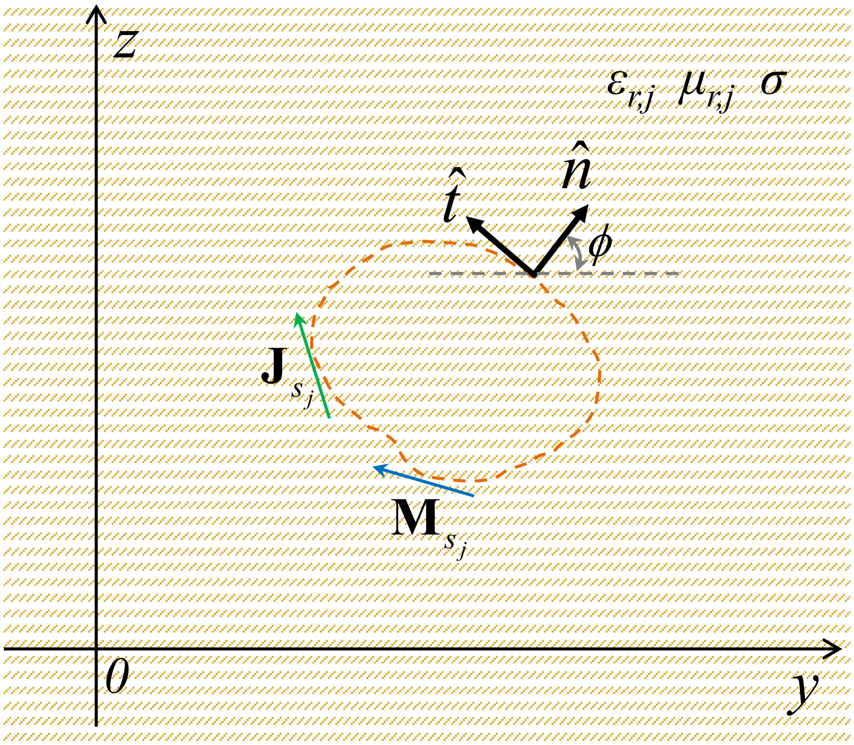

Figure 5.3 Internal equivalent problem

$$0 = \frac{1}{2}\mathbf{M}_s - \hat{n} \times \mathbf{E}_h^s\left(\mathbf{J}_s, \mathbf{M}_s\right) \tag{5.2}$$

$$\hat{n} \times \mathbf{H}^i = \frac{1}{2}\mathbf{J}_s - \hat{n} \times \mathbf{H}_l^s\left(\mathbf{J}_s, \mathbf{M}_s\right) \tag{5.3}$$

$$0 = -\frac{1}{2}\mathbf{J}_s - \hat{n} \times \mathbf{H}_h^s\left(\mathbf{J}_s, \mathbf{M}_s\right) \tag{5.4}$$

where $\hat{n}$ is the outward unit vector normal to the strip contour as shown in Figure 5.3. The subscript l represents for external layered medium, while h represents for internal homogeneous medium. Then, let's combine two EFIEs and two MFIEs linearly, and take the linear combination coefficients as 1. We now get the famous PMCHWT formulation [78–80], and can be written as:

$$-\mathbf{E}^i|_{\tan} = \left[\mathbf{E}_h^s\left(\mathbf{J}_s, \mathbf{M}_s\right) + \mathbf{E}_l^s\left(\mathbf{J}_s, \mathbf{M}_s\right)\right]|_{\tan} \tag{5.5}$$

$$-\mathbf{H}^i|_{\tan} = \left[\mathbf{H}_h^s\left(\mathbf{J}_s, \mathbf{M}_s\right) + \mathbf{H}_l^s\left(\mathbf{J}_s, \mathbf{M}_s\right)\right]|_{\tan} \tag{5.6}$$

The general PMCHWT formulations (5.5) and (5.6) are reduced to 2D-PMCHWT by using Green's functions and surface equivalent electric and magnetic currents:

$$-E_x^i = \langle G_{xx}^{EJ}, J_x \rangle + \langle G_{xt}^{EJ}, J_t \rangle + \langle G_{xx}^{EM}, M_x \rangle + \langle G_{xt}^{EM}, M_t \rangle \tag{5.7}$$

$$-E_t^i = \langle G_{tx}^{EJ}, J_x \rangle + \langle G_{tt}^{EJ}, J_t \rangle + \langle G_{tx}^{EM}, M_x \rangle + \langle G_{tt}^{EM}, M_t \rangle \tag{5.8}$$

$$-H_x^i = \langle G_{xx}^{HJ}, J_x \rangle + \langle G_{xt}^{HJ}, J_t \rangle + \langle G_{xx}^{HM}, M_x \rangle + \langle G_{xt}^{HM}, M_t \rangle \tag{5.9}$$

$$-H_t^i = \langle G_{tx}^{HJ}, J_x \rangle + \langle G_{tt}^{HJ}, J_t \rangle + \langle G_{tx}^{HM}, M_x \rangle + \langle G_{tt}^{HM}, M_t \rangle \tag{5.10}$$

where

$$G_{\alpha\beta}^{PQ}(\boldsymbol{\rho}, \boldsymbol{\rho'}) = \hat{\alpha} \cdot \bar{\mathbf{G}}^{PQ}(\boldsymbol{\rho}, \boldsymbol{\rho'}) \cdot \hat{\beta} \tag{5.11}$$

and $(\alpha, \beta) \in \{x, t\}$. x is the propagation direction (longitudinal direction), and t represents the transverse direction of the cross section contour on the $y-z$ plane. $\bar{\mathbf{G}}^{PQ}(\boldsymbol{\rho}, \boldsymbol{\rho'})$ is the dyadic Green's function (DGF) relating P-type fields at $\boldsymbol{\rho}$ and Q-type current at $\boldsymbol{\rho'}$, which are defined as the following:

$$\bar{\mathbf{G}}^{PQ} = \sum_{i \in \{x,y,z\}} \sum_{j \in \{x,y,z\}} \hat{i}\hat{j} g_{ij}^{PQ} \tag{5.12}$$

and the g_{ij}^{PQ} are the scalar Green's functions which include both the internal and external regions.

$$g_{ij}^{PQ} = g_{hij}^{PQ} + g_{lij}^{PQ} \tag{5.13}$$

where $P \in \{E, H\}$, $Q \in \{J, M\}$, $(i, j) \in \{x, y, z\}$.

5.3 Dyadic Green's Functions (DGF)

5.3.1 The DGF of the internal problem

The dyadic Green's functions (DGF) of the internal problem are derived from the general three-dimensional DGF in homogeneous medium through the auxiliary potential functions with **A** and **F**. First, we look at the electric field generated by the electric current.

$$\mathbf{E}^e = -j\omega\mathbf{A} - \frac{j}{\omega\mu\varepsilon}\nabla(\nabla\cdot\mathbf{A}) = -j\omega\mu\iint_s \left[\bar{\mathbf{I}} + \frac{1}{k^2}\nabla\nabla\right] g\cdot\mathbf{J}(\mathbf{r}')ds' \tag{5.14}$$

In order to derive the internal problem's DGF, let's substitute $\mathbf{J}(\mathbf{r}') = \delta(\boldsymbol{\rho}' - \boldsymbol{\rho}'')e^{-j\beta x'}$ into (5.14):

$$\mathbf{E}^e(x,\boldsymbol{\rho},\boldsymbol{\rho}'') = -j\omega\mu\left[\bar{\mathbf{I}} + \frac{1}{k^2}\nabla_t\nabla_t - \frac{j\beta}{k^2}(\nabla_t\hat{x} + \hat{x}\nabla_t) - \frac{\beta^2}{k^2}\hat{x}\hat{x}\right] I(x,\boldsymbol{\rho},\boldsymbol{\rho}'') \tag{5.15}$$

where $\nabla_t g = \hat{y}\partial g/\partial y + \hat{z}\partial g/\partial z$, and

$$I(x,\boldsymbol{\rho},\boldsymbol{\rho}'') = \int_{x'=-\infty}^{+\infty} g(\boldsymbol{\rho},\boldsymbol{\rho}';x,x')e^{-j\beta x'}dx' = e^{-j\beta x}H(\boldsymbol{\rho},\boldsymbol{\rho}'') \tag{5.16}$$

$$I_x = \int_{x'=-\infty}^{+\infty} \frac{\partial g}{\partial x}e^{-j\beta x'}dx' = -j\beta I \tag{5.17}$$

$$I_{xx} = \int_{x'=-\infty}^{+\infty} \frac{\partial^2 g}{\partial x^2}e^{-j\beta x'}dx' = -\beta^2 I \tag{5.18}$$

$$H(\boldsymbol{\rho},\boldsymbol{\rho}'') = \frac{1}{4j}H_0^{(2)}\left(|\boldsymbol{\rho}-\boldsymbol{\rho}''|\sqrt{k^2-\beta^2}\right) \tag{5.19}$$

The integral definition of (5.16) is from [60].

From the above derivation, we can see that the current $\mathbf{J}(\boldsymbol{\rho}')e^{-j\beta x}$ will generate field $\mathbf{E}^e(\boldsymbol{\rho})e^{-j\beta x}$. By depressing propagation term $e^{-j\beta x}$, we only focus on field $\mathbf{E}^e(\boldsymbol{\rho})$ generated by current $\mathbf{J}(\boldsymbol{\rho}')$ through the DFG as:

$$\mathbf{E}^e(\boldsymbol{\rho}) = -j\omega\mu\langle\bar{\mathbf{G}}^{EJ},\mathbf{J}\rangle = -j\omega\mu\int_c \bar{\mathbf{G}}^{EJ}\cdot\mathbf{J}(\boldsymbol{\rho}')dl' \tag{5.20}$$

where

$$\bar{\mathbf{G}}^{EJ}(\boldsymbol{\rho},\boldsymbol{\rho}') = \left[\bar{\mathbf{I}} + \frac{1}{k^2}\nabla_t\nabla_t - \frac{j\beta}{k^2}(\nabla_t\hat{x} + \hat{x}\nabla_t) - \frac{\beta^2}{k^2}\hat{x}\hat{x}\right] H(\boldsymbol{\rho},\boldsymbol{\rho}') \tag{5.21}$$

Then, let's consider the electric field generated by the magnetic current:

$$\mathbf{E}^h = -\frac{1}{\varepsilon}\nabla \times \mathbf{F} = \iint_s \bar{\mathbf{G}}^{EM}(\mathbf{r}, \mathbf{r}') \cdot \mathbf{M}(\mathbf{r}')ds' \tag{5.22}$$

where

$$\bar{\mathbf{G}}^{EM}(\mathbf{r}, \mathbf{r}') = \begin{bmatrix} 0 & \frac{\partial g}{\partial z} & -\frac{\partial g}{\partial y} \\ -\frac{\partial g}{\partial z} & 0 & \frac{\partial g}{\partial x} \\ \frac{\partial g}{\partial y} & -\frac{\partial g}{\partial x} & 0 \end{bmatrix} = -\nabla g \times \bar{\mathbf{I}} \tag{5.23}$$

such that:

$$\mathbf{E}^h(\boldsymbol{\rho}) = \langle \bar{\mathbf{G}}^{EM}, \mathbf{M} \rangle = \int_c \bar{\mathbf{G}}^{EM} \cdot \mathbf{M}(\boldsymbol{\rho}')dl' \tag{5.24}$$

where

$$\bar{\mathbf{G}}^{EM}(\boldsymbol{\rho}, \boldsymbol{\rho}') = \left[\hat{x}\hat{y}\partial_z - \hat{x}\hat{z}\partial_y - \hat{y}\hat{x}\partial_z - j\beta\hat{y}\hat{z} + \hat{z}\hat{x}\partial_y + j\beta\hat{z}\hat{y}\right] H(\boldsymbol{\rho}, \boldsymbol{\rho}') \tag{5.25}$$

5.3.2 The spectral domain DGF of the external problem

Consider a general multilayered medium which is transversely unbounded with respect to the z axis as shown in Figure 5.4. The fields must obey the Maxwell's equations:

$$\begin{aligned} \nabla \times \mathbf{E} &= -j\omega\mu_0\mu_r\mathbf{H} - \mathbf{M} \\ \nabla \times \mathbf{H} &= j\omega\varepsilon_0\varepsilon_r\mathbf{E} + \mathbf{J} \end{aligned} \tag{5.26}$$

Assuming the wave is propagating along the x direction with a propagation constant β, we can solve the hybrid modes solution by decoupling the field into two independent configurations as TE^z(LSE) and TM^z(LSM) modes [60]. Therefore, the Fourier transform is only applied over y:

$$\tilde{f}(\alpha, z) = \int_{-a}^{a} f(y, z)e^{j\alpha y}dy \tag{5.27}$$

$$f(y, z) = \frac{1}{2\pi}\int_{-\infty}^{\infty} \tilde{f}(\alpha, z)e^{-j\alpha y}d\alpha \tag{5.28}$$

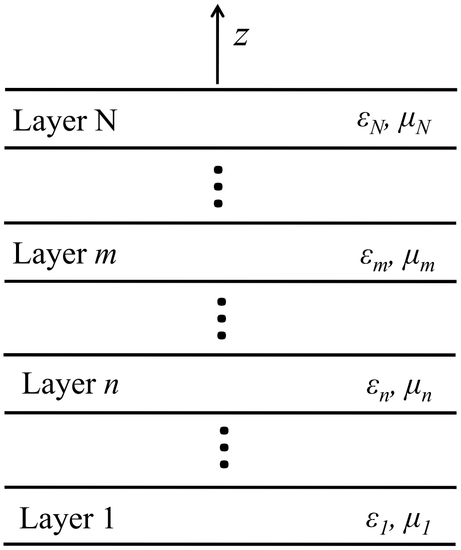

Figure 5.4 A transversely unbounded multilayered medium.

The spatial transverse coordinate $\boldsymbol{\rho} = \hat{x}x + \hat{y}y$ is replaced by its spectral counterpart $\mathbf{k}_\rho = \hat{x}\beta + \hat{y}\alpha$, and s is the transverse parametric variable on $x-y$ plane. The Maxwell's equations (5.26) can be rewrite as [46]:

$$\frac{d}{dz}\tilde{\mathbf{E}}_s = \frac{1}{j\omega\varepsilon_0\varepsilon_r}\left(k_0^2\mu_r\varepsilon_r\bar{\mathbf{I}} - \mathbf{k}_\rho\mathbf{k}_\rho\right)\cdot\left(\tilde{\mathbf{H}}_s\times\hat{z}\right) + \frac{\tilde{J}_z}{\omega\varepsilon_0\varepsilon_r}\mathbf{k}_\rho - \tilde{\mathbf{M}}_s\times\hat{z} \tag{5.29a}$$

$$\frac{d}{dz}\tilde{\mathbf{H}}_s = \frac{1}{j\omega\mu_0\mu_r}\left(k_0^2\mu_r\varepsilon_r\bar{\mathbf{I}} - \mathbf{k}_\rho\mathbf{k}_\rho\right)\cdot\left(\hat{z}\times\tilde{\mathbf{E}}_s\right) + \frac{\tilde{M}_z}{\omega\mu_0\mu_r}\mathbf{k}_\rho - \hat{z}\times\tilde{\mathbf{J}}_s \tag{5.29b}$$

$$-j\omega\varepsilon_0\varepsilon_r\tilde{E}_z = j\mathbf{k}_\rho\cdot\left(\tilde{\mathbf{H}}_s\times\hat{z}\right) + \tilde{J}_z \tag{5.29c}$$

$$-j\omega\mu_0\mu_r\tilde{H}_z = j\mathbf{k}_\rho\cdot\left(\hat{z}\times\tilde{\mathbf{E}}_s\right) + \tilde{M}_z \tag{5.29d}$$

We can simplify the subsequent analysis by rotating the spectral domain transverse components in the (x, y) coordinate by an angle θ to the new coordinate (u, v) as shown in Figure 5.5:

$$\begin{bmatrix} \hat{u} \\ \hat{v} \end{bmatrix} = \begin{bmatrix} \cos\theta & \sin\theta \\ -\sin\theta & \cos\theta \end{bmatrix}\begin{bmatrix} \hat{x} \\ \hat{y} \end{bmatrix} \tag{5.30}$$

$$\cos\theta = \frac{\beta}{k_\rho}, \ \sin\theta = \frac{\alpha}{k_\rho} \tag{5.31}$$

Then, as reported in [81], two decoupled sets of transmission line equations are obtained:

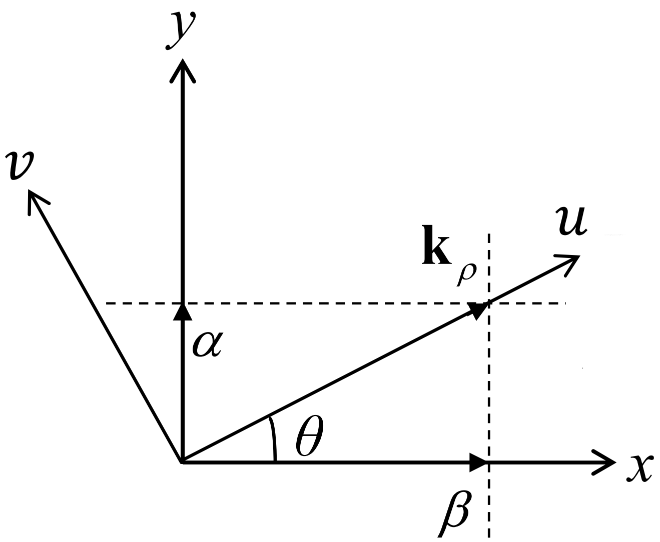

Figure 5.5 Spectral domain coordinate rotation from (x, y) to (u, v).

$$\frac{d}{dz}\tilde{E}_u^e = -jk_z Z^e \tilde{H}_v^e + \frac{k_\rho}{\omega\varepsilon_0\varepsilon_r}\tilde{J}_z - \tilde{M}_v \tag{5.32a}$$

$$\frac{d}{dz}\tilde{H}_v^e = -jk_z Y^e \tilde{E}_u^e - \tilde{J}_u \tag{5.32b}$$

$$\tilde{E}_z^e = -\frac{1}{j\omega\varepsilon_0\varepsilon_r}\left(jk_\rho \tilde{H}_v^e + \tilde{J}_z\right) \tag{5.32c}$$

and

$$\frac{d}{dz}\tilde{E}_v^h = -jk_z Z^h \tilde{H}_u^h + \tilde{M}_u \tag{5.33a}$$

$$\frac{d}{dz}\tilde{H}_u^h = -jk_z Y^h \tilde{E}_v^h - \frac{k_\rho}{\omega\mu_0\mu_r}\tilde{M}_z - \tilde{J}_v \tag{5.33b}$$

$$\tilde{H}_z^h = \frac{1}{j\omega\mu_0\mu_r}\left(jk_\rho\tilde{E}_v^h - \tilde{M}_z\right) \tag{5.33c}$$

where the superscript e and h represent the TM and TE respectively, and

$$Z^e = \frac{1}{Y^e} = \frac{k_z}{\omega\varepsilon_0\varepsilon_r},\; Z^h = \frac{1}{Y^h} = \frac{\omega\mu_0\mu_r}{k_z} \tag{5.34a}$$

$$k_z = \sqrt{k_0^2\varepsilon_r\mu_r - k_\rho^2} \tag{5.34b}$$

If we consider the spectral domain electric and magnetic fields $\tilde{E}_u^e, \tilde{H}_v^e$ as voltage and current V^e, I^e on a TM transmission line. And $\tilde{E}_v^h, \tilde{H}_u^h$ can be considered as voltage and current V^h, I^h on a TE transmission line. We can express the transverse electric and magnetic fields as [46]:

$$\tilde{\mathbf{E}}_s = \hat{u}V^e + \hat{v}V^h \tag{5.35}$$

$$\tilde{\mathbf{H}}_s \times \hat{z} = \hat{u}I^e + \hat{v}I^h \tag{5.36}$$

Therefore, the spectral fields now can be expressed as [46]:

$$\tilde{\mathbf{E}} = \hat{u}V^e + \hat{v}V^h - \hat{z}\frac{1}{j\omega\varepsilon_0\varepsilon_r}\left(jk_\rho I^e + \tilde{J}_z\right) \tag{5.37}$$

$$\tilde{\mathbf{H}} = -\hat{u}I^h + \hat{v}I^e + \hat{z}\frac{1}{j\omega\mu_0\mu_r}\left(jk_\rho V^h - \tilde{M}_z\right) \tag{5.38}$$

We obtain the spectral domain DGF in the (u, v, z) coordinate first, and then rotate back to the (x, y, z) coordinate by using the formula:

$$\begin{bmatrix} A_x \\ A_y \\ A_z \end{bmatrix} = T^{-1}\begin{bmatrix} \tilde{g}_{uu} & \tilde{g}_{uv} & \tilde{g}_{uz} \\ \tilde{g}_{vu} & \tilde{g}_{vv} & \tilde{g}_{vz} \\ \tilde{g}_{zu} & \tilde{g}_{zv} & \tilde{g}_{zz} \end{bmatrix} T \begin{bmatrix} J_x \\ J_y \\ J_z \end{bmatrix} \tag{5.39}$$

where T is the rotation transform matrix and its inverse matrix T^{-1}:

$$T = \begin{bmatrix} \cos\theta & \sin\theta & 0 \\ -\sin\theta & \cos\theta & 0 \\ 0 & 0 & 1 \end{bmatrix},\; T^{-1} = T^T = \begin{bmatrix} \cos\theta & -\sin\theta & 0 \\ \sin\theta & \cos\theta & 0 \\ 0 & 0 & 1 \end{bmatrix} \tag{5.40}$$

The spectral domain DGF in the (u, v, z) coordinate is given as [46]:

$$\begin{aligned}\tilde{\bar{\mathbf{G}}}_l^{EJ} &= -\hat{u}\hat{u}V_i^e - \hat{v}\hat{v}V_i^h + \hat{z}\hat{u}\frac{k_\rho}{\omega\varepsilon_m}I_i^e + \hat{u}\hat{z}\frac{k_\rho}{\omega\varepsilon'_n}V_v^e \\ &+ \hat{z}\hat{z}\frac{1}{j\omega\varepsilon'_n}\left[\frac{k_\rho^2}{j\omega\varepsilon_m}I_v^e - \delta(z-z')\right]\end{aligned} \tag{5.41}$$

$$\tilde{\bar{\mathbf{G}}}_l^{HJ} = \hat{u}\hat{v}I_i^h - \hat{v}\hat{u}I_i^e - \hat{z}\hat{v}\frac{k_\rho}{\omega\mu_m}V_i^h + \hat{v}\hat{z}\frac{k_\rho}{\omega\varepsilon'_n}I_v^e \tag{5.42}$$

$$\tilde{\bar{\mathbf{G}}}_l^{EM} = -\hat{u}\hat{v}V_v^e + \hat{v}\hat{u}V_v^h + \hat{z}\hat{v}\frac{k_\rho}{\omega\varepsilon_m}I_v^e - \hat{v}\hat{z}\frac{k_\rho}{\omega\mu'_n}V_i^h \tag{5.43}$$

$$\begin{aligned}\tilde{\bar{\mathbf{G}}}_l^{HM} &= -\hat{u}\hat{u}I_v^h - \hat{v}\hat{v}I_v^e + \hat{z}\hat{u}\frac{k_\rho}{\omega\mu_m}V_v^h + \hat{u}\hat{z}\frac{k_\rho}{\omega\mu'_n}I_i^h \\ &+ \hat{z}\hat{z}\frac{1}{j\omega\mu'_n}\left[\frac{k_\rho^2}{j\omega\mu_m}V_i^h - \delta(z-z')\right]\end{aligned} \tag{5.44}$$

V_i^p, V_v^p, I_i^p, and I_v^p are called as the transmission line Green's functions. ε_m and μ_m are referred to field points in layer m, while ε'_n and μ'_n are referred to source points in layer n. Consider the case that the source and observation points are in the same layer, the transmission line Green's functions can be expressed as [46]:

$$V_i^p(z, z') = \frac{Z_n^p}{2}\left[e^{-jk_{zn}|z-z'|} + \frac{1}{D_n^p}\sum_{s=1}^{4} R_{ns}^p e^{-jk_{zn}l_{ns}}\right] \tag{5.45}$$

$$V_v^p(z, z') = \frac{1}{2}\left[\pm e^{-jk_{zn}|z-z'|} - \frac{1}{D_n^p}\sum_{s=1}^{4}(-1)^s R_{ns}^p e^{-jk_{zn}l_{ns}}\right] \tag{5.46}$$

$$I_i^p(z, z') = \frac{1}{2}\left[\pm e^{-jk_{zn}|z-z'|} - \frac{1}{D_n^p}\sum_{s=1}^{4}(-1)^{\lfloor \frac{s}{2} \rfloor} R_{ns}^p e^{-jk_{zn}l_{ns}}\right] \tag{5.47}$$

$$I_v^p(z, z') = \frac{1}{2Z_n^p}\left[e^{-jk_{zn}|z-z'|} + \frac{1}{D_n^p}\sum_{s=1}^{4}(-1)^{\lfloor \frac{s+1}{2} \rfloor} R_{ns}^p e^{-jk_{zn}l_{ns}}\right] \tag{5.48}$$

where $p \in e, h$, and n is the index of the layer:

$$D_n^p = 1 - \overleftarrow{\Gamma}_n^p \overrightarrow{\Gamma}_n^p t_n^p \tag{5.49a}$$

$$R^p_{n_1} = \overrightarrow{\Gamma}^p_n \tag{5.49b}$$

$$R^p_{n_2} = \overleftarrow{\Gamma}^p_n \tag{5.49c}$$

$$R^p_{n_3} = R^p_{n4} = \overleftarrow{\Gamma}^p_n \overrightarrow{\Gamma}^p_n \tag{5.49d}$$

and d_n is the thickness of n^{th} layer and defined as $z_{n+1} - z_n$:

$$l_{n1} = 2z_{n+1} - (z + z') \tag{5.50a}$$

$$l_{n2} = (z + z') - 2z_n \tag{5.50b}$$

$$l_{n3} = 2d_n + (z - z') \tag{5.50c}$$

$$l_{n4} = 2d_n - (z - z') \tag{5.50d}$$

$\overleftarrow{\Gamma}^p_n$ and $\overrightarrow{\Gamma}^p_n$ are the voltage reflection coefficients looking to the $-z$ and $+z$ direction, respectively, out of the terminals of section n. These coefficients are calculated from the iterative relations:

$$\overleftarrow{\Gamma}^p_n = \frac{\Gamma^p_{n-1,n} + \overleftarrow{\Gamma}^p_{n-1} t^p_{n-1}}{1 + \Gamma^p_{n-1,n} \overleftarrow{\Gamma}^p_{n-1} t^p_{n-1}} \tag{5.51a}$$

$$\overrightarrow{\Gamma}^p_n = \frac{\Gamma^p_{n+1,n} + \overrightarrow{\Gamma}^p_{n+1} t^p_{n+1}}{1 + \Gamma^p_{n+1,n} \overrightarrow{\Gamma}^p_{n+1} t^p_{n+1}} \tag{5.51b}$$

where $t^p_n = e^{-j2k_{zn}d_n}$ and:

$$\Gamma^p_{m,n} = \frac{Z^p_m - Z^p_n}{Z^p_m + Z^p_n} \tag{5.52}$$

$$Z^e_n = \frac{k_{zn}}{\omega \varepsilon_0 \varepsilon_{r,n}} \tag{5.53}$$

$$Z_n^h = \frac{\omega\mu_0\mu_{r,n}}{k_{zn}} \tag{5.54}$$

$$k_{zn} = \sqrt{k_0^2\varepsilon_{r,n}\mu_{r,n} - (\beta^2+\alpha^2)} \tag{5.55}$$

In view of (5.40), (5.41), (5.42), (5.43) and (5.44), the spectral domain DGF in the (x, y, z) coordinate is now written as matrix form:

$$\tilde{\tilde{\mathbf{G}}}_l^{EJ} = \begin{bmatrix} -\cos^2\theta V_i^e - \sin^2\theta V_i^h & -\sin\theta\cos\theta(V_i^e - V_i^h) & \cos\theta\frac{k_\rho}{\omega\varepsilon_n'}V_v^e \\ -\sin\theta\cos\theta(V_i^e - V_i^h) & -\sin^2\theta V_i^e - \cos^2\theta V_i^h & \sin\theta\frac{k_\rho}{\omega\varepsilon_n'}V_v^e \\ \cos\theta\frac{k_\rho}{\omega\varepsilon_m}I_i^e & \sin\theta\frac{k_\rho}{\omega\varepsilon_m}I_i^e & \frac{1}{j\omega\varepsilon_n'}\left[\frac{k_\rho^2}{j\omega\varepsilon_m}I_v^e - \delta(z-z')\right] \end{bmatrix} \tag{5.56}$$

$$\tilde{\tilde{\mathbf{G}}}_l^{EM} = \begin{bmatrix} -\sin\theta\cos\theta(V_v^h - V_v^e) & -\sin^2\theta V_v^h - \cos^2\theta V_v^e & \sin\theta\frac{k_\rho}{\omega\mu_n'}V_i^h \\ \cos^2\theta V_v^h + \sin^2\theta V_v^e & \sin\theta\cos\theta(V_v^h - V_v^e) & -\cos\theta\frac{k_\rho}{\omega\mu_n'}V_i^h \\ -\sin\theta\frac{k_\rho}{\omega\varepsilon_m}I_v^e & \cos\theta\frac{k_\rho}{\omega\varepsilon_m}I_v^e & 0 \end{bmatrix} \tag{5.57}$$

$$\tilde{\tilde{\mathbf{G}}}_l^{HJ} = \begin{bmatrix} \sin\theta\cos\theta(I_i^e - I_i^h) & \sin^2\theta I_i^e + \cos^2\theta I_i^h & -\sin\theta\frac{k_\rho}{\omega\varepsilon_n'}I_v^e \\ -\cos^2\theta I_i^e - \sin^2\theta I_i^h & -\sin\theta\cos\theta(I_i^e - I_i^h) & -\cos\theta\frac{k_\rho}{\omega\varepsilon_n'}I_v^e \\ \sin\theta\frac{k_\rho}{\omega\mu_m}V_i^h & -\cos\theta\frac{k_\rho}{\omega\mu_m}V_i^h & 0 \end{bmatrix} \tag{5.58}$$

$$\tilde{\tilde{\mathbf{G}}}_l^{HM} = \begin{bmatrix} -\cos^2\theta I_v^h - \sin^2\theta I_v^e & -\sin\theta\cos\theta(I_v^h - I_v^e) & \cos\theta\frac{k_\rho}{\omega\mu_n'}I_i^h \\ -\sin\theta\cos\theta(I_v^h - I_v^e) & -\sin^2\theta I_v^h - \cos^2\theta I_v^e & \sin\theta\frac{k_\rho}{\omega\mu_n'}I_i^h \\ \cos\theta\frac{k_\rho}{\omega\mu_m}V_v^h & \sin\theta\frac{k_\rho}{\omega\mu_m}V_v^h & \frac{1}{j\omega\mu_n'}\left[\frac{k_\rho^2}{j\omega\mu_m}V_i^h - \delta(z-z')\right] \end{bmatrix} \tag{5.59}$$

5.4 Current Basis Functions and Shielded Environment

5.4.1 Current basis functions

The surface of the metal strip with an arbitrary cross section is divided into N_s pieces. As shown in Figure 5.6, $\hat{t}_i$ and $\hat{n}_i$ are the unit tangential and normal vector to the i^{th} segment. ϕ_i is the polar angle defining the outward normal vector of the i^{th} segment.

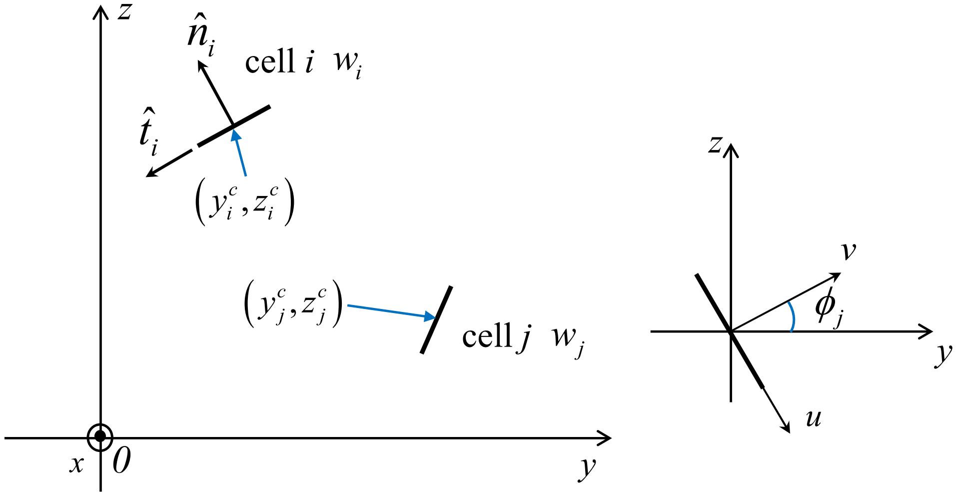

Figure 5.6 Spectral domain coordinate rotation from (x, y) to (u, v)

$$\hat{n}_i = \cos\phi_i \hat{y} + \sin\phi_i \hat{z} \tag{5.60a}$$

$$\hat{t}_i = -\sin\phi_i \hat{y} + \cos\phi_i \hat{z} \tag{5.60b}$$

And u and v are parametric variables describing the local coordinate for each segment:

$$u = \sin\phi_i (y - y_i^c) - \cos\phi_i (z - z_i^c) \tag{5.61a}$$

$$v = \cos\phi_i(y - y_i^c) + \sin\phi_i(z - z_i^c) \tag{5.61b}$$

$$y = \sin\phi_i u + \cos\phi_i v + y_i^c \tag{5.61c}$$

$$z = -\cos\phi_i u + \sin\phi_i v + z_i^c \tag{5.61d}$$

where (y_i^c, z_i^c) is the coordinate of the center point of i^{th} segment. And y, z have the following relation in each segment:

$$y = f(z) = -\tan\phi_i(z - z_i^c) + y_i^c \tag{5.62}$$

The longitudinal (x) current is expanded as a linear combination of pulse basis-piecewise constant, and the transverse (t) current on the strip can be written as a linear combination of rooftop functions-piecewise linear:

$$\mathbf{J}_s = \hat{x}\sum_{j=1}^{N_s} J_{xj}b_{xj} + \hat{t}\sum_{j=1}^{N_s} J_{tj}b_{tj} \tag{5.63}$$

$$\mathbf{M}_s = \hat{x}\sum_{j=1}^{N_s} M_{xj}b_{xj} + \hat{t}\sum_{j=1}^{N_s} M_{tj}b_{tj} \tag{5.64}$$

where J_{xj}, J_{tj}, M_{xj}, and M_{tj} are unknown coefficients need to solve, and b_{xj} is the pulse basis function and b_{tj} is the rooftop basis function:

$$b_{xj} = \Pi(u/w_j)\delta^k(v) \tag{5.65}$$

$$b_{tj} = \begin{cases} \frac{u-u_{j-1}}{w_j}\delta^k(v), & u_{j-1} \le u \le u_j \\ \frac{u_{j+1}-u}{w_{j+1}}\delta^k(v), & u_j \le u \le u_{j+1} \end{cases} \tag{5.66}$$

where $\Pi(x)$ is the rectangular function, and $\delta^k(x)$ is the Kronecker delta function:

$$\Pi(x) = \begin{cases} 1, & |x| < \frac{1}{2} \\ \frac{1}{2}, & |x| = \frac{1}{2} \\ 0, & |x| > \frac{1}{2} \end{cases} \tag{5.67}$$

$$\delta^k(x) = \begin{cases} 1, & x = 0 \\ 0, & x \neq 0 \end{cases} \tag{5.68}$$

5.4.2 Shielded environment and boundary conditions

The external problem is defined in a shielded environment. We represent the effect of the two side walls by a set of image source radiating in a laterally unbounded medium. First, let's look at electric current sources J_x and J_y located at (y, z) inside the rectangular shield and their images located at $(-y, z)$, as illustrated in Figure 5.7. The two-source set (the original source plus the image) forms the basic image set (BIS) [46].

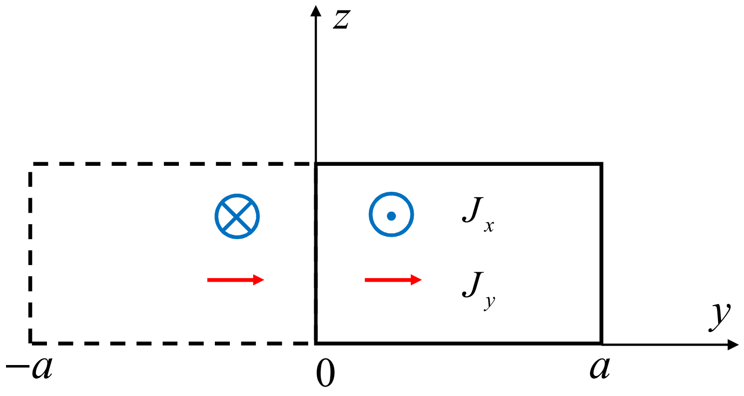

Figure 5.7 Electric current sources inside a rectangular shield and their images due to the y=0 PEC plane.

To maintain the correct boundary conditions at the two side walls, the BIS must be imaged in the $y = a$ PEC plane, and the new image set must again be imaged in the $y = 0$ planes, etc. Thus, a periodic lattice of BISs is obtained, which periods $2a$ along the y axis. The currents are infinitely periodic functions, which is denoted as a superscript p.

$$\mathbf{J}^p_\lambda = \sum_{j=1}^{N_s} J_{\lambda j} b^{Jp}_{\lambda j}, \quad \mathbf{M}^p_\lambda = \sum_{j=1}^{N_s} M_{\lambda j} b^{Mp}_{\lambda j} \tag{5.69}$$

where

$$b^{Qp}_{\lambda j}(y',z') = \begin{cases} b^{Qp}_{\lambda j}(y')\delta^{k}(z'-z^{c}_{j}), & |\phi_j| = \frac{\pi}{2} \\ b_{\lambda j}(z')\delta^{Qp}_{\lambda j}(y') \quad , & |\phi_j| \neq \frac{\pi}{2} \end{cases} \tag{5.70}$$

and $Q = J$ or M, $\lambda = x$ or t. Then, due to the image theory, we have:

$$b^{Qp}_{xj}(y') = \sum_{n=-\infty}^{\infty} \left[b_{xj}(y'-2na) + C^{Q}_{x} b_{xj}(-y'-2na) \right] \tag{5.71}$$

$$\begin{aligned} \hat{t}b^{Qp}_{tj}(y') =& \hat{y} \sum_{n=-\infty}^{\infty} \left[b_{yj}(y'-2na) + C^{Q}_{y} b_{yj}(-y'-2na) \right] + \\ & \hat{z} \sum_{n=-\infty}^{\infty} \left[b_{zj}(y'-2na) + C^{Q}_{z} b_{zj}(-y'-2na) \right] \end{aligned} \tag{5.72}$$

$$\delta^{Qp}_{xj}(y') = \sum_{n=-\infty}^{\infty} \left[\delta^{k}(y'-y^{c}_{j}-2na) + C^{Q}_{x} \delta^{k}(y'+y^{c}_{j}-2na) \right] \tag{5.73}$$

$$\begin{aligned} \hat{t}\delta^{Qp}_{tj}(y') =& \hat{y} \sum_{n=-\infty}^{\infty} \left[\delta^{k}(y'-y^{c}_{j}-2na) + C^{Q}_{y} \delta^{k}(y'+y^{c}_{j}-2na) \right] + \\ & \hat{z} \sum_{n=-\infty}^{\infty} \left[\delta^{k}(y'-y^{c}_{j}-2na) + C^{Q}_{z} \delta^{k}(y'+y^{c}_{j}-2na) \right] \end{aligned} \tag{5.74}$$

where

$$C^{Q}_{x} = C^{Q}_{z} \begin{cases} -1, & Q = J \\ +1, & Q = M \end{cases} \quad , \quad C^{Q}_{y} = \begin{cases} +1, & Q = J \\ -1, & Q = M \end{cases} \tag{5.75}$$

The testing and basis functions are infinite periodic function, which can be expanded as Fourier series:

$$f(y') = \frac{1}{2a} \sum_{n=-\infty}^{\infty} \tilde{f}(\alpha_n) e^{-j\alpha_n y'} \tag{5.76}$$

$$\tilde{f}(\alpha_n) = \int_{-a}^{a} f(y') e^{j\alpha_n y'} dy' \tag{5.77}$$

where $\alpha_n = n\pi/a$.

5.5 Matrix Equations and Method of Moments

With the integral equation (2D-PMCHWT) and the Green's functions available, also by introducing the pulse basis and triangular basis, the method of moments (MoM) is employed to solve the integral equation. The matrix equation is written as:

$$\begin{bmatrix} K_{mn}^{E_xJ_x} & K_{mn}^{E_xJ_t} & K_{mn}^{E_xM_x} & K_{mn}^{E_xM_t} \\ K_{mn}^{E_tJ_x} & K_{mn}^{E_tJ_t} & K_{mn}^{E_tM_x} & K_{mn}^{E_tM_t} \\ K_{mn}^{H_xJ_x} & K_{mn}^{H_xJ_t} & K_{mn}^{H_xM_x} & K_{mn}^{H_xM_t} \\ K_{mn}^{H_tJ_x} & K_{mn}^{H_tJ_t} & K_{mn}^{H_xM_x} & K_{mn}^{H_tM_t} \end{bmatrix} \begin{bmatrix} a \\ b \\ c \\ d \end{bmatrix} = \begin{bmatrix} 0 \\ 0 \\ 0 \\ 0 \end{bmatrix} \tag{5.78}$$

Each matrix element consists two parts: internal part $H_{mn}^{P_\alpha Q_\beta}$ and external part $L_{mn}^{P_\alpha Q_\beta}$:

$$K_{mn}^{P_\alpha Q_\beta} = H_{mn}^{P_\alpha Q_\beta} + L_{mn}^{P_\alpha Q_\beta} \tag{5.79}$$

where $m, n = 1, \ldots, N_s$, $P \in \{E, H\}$, $Q \in \{J, M\}$, and $(\alpha, \beta) \in \{x, t\}$. The propagation constant β, for each frequency point ω can be found by solving the determinant of (5.78) equal to zero.

5.5.1 Internal part

From the Green's function and basis function introduced above and by using the Galerkin method, we have the following integral:

$$H_{mn}^{P_\alpha Q_\beta} = \langle t_m^\alpha, G_{\alpha\beta}^{PQ}, b_n^\beta \rangle = \langle \hat{\alpha} t_m^\alpha, \bar{\mathbf{G}}^{PQ}, \hat{\beta} b_n^\beta \rangle \tag{5.80}$$

(1) As $P = E$ and $Q = J$, we have:

$$\begin{aligned} &\frac{H_{mn}^{E_\alpha J_\beta}}{-j\omega\mu} = \langle \hat{\alpha} t_m^\alpha, \bar{\mathbf{G}}^{EJ}, \hat{\beta} b_n^\beta \rangle \qquad (5.81) \\ &= \langle \hat{\alpha} t_m^\alpha, \left[\bar{\mathbf{I}} + \frac{1}{k^2} \nabla_t \nabla_t - \frac{j\beta}{k^2} (\nabla_t \hat{x} + \hat{x} \nabla_t) - \frac{\beta^2}{k^2} \hat{x}\hat{x} \right], \hat{\beta} b_n^\beta \rangle \\ &= \langle \hat{\alpha} t_m^\alpha, H, \hat{\beta} b_n^\beta \rangle + \frac{1}{k^2} \langle \hat{\alpha} t_m^\alpha, \nabla_t \nabla_t H, \hat{\beta} b_n^\beta \rangle - \frac{j\beta}{k^2} \langle \hat{\alpha} t_m^\alpha, (\nabla_t \hat{x} + \hat{x} \nabla_t) H, \hat{\beta} b_n^\beta \rangle - \frac{\beta^2}{k^2} \langle \hat{\alpha} t_m^\alpha, \hat{x}\hat{x} H, \hat{\beta} b_n^\beta \rangle \\ &= \langle \hat{\alpha} t_m^\alpha, H, \hat{\beta} b_n^\beta \rangle - \frac{1}{k^2} \langle \nabla_t \cdot \hat{\alpha} t_m^\alpha, H, \nabla_t \cdot \hat{\beta} b_n^\beta \rangle + \frac{j\beta}{k^2} \langle \nabla_t \cdot \hat{\alpha} t_m^\alpha, H, \hat{x} \cdot \hat{\beta} b_n^\beta \rangle \\ &\quad - \frac{j\beta}{k^2} \langle \hat{x} \cdot \hat{\alpha} t_m^\alpha, H, \nabla_t \cdot \hat{\beta} b_n^\beta \rangle - \frac{\beta^2}{k^2} \langle \hat{x} \cdot \hat{\alpha} t_m^\alpha, H, \hat{x} \cdot \hat{\beta} b_n^\beta \rangle \end{aligned}$$

Since:

$$\langle \mathbf{t}_m, \nabla_t \nabla_t H, \mathbf{b}_n \rangle = -\langle \nabla_t \cdot \mathbf{t}_m, H, \nabla_t \cdot \mathbf{b}_n \rangle \tag{5.82}$$

$$\langle \mathbf{t}_m, \nabla_t \hat{x} H, \mathbf{b}_n \rangle = -\langle \nabla_t \cdot \mathbf{t}_m, H, \hat{x} \cdot \mathbf{b}_n \rangle \tag{5.83}$$

$$\langle \mathbf{t}_m, \hat{x} \nabla_t H, \mathbf{b}_n \rangle = \langle \hat{x} \cdot \mathbf{t}_m, H, \nabla_t \cdot \mathbf{b}_n \rangle \tag{5.84}$$

$$\nabla_t \cdot \mathbf{f}_m = -\frac{\partial f_m^t}{\partial u} \tag{5.85}$$

Such that:

$$\frac{H_{mn}^{E_x J_x}}{-j\omega\mu} = \langle t_m^x, H, b_n^x \rangle - \frac{\beta^2}{k^2} \langle t_m^x, H, b_n^x \rangle \tag{5.86}$$

$$\frac{H_{mn}^{E_x J_t}}{-j\omega\mu} = \frac{j\beta}{k^2} \langle t_m^x, H, \frac{\partial b_n^t}{\partial u} \rangle \tag{5.87}$$

$$\frac{H_{mn}^{E_t J_x}}{-j\omega\mu} = -\frac{j\beta}{k^2} \langle \frac{\partial t_m^t}{\partial u}, H, b_n^x \rangle \tag{5.88}$$

$$\frac{H_{mn}^{E_t J_t}}{-j\omega\mu} = \langle t_m^t, H, b_n^t \rangle - \frac{1}{k^2} \langle \frac{\partial t_m^t}{\partial u}, H, \frac{\partial b_n^t}{\partial u} \rangle \tag{5.89}$$

(2) As $P = E$ and $Q = M$, we have:

$$\begin{aligned} H_{mn}^{E_\alpha M_\beta} &= \langle \hat{\alpha} t_m^\alpha, \bar{\mathbf{G}}^{EM}, \hat{\beta} b_n^\beta \rangle \qquad (5.90) \\ &= \langle \hat{\alpha} t_m^\alpha, [\hat{x}\hat{y}\partial_z - \hat{x}\hat{z}\partial_y - \hat{y}\hat{x}\partial_z - j\beta\hat{y}\hat{z} + \hat{z}\hat{x}\partial_y + j\beta\hat{z}\hat{y}]\, H, \hat{\beta} b_n^\beta \rangle \\ &= \langle \hat{x} \cdot \hat{\alpha} t_m^\alpha, \frac{\partial H}{\partial z}, \hat{y} \cdot \hat{\beta} b_n^\beta \rangle - \langle \hat{x} \cdot \hat{\alpha} t_m^\alpha, \frac{\partial H}{\partial y}, \hat{z} \cdot \hat{\beta} b_n^\beta \rangle - \langle \hat{y} \cdot \hat{\alpha} t_m^\alpha, \frac{\partial H}{\partial z}, \hat{x} \cdot \hat{\beta} b_n^\beta \rangle \\ &+ \langle \hat{z} \cdot \hat{\alpha} t_m^\alpha, \frac{\partial H}{\partial y}, \hat{x} \cdot \hat{\beta} b_n^\beta \rangle - j\beta \langle \hat{y} \cdot \hat{\alpha} t_m^\alpha, H, \hat{z} \cdot \hat{\beta} b_n^\beta \rangle + j\beta \langle \hat{z} \cdot \hat{\alpha} t_m^\alpha, H, \hat{y} \cdot \hat{\beta} b_n^\beta \rangle \end{aligned}$$

Such that:

$$H_{mn}^{E_x M_x} = 0 \tag{5.91}$$

$$H_{mn}^{E_xM_t} = \langle t_m^x, \frac{\partial H}{\partial z}, \hat{y}\cdot\hat{t}b_n^t\rangle - \langle t_m^x, \frac{\partial H}{\partial y}, \hat{z}\cdot\hat{t}b_n^t\rangle = -\langle t_m^x, \frac{\partial H}{\partial y}\cos\phi_n + \frac{\partial H}{\partial z}\sin\phi_n, b_n^t\rangle \tag{5.92}$$

$$H_{mn}^{E_tM_x} = \langle \hat{z}\cdot\hat{t}t_m^t, \frac{\partial H}{\partial y}, b_n^x\rangle - \langle \hat{y}\cdot\hat{t}t_m^t, \frac{\partial H}{\partial z}, b_n^x\rangle = \langle t_m^t, \frac{\partial H}{\partial y}\cos\phi_m + \frac{\partial H}{\partial z}\sin\phi_m, b_n^x\rangle \tag{5.93}$$

$$\begin{aligned} H_{mn}^{E_tM_t} &= -j\beta\left[\langle \hat{y}\cdot\hat{t}t_m^t, H, \hat{z}\cdot\hat{t}b_n^t\rangle - \langle \hat{z}\cdot\hat{t}t_m^t, H, \hat{y}\cdot\hat{t}b_n^t\rangle\right] \qquad (5.94) \\ &= -j\beta\langle t_m^t, (-\sin\phi_m\cos\phi_n + \cos\phi_m\sin\phi_n)H, b_n^t\rangle \end{aligned}$$

By using the dual prosperity, we can directly write the following matrix elements:

$$H_{mn}^{H_\alpha J_\beta} = -H_{mn}^{E_\alpha M_\beta} \tag{5.95}$$

$$H_{mn}^{H_\alpha M_\beta} = \frac{\varepsilon}{\mu}H_{mn}^{E_\alpha J_\beta} \tag{5.96}$$

5.5.2 External part

By using the spatial domain layered dyadic Green's function $\bar{\mathbf{G}}_l^{PQ}$, we have the following integral:

$$L_{mn}^{P_\alpha Q_\beta} = \langle \hat{\alpha}t_{\alpha i}^{Pp}, \bar{\mathbf{G}}_l^{PQ}, \hat{\beta}b_{\beta j}^{Qp}\rangle \tag{5.97}$$

Then, according to the pulse or triangular basis, we divide the integral into four different kinds:

$$L_{mn}^{P_xQ_x} = \langle \hat{x}t_{xi}^{Pp}, \bar{\mathbf{G}}_l^{PQ}, \hat{x}b_{xj}^{Qp}\rangle = l_{m,n}^{P_xQ_x} \tag{5.98}$$

$$L_{mn}^{P_xQ_t} = \langle \hat{x}t_{xi}^{Pp}, \bar{\mathbf{G}}_l^{PQ}, \hat{t}b_{tj}^{Qp}\rangle = \sum_{n_t\in\{n_t^+, n_t^-\}} l_{m,n_t}^{P_xQ_t} \tag{5.99}$$

$$L_{mn}^{P_tQ_x} = \langle \hat{t}t_{ti}^{Pp}, \bar{\mathbf{G}}_l^{PQ}, \hat{x}b_{xj}^{Qp}\rangle = \sum_{m_t\in\{m_t^+, m_t^-\}} l_{m_t,n}^{P_tQ_x} \tag{5.100}$$

$$L_{mn}^{P_tQ_t} = \langle \hat{t}t_{ti}^{Pp}, \bar{\mathbf{G}}_l^{PQ}, \hat{t}b_{tj}^{Qp}\rangle = \sum_{m_t\in\{m_t^+,m_t^-\}} \sum_{n_t\in\{n_t^+,n_t^-\}} l_{m_t,n_t}^{P_tQ_t} \tag{5.101}$$

where

$$l_{i,j}^{P_\alpha Q_\beta} = \int_{\text{cell } i} t_{\alpha i}^{Pp}(y,z)du \int_{\text{cell } j} G_{l\alpha\beta}^{PQ}(y,y';z,z')b_{\beta j}^{Qp}(y',z')du' \tag{5.102}$$

Then, we need to transfer the spatial integrals (5.102) to summations in spectral domain, because the spectral domain Green's functions are well defined in close form.

(1) $|\phi_i| = \frac{\pi}{2}$ and $|\phi_j| = \frac{\pi}{2}$

$$l_{i,j}^{P_\alpha Q_\beta} = \sin\phi_i \sin\phi_j \tilde{l}_{i,j}^{P_\alpha Q_\beta} \tag{5.103}$$

By using the integral definition of the delta function and the Parseval's theorem, also with the fact that the testing function is a pure real function so that the complex conjugate function is itself, we obtain:

$$\tilde{l}_{i,j}^{P_\alpha Q_\beta} = \frac{\pi}{2a^2} \sum_{n=-\infty}^{\infty} \tilde{t}_{\alpha i}^{Pp*}(\alpha_n) \tilde{G}_{l\alpha\beta}^{PQ}(\alpha_n; z_i^c, z_j^c) \tilde{b}_{\beta j}^{Qp}(\alpha_n) \tag{5.104}$$

where $\tilde{b}_{\beta j}^{Qp}$ are the Fourier transforms of the basis functions defined in (5.71) and (5.72):

$$\tilde{b}_{\beta j}^{Qp}(\alpha_n) = \int_{-a}^{a} b_{\beta j}^{Qp}(y') e^{j\alpha_n y'} dy' \tag{5.105}$$

and $\tilde{t}_{\alpha i}^{Pp}$ are the Fourier transforms of the testing functions. The testing functions are the same as the basis functions by using the Galerkin method. The superscript $*$ means the complex conjugate.

(2) $|\phi_i| \neq \frac{\pi}{2}$ and $|\phi_j| = \frac{\pi}{2}$

$$l_{i,j}^{P_\alpha Q_\beta} = -\cos\phi_i \sin\phi_j \tilde{l}_{i,j}^{P_\alpha Q_\beta} \tag{5.106}$$

where

$$\tilde{l}_{i,j}^{P_\alpha Q_\beta} = \frac{\pi}{2a^2} \sum_{n=-\infty}^{\infty} \tilde{\delta}_{\alpha i}^{Pp*}(\alpha_n) \tilde{b}_{\beta j}^{Qp}(\alpha_n) \int_{\text{cell } i} t_{\alpha i}(z) \tilde{G}_{l\alpha\beta}^{PQ}(\alpha_n; z, z_j^c) dz \tag{5.107}$$

where $\tilde{\delta}_{\alpha i}^{Pp}$ are the Fourier transforms of the delta functions defined in (5.73) and (5.74):

$$\tilde{\delta}_{\alpha i}^{Pp}(\alpha_n) = \int_{-a}^{a} \delta_{\alpha i}^{Pp}(y') e^{j\alpha_n y'} dy' \tag{5.108}$$

(3) $|\phi_i| = \frac{\pi}{2}$ and $|\phi_j| \neq \frac{\pi}{2}$

$$l_{i,j}^{P_\alpha Q_\beta} = -\sin\phi_i \cos\phi_j \tilde{l}_{i,j}^{P_\alpha Q_\beta} \tag{5.109}$$

where

$$\tilde{l}_{i,j}^{P_\alpha Q_\beta} = \frac{\pi}{2a^2} \sum_{n=-\infty}^{\infty} \tilde{t}_{\alpha i}^{Pp*}(\alpha_n)\tilde{\delta}_{\beta j}^{Qp}(\alpha_n) \int_{\text{cell } j} b_{\beta j}(z')\tilde{G}_{l\alpha\beta}^{PQ}(\alpha_n; z_i^c, z')dz' \tag{5.110}$$

(4) $|\phi_i| \neq \frac{\pi}{2}$ and $|\phi_j| \neq \frac{\pi}{2}$

$$l_{i,j}^{P_\alpha Q_\beta} = \cos\phi_i \cos\phi_j \tilde{l}_{i,j}^{P_\alpha Q_\beta} \tag{5.111}$$

where

$$\tilde{l}_{i,j}^{P_\alpha Q_\beta} = \frac{\pi}{2a^2} \sum_{n=-\infty}^{\infty} \tilde{\delta}_{\alpha i}^{Pp*}(\alpha_n)\tilde{\delta}_{\beta j}^{Qp}(\alpha_n) \int_{\text{cell } i} t_{\alpha i}(z)dz \int_{\text{cell } j} b_{\beta j}(z')\tilde{G}_{l\alpha\beta}^{PQ}(\alpha_n; z, z')dz' \tag{5.112}$$

5.6 Numerical Results

The technique is validated by an open rectangular cross section microstrip line sketched in the Figure 5.8. We set the length of the shielded box twenty times as w to approximate the open structure. The thickness of the PEC strip is varying, with $d/w = 0.2117$ and $\varepsilon_r = 9.8$. In Figure 5.8, the dispersion curves for the fundamental mode of a rectangular cross section microstrip line with different strip thickness are shown and compared with very good agreement to the results obtained by Coluccini *et al.* [47], by directly deriving an integral-differential equation formulation in the spectral domain that is subsequently reduced to a numerically stable one-dimensional electric field integral equation (EFIE) to handle the open case perfectly conducting microstrip lines with polygonal cross section.

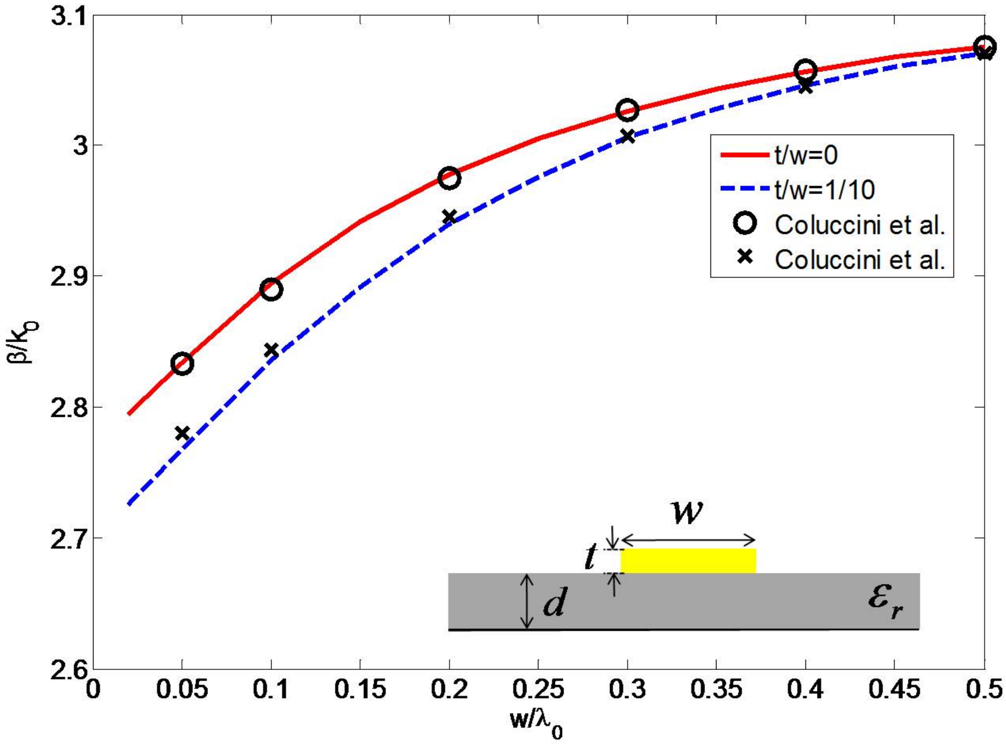

Figure 5.8 Dispersion curves for the fundamental mode of the rectangular cross section microstrip line with different strip thickness.

CHAPTER 6. CONCLUSIONS

In the first part of the dissertation, the current distribution and internal impedance have been studied by using integral equation methods. A rigorous volume integral equation (VIE) is developed for the current distribution over two-dimensional conducting cylinder with arbitrary cross section. It can be reduced to the widely-used quasi-static VIE in very low frequency. The accurate VIE gives almost the same results as the SIE, but the quasi-static VIE is not accurate enough for the current distribution as there is a constant ratio between the quasi-static VIE and SIE. Two more leading terms from the Hankel function have been added into the integral kernel to solve this problem. The current distributions calculated from different integral equations are compared and explained. The comparison of different definitions and boundary conditions for calculation of the internal impedance shows that it is mainly the different boundary conditions result in the different values of internal impedance. The different definitions will give the same internal impedance based on constant boundary value condition.

In the second part of the dissertation, the acceleration methods of the spectral domain approach (SDA) and approaches to handle the arbitrary cross section finite conductivity multilayered microstrip have been studied. Acceleration of the infinite series summation is the most difficult and important part in SDA, and asymptotic techniques as leading term extraction is the most complicated and time consuming procedure in the approaches like mid-point summation (MPS) and super convergent series (SCS). With the help of our proposed approach, the complexity of the SDA can be dramatically decreased because no asymptotic technique involves or only first leading term extraction needed. By using this approach, results are achieved as accurate as or even more accurate than the results obtained by using high order leading term extraction in MPS or SCS. Furthermore, the proposed approach is very simple and easy to implement. Then this acceleration approach is extended to handle the multiple metal lines and multilayered shielded microstrip lines by recasting the summation kernel into a suitable form for applying the Levin's transformation. It achieves convergence rates as fast as or even faster than high order asymptotic extraction techniques. This technique shows more advantages when it is extended to deal with the case of multilayered substrates and multiple strips, for which the spectral domain Green's function and basis functions are more complicated. The 2D PMCHWT formulation is developed along with the method of moments (MoM) to deal with the finite thickness (or arbitrary cross sections) and finite conductivity of the metal strips embedded in generalized multilayered shielded microstrip. The spatial and spectral domain dyadic Green's functions are used and the basis functions are chosen as pulse and triangular basis functions. The spatial integration is directly calculated in homogeneous medium in the internal region. While the spatial integration is transfered to the spectral domain summation by using Fourier transform and Parseval's theorem in the external region.

BIBLIOGRAPHY

[1] B. D. Hatton, K. Landskron, W. J. Hunks, M. R. Bennett, D. Shukaris, D. D. Perovic, and G. A. Ozin, "Materials chemistry for low-k materials," *Materials Today*, vol. 9, no. 3, pp. 22–31, Mar. 2006.

[2] *http://en.wikipedia.org/wiki/Signal-integrity.*

[3] *http://en.wikipedia.org/wiki/Parasitic-extraction.*

[4] A. Press, "Resistance and reactance of massed rectangular conductors," *Phys. Rev.*, vol. 8, no. 4, pp. 417–422, Oct. 1916.

[5] D. Cockcroft, "Skin effect in rectangular conductors at high frequencies," *Proc. Roy. Soc.*, vol. 122, no. 790, pp. 533–542, Feb. 1929.

[6] S. J. Haefner, "Alternating-current resistance of rectangular conductors," *Proc. IRE*, vol. 25, no. 4, pp. 434–447, Apr. 1937.

[7] P. Silvester, "Modal network theory of skin effect in flat conductors," *Proc. IEEE*, vol. 54, no. 9, pp. 1147–1151, Sep. 1966.

[8] ——, "The accurate calculation of skin effect in conductors of complicated shape," *IEEE Trans. Power App. Syst.*, vol. 87, no. 3, pp. 735–742, Mar. 1968.

[9] P. Hammond and J. Penman, "Calculation of eddy currents by dual energy methods," *Proc. Inst. Elect. Eng.*, vol. 125, pp. 701–708, 1978.

[10] E. Denlinger, “Losses of microstrip lines,” *IEEE Trans. Microw. Theory Tech.*, vol. 28, no. 6, pp. 513–522, Jun. 1980.

[11] L. Olson, “Application of the finite element method to determine the electrical resistance, inductance, capacitance parameters for the circuit package environment,” *IEEE Trans. Compon., Hybrids, Manuf. Technol.*, vol. 5, no. 4, pp. 486–492, Dec. 1982.

[12] M. Krakowski and H. Morawska, “Skin effect and eddy currents in a thin tape,” *Arch. Elektrotech.*, vol. 66, no. 2, pp. 95–98, Mar. 1983.

[13] P. Waldow and I. Wolff, “The skin-effect at high frequencies,” *IEEE Trans. Microw. Theory Tech.*, vol. 33, no. 10, pp. 1076–1082, Oct. 1985.

[14] A. Djordjevic, T. Sarkar, and S. Rao, “Analysis of finite conductivity cylindrical conductors excited by axially-independent tm electromagnetic field,” *IEEE Trans. Microw. Theory Tech.*, vol. 33, no. 10, pp. 960–966, Oct. 1985.

[15] R. B. Wu and J. C. Yang, “Boundary integral equation formulation of skin effect problems in multiconductor transmission lines,” *IEEE Trans. Magn.*, vol. 25, no. 4, pp. 3013–3015, Jul. 1989.

[16] R. Faraji-Dana and Y. Chow, “The current distribution and ac resistance of a microstrip structure,” *IEEE Trans. Microw. Theory Tech.*, vol. 38, no. 9, pp. 1268–1277, Sep. 1990.

[17] ——, “Ac resistance of two coupled strip conductors,” *Proc. Inst. Elect. Eng. Microw., Antennas, Propag.*, vol. 138, no. 1, pp. 37–45, Feb. 1991.

[18] M. Tsuk and J. Kong, “A hybrid method for the calculation of the resistance and inductance of transmission lines with arbitrary cross sections,” *IEEE Trans. Microw. Theory Tech.*, vol. 39, no. 8, pp. 1338–1347, Aug. 1991.

[19] S. Ramo, J. R. Whinnery, and T. V. Duzer, *Fields and Waves in Communication Electronics.* New York: Wiley, 1984.

[20] G. Antonini, A. Orlandi, and C. R. Paul, “Internal impedance of conductors of rectangular cross section,” *IEEE Trans. Microw. Theory Tech.*, vol. 47, no. 7, pp. 979–985, Jul. 1999.

[21] F. Medina and R. Marques, “Comments on ‘internal impedance of conductors of rectangular cross section’,” *IEEE Trans. Microw. Theory Tech.*, vol. 49, no. 8, pp. 1511–1512, Aug. 2001.

[22] G. Antonini, A. orlandi, and C. R. Paul, “Authors’ reply,” *IEEE Trans. Microw. Theory Tech.*, vol. 49, no. 8, pp. 1512–1513, Aug. 2001.

[23] W. Heinrich, “Comments on ‘internal impedance of conductors of rectangular cross section’,” *IEEE Trans. Microw. Theory Tech.*, vol. 49, no. 3, pp. 580–581, Mar. 2001.

[24] P. Silvester, *Modern Electromagnetic Fields.* Englewood Cliffs, New York: Prentice-Hall, 1968.

[25] A. Rong and A. C. Cangellaris, “Note on the definition and calculation of the per-unit-length internal impedance of a uniform conducting wire,” *IEEE Trans. Electromagn. Compat.*, vol. 49, no. 3, pp. 677–681, Aug. 2007.

[26] A. F. Peterson, S. L. Ray, and R. Mittra, *Computational Methods for Electromagnetics.* New York: IEEE Press, 1998.

[27] I. Toyoda, M. Matsuhara, and N. Kumagai, “Extended integral equation formulation for scattering problems from a cylindrical scatterer,” *IEEE Trans. Antennas Propag.*, vol. 36, no. 11, pp. 1580–1586, Nov. 1988.

[28] C. You, M. M. Tentzeris, and W. Hwang, "Multilayer effects on microstrip antennas for their integration with mechanical structures," *IEEE Trans. Antennas Propag.*, vol. 55, no. 4, pp. 1051–1058, Apr. 2007.

[29] S. Jain, "Accurate and efficient modeling of interconnects in lossy layered media," Ph.D. dissertation, Iowa State University, Ames, Iowa, 2011.

[30] *www.ansys.com.*

[31] G. Cano, F. Medina, and M. Horno, "On the efficient implementation of SDA for boxed strip-like and slot-like structures," *IEEE Trans. Microw. Theory Tech.*, vol. 46, no. 11, pp. 1801–1806, Nov. 1998.

[32] J. L. Tsalamengas and G. Fikioris, "Rapidly converging spectral-domain analysis of rectangularly shielded layered microstrip lines," *IEEE Trans. Microw. Theory Tech.*, vol. 51, no. 6, pp. 1729–1734, Jun. 2003.

[33] J. Song and S. Jain, "Midpoint summation: A method for accurate and efficient summation of series appearing in electromagnetics," *IEEE Antennas Wireless Propag. Lett.*, vol. 9, pp. 1084–1087, 2010.

[34] S. Jain and J. Song, "Accelerated spectral domain approach for shielded microstrip lines by approximating summation with super convergent series," *IEEE Trans. Magn.*, vol. 49, no. 2, pp. 803–806, Feb. 2013.

[35] S. Jain, J. Song, T. Kamgaing, and Y. S. Mekonnen, "Acceleration of spectral domain approach for generalized multilayered shielded microstrip interconnects using two fast convergent series," *IEEE Trans. Compon., Packag., Manuf. Technol.*, vol. 3, no. 3, pp. 401–410, Mar. 2013.

[36] K. Michalski, "Extrapolation methods for Sommerfeld integral tails," *IEEE Trans. Antennas Propag.*, vol. 46, no. 10, pp. 1405–1418, Oct. 1998.

[37] N. Kinayman and M. I. Aksun, "Comparative study of acceleration techniques for integrals and series in electromagnetic problems," *Radio Sci.*, vol. 30, pp. 1713–1722, 1995.

[38] D. Levin, "Nonlinear transformations of divergent and slowly convergent sequences," *J. Math. Phys.*, vol. 34, pp. 1–42, 1955.

[39] P. Wynn, "On a device for computing the $e_m(s_n)$ transformation," *Math. Tables Aids Comput.*, vol. 10, pp. 91–96, 1956.

[40] D. Levin, "Development of nonlinear transformations for improving convergence of sequences," *Int. J. Comput. Math. Sec. B*, vol. 3, pp. 371–388, 1973.

[41] M. Blakemore, G. A. Evans, and J. Hyslop, "Comparison of some methods for evaluating infinite range oscillatory integrals," *J. Comput. Phys.*, vol. 22, pp. 352–376, 1976.

[42] C. W. Kuo and T. Itoh, "A flexible approach combining the spectral domain method and impedance boundary condition for the analysis of microstrip lines," *IEEE Microwave Guided Wave Letters*, vol. 1, no. 7, pp. 172–174, Jul. 1991.

[43] D. Nghiem, J. Williams, and D. Jackson, "A general analysis of propagation along multiple layer superconducting stripline and microstrip transmission lines," *IEEE Trans. Microw. Theory Tech.*, vol. 39, no. 9, pp. 1553–1565, Sep. 1991.

[44] J. Pond, C. Krowne, and W. Carter, "On the application of complex resistive boundary conditions to model transmission lines consisting of very thin superconductors," *IEEE Trans. Microw. Theory Tech.*, vol. 37, no. 1, pp. 181–190, Jan. 1989.

[45] F. Olyslager, D. Zutter, and K. Blomme, "Rigorous analysis of the propagation characteristics of general lossless and lossy multiconductor transmission lines in

multilayered media," *IEEE Trans. Microw. Theory Tech.*, vol. 41, no. 1, pp. 79–88, Jan. 1993.

[46] K. Michalski and J. Mosig, "Multilayered media Greens functions in integral equation formulations," *IEEE Trans. Antennas Propag.*, vol. 45, no. 3, pp. 508–519, Mar. 1997.

[47] G. Coluccini, M. Lucido, and G. Panariello, "Spectral domain analysis of open single and coupled microstrip lines with polygonal cross-section in bound and leaky regimes," *IEEE Trans. Microw. Theory Tech.*, vol. 61, no. 2, pp. 736–745, Feb. 2013.

[48] R. F. Harrington, *Field Computation by Moment Methods.* New York: MacMillan, 1968.

[49] M. Abramowitz and I. A. Stegun, *Handbook of Mathematical Functions.* New York: Dover, 1970.

[50] T. Demeester and D. D. Zutter, "Internal impedance of composite conductors with arbitrary cross section," *IEEE Trans. Electromagn. Compat.*, vol. 51, no. 1, pp. 101–107, Feb. 2009.

[51] K. Mei and J. V. Bladel, "Scattering by perfectly conducting rectangular cylinders," *IEEE Trans. Antennas Propag.*, vol. 11, no. 2, pp. 185–192, Mar. 1963.

[52] T. Demeester and D. D. Zutter, "Comments on scattering by perfectly conducting rectangular cylinders," *IEEE Trans. Antennas Propag.*, vol. 12, no. 2, pp. 235–236, Mar. 1964.

[53] M. Lucido, G. Panariello, and F. Schettino, "Scattering by polygonal cross-section dielectric cylinders at oblique incidence," *IEEE Trans. Antennas Propag.*, vol. 58, no. 2, pp. 540–551, Feb. 2010.

[54] C. L. Holloway and E. F. Kuester, "DC internal inductance for a conductor of rectangular cross section," *IEEE Trans. Electromagn. Compat.*, vol. 51, no. 2, pp. 338–344, May 2009.

[55] T. Itoh and R. Mittra, "Spectral-domain approach for calculating the dispersion characteristics of microstrip lines," *IEEE Trans. Microw. Theory Tech.*, vol. 21, no. 7, pp. 496–599, Jul. 1973.

[56] T. Itoh, "Spectral domain immitance approach for dispersion characteristics of generalized printed transmission lines," *IEEE Trans. Microw. Theory Tech.*, vol. 28, no. 7, pp. 733–736, Jul. 1980.

[57] J. R. Mosig and A. Melconi, "The summation by parts algorithm—a new efficient technique for the rapid calculation of certain series arising in shielded planar structures," *IEEE Trans. Microw. Theory Tech.*, vol. 50, no. 1, pp. 215–218, Jan. 2002.

[58] C. A. Balanis, *Advanced Engineering Electromagnetics.* New York: Wiley, 1989.

[59] R. E. Collin, *Field Theory of Guided Waves.* Piscataway, NJ: IEEE Press, 1991.

[60] J. Song, *Lecture Notes on Advanced Electromagnetic Field Theory II*, 2012.

[61] T. Itoh and R. Mittra, "Technique for computing dispersion characteristics of shielded microstrip lines," *IEEE Trans. Microw. Theory Tech.*, vol. 22, no. 10, pp. 896–898, Oct. 1974.

[62] J. B. Knorr and A. Tufekcioglu, "Spectral-domain calculation of microstrip characteristic impedance," *IEEE Trans. Microw. Theory Tech.*, vol. 23, no. 9, pp. 725–728, Sep. 1975.

[63] R. H. Jansen, "High-speed computation of single and coupled microstrip parameters including dispersion, higher order modes, loss and finite strip thickness," *IEEE Trans. Microw. Theory Tech.*, vol. 26, no. 7, pp. 75–87, Feb. 1978.

[64] D. Mirshekar-Syahkal, *Spectral Domain Method for Microwave Integrated Circuits.* New York: Wiley, 1990.

[65] W. Shu, "Electromagnetic waves in double negative metamaterials and study on numerical resonances in the method of moments," Ph.D. dissertation, Iowa State University, Ames, Iowa, 2008.

[66] Z. Zeng, J. Song, and L. Zhang, "DC limit of microstrip analysis using the spectral domain approach with both transverse and longitudinal currents," *IEEE Antennas Wireless Propag. Lett.*, vol. 6, pp. 560–563, 2007.

[67] A. Sidi, "The numerical evaluation of very oscillatory infinite integrals by extrapolation," *Math. Comput.*, vol. 38, no. 158, pp. 517–529, 1982.

[68] ——, "Extrapolation methods for divergent oscillatory infinite integrals that are defined in the sense of summability," *J. Comput. Appl. Math.*, vol. 17, pp. 105–114, 1987.

[69] J. Wimp, *Sequence transformations and their applications.* New York: Wiley, 1989.

[70] J. E. Kiefer and G. H. Weiss, "A comparison of two methods for accelerating the convergence of fourier series," *Comput. Math. Appl.*, vol. 7, pp. 527–535, 1981.

[71] D. A. Smith and W. F. Ford, "Acceleration of linear and logarithmic convergence," *SIAM J. Numer. Anal.*, vol. 16, pp. 223–240, 1979.

[72] H. M. Edward, *Riemanns Zeta Function.* N. Chemsford, MA: Courier Dover, 2001.

[73] H. H. H. Homeier, "A levin-type algorithm for accelerating the convergence of fourier series," *Numer. Algorithms*, vol. 3, pp. 245–254, 1992.

[74] S. Jain, J. Song, T. Kamgaing, and Y. S. Mekonnen, "Efficient and accurate modeling of effective medium for interconnects in lossy shielded layered medium using

fast convergent series," in *Proc. IEEE 62nd Electronic Components and Technology Conference (ECTC'12)*, San Diego, CA, May 2012, pp. 133–139.

[75] K. Sainath, F. L. Teixeira, and B. Donderici, "Complex-plane generalization of scalar levin transforms: A robust, rapidly convergent method to compute potentials and fields in multi-layered media," *J. Comp. Phys.*, vol. 269, pp. 403–422, 2014.

[76] H. S. Xu, J. M. Song, T. Kamgaing, and Y. S. Mekonnen, "Acceleration of spectral domain immitance approach for generalized multilayered shielded microstrips using the levin's transformation," *IEEE Antennas Wireless Propag. Lett.*, vol. 14, pp. 92–95, 2015.

[77] H. Xu, K. Chen, J. Song, T. Kamgaing, and Y. S. Mekonnen, "A novel approach to accelerate spectral domain approach for shielded microstrip lines using the levin transformation and summation-by-parts," *Radio Sci.*, vol. 49, no. 8, pp. 573–582, Aug. 2014.

[78] A. J. Poggio and E. K. Miller, *Integral equation solutions of three-dimensional scattering problems.* Ed. Oxford, U.K.: Pregamon Press, 1973.

[79] T. K. Wu and L. L. Tsai, "Scattering from arbitrarily-shaped lossy dielectric bodies of revolution," *Radio Sci.*, vol. 12, pp. 709–718, 1977.

[80] Y. Chang and R. F. Harrington, "A surface formulation for characteristic modes of material bodies," *IEEE Trans. Antennas Propag.*, vol. 25, pp. 789–795, Nov. 1977.

[81] F. Ling, "Fast electromagnetic modeling of multilayer microstrip antennas and circuits," Ph.D. dissertation, University of Illinois at Urbana-Champaign, Urbana, Illinois, 2000.

BIOGRAPHICAL SKETCH

Hongsheng Xu was born March 17, 1987 in Nanjing, Jiangsu Province, China. He received the Bachelor of Science in Electrical Engineering from Southeast University in 2009 and the Ph.D. from Iowa State University in 2015.

He has served as a Research Assistant in Dr. Jiming Song's group and Teaching Assistant in the Department of Electrical and Computer Engineering at Iowa State University. His current research interests include electromagnetic modeling using numerical techniques, power system and smart grids. He received the China Scholarship Council (CSC) fellowship in 2010.

PUBLICATIONS

1. H. S. Xu, S. Jain, J. M. Song, T. Kamgaing, and Y. S. Mekonnen, "Acceleration of spectral domain immitance approach for generalized multilayered shielded microstrips using the Levin's transformation," *IEEE Antennas Wireless Propagation Lett.*, vol. 14, pp. 92-95, 2015.

2. H. Xu, K. Chen, J. Song, T. Kamgaing, and Y. S. Mekonnen, "A novel approach to accelerate spectral domain approach for shield microstrip lines using the Levin transformations and summation-by-parts," *Radio Science*, vol. 48, no. 8, pp. 573-582, Aug. 2014

3. H. Xu, J. Song, T. Kamgaing and Y. S. Mekonnen, "The extrapolation methods in acceleration of SDA for shielded microstrip lines," *in Proc. IEEE AP-S Int. Symp.*, Memphis, Tennessee, USA, paper 342.7, Jul. 6-11, 2014.

4. H. Xu, J. Song, and T. Kamgaing, "Current distribution and internal impedance of interconnects," *21st Conference on Electrical Performance of Electronic Packaging and System* (EPEPS), Tempe, Arizona, USA, pp. 307-310, 2012.

5. H. Xu, J. Song, and T. Kamgaing, "An accurate volume integral equation for calculation of the current distribution," *28th International Review of Progress in Applied Computational Electromagnetics* (ACES), Columbus, Ohio, USA, pp. 208-213, 2012.

6. H. F. Ma, X. Chen, X. M. Yang, H. S. Xu, Q. Cheng, and T. J. Cui, "A Broadband

Metamaterial Cylindrical Lens Antenna," *Chinese Science Bulletin*, vol. 55, 2066-2070, 2010.

7. H. F. Ma, X. Chen, H. S. Xu, X. M. Yang, W. X. Jiang, and T. J. Cui, "Experiments on high-performance beam-scanning antennas made of gradient-index metamaterials," *Appl. Phys. Lett.*, vol. 95, 094107, 2009.

8. Q. H. Sun, Q. Cheng, H. S. Xu, B. Zhou, and T. J. Cui, "A new type of band-pass FSS based on metamaterial structures," *2008 International Workshop on Metamaterials*, Nanjing, Jiangsu, China, pp. 267-269, 2008.

9. Q. Cheng, X. Y. Zhou, B. Zhou, H. S. Xu and T. J. Cui, "A Superstrate for Microstrip Patch Antennas," *2008 International Workshop on Metamaterials*, Nanjing, Jiangsu, China, pp. 382-384, 2008.